THESIS FOR THE DEGREE OF DOCTOR OF PHILOSOPHY (PhD)

Contribution of voltage-gated cation channels to immunity: function and importance of localization within the membrane

by Orsolya Szilágyi

Supervisor: Péter Béla Hajdu, PhD

UNIVERSITY OF DEBRECEN

DOCTORAL SCHOOL OF MOLECULAR MEDICINE

Debrecen, 2013

TABLE OF CONTENTS

LIST OF ABBREVIATIONS

Ag	antigen
APC	antigen presenting cell
CD	cluster of differentiation
CHO	Chinese hamster ovary
ChTX	charybdotoxin
CRAC	calcium release-activated calcium channel
DAG	diacyl glycerol
DC	dendritic cell
DLG	discs large protein
DMEM	Dulbecco's Modified Eagle's Medium
GM-CSF	granulocyte-macrophage colony-stimulating factor
GST	glutathione S-transferase
HEK	human embryonic kidney
IDC	immature dendritic cell
IKCa1	intermediate-conductance Ca^{2+}-activated K^+ channel
IL	interleukin
IP_3	inositol 1,4,5-trisphosphate
IS	immunological synapse
LB	Luria-Bertani broth
Lck	lymphocyte-specific protein tyrosin kinase
LFA-1	lymphocyte function-associated antigen-1
MAGUK	membrane-associated guanylate kinase
MDC	mature dendritic cell
mGFP	monomeric green fluorescent protein
MHC	major histocompatibility complex
NF-AT	nuclear factor of activated T-cells
PBS	phosphate-buffered saline
PIP_2	phosphatidylinositol 4,5-bisphosphate
PKC	protein kinase C
PLC-γ	phospholipase C-γ
PSD-95	post-synaptic density protein-95
RPMI	Roswell Park Memorial Institute Medium

SAP97	synapse-associated protein 97
SDS	sodium dodecyl sulfate
SEE	Staphylococcus enterotoxin E
SLE	systemic lupus erythematosus
SMAC	supramolecular activation cluster
SOB	super optimal broth
SOC	super optimal broth with catabolite repression
STIM1	stromal interaction molecule 1
STX	saxitoxin
TAE	Tris-acetate-EDTA
TBS	Tris-buffered saline
TEA	tetraethylammonium
T_{CM}	central memory T cell
TCR	T cell receptor
T_{EM}	effector memory T cell
TTX	tetrodotoxin
VGPC	voltage-gated potassium channel
VGSC	voltage-gated sodium channel
WT	wild-type
YT	yeast extract triptone

1. INTRODUCTION

Obtaining an appropriate immune response requires a coordinated interplay between several immune cells. The reactivity of these cells greatly depends on activating signaling cascades, which are in part regulated by ion channels. These proteins were first described as transmembrane molecules that allow the passage of different ions through cellular membranes. Initially, their importance has been shown on excitable cells, where they control the membrane potential, eventually creating action potentials. However, by now it is well known, that ion channels can be found on every cell type, where they affect various cellular functions, mainly through the regulation of the membrane potential and possibly through the interaction with various intracellular scaffolding proteins.

Dendritic cells (DC) are one of the major professional antigen presenting cell (APC) types. Upon antigen encounter immature dendritic cells (IDC) differentiate into mature DC (MDC), which present the processed antigen to T lymphocytes through major histocompatibility complex II (MHCII) molecules. Therefore it is crucial that the differentiation process is under strict control, since the lack of maturation or unwanted maturation could both cause serious immune defects. A voltage-gated sodium channel, Nav1.7, has been described as the major sodium channel of human monocyte-derived immature dendritic cells [1]. We have shown in this study, that it is expressed especially on one IDC subset, which can skew the immune response towards a more immunogenic direction. We propose that by the regulation of the membrane potential, this channel constrains IDC to only become activated at an appropriate signal intensity threshold, hence preventing unnecessary DC activation.

Antigen presentation requires the physical interaction of antigen presenting cells with T cells, their coupling is termed the immunological synapse (IS), analogous to neuronal synapses. This is an extremely complicated supra-molecular cluster, which involves the rearrangement of several proteins in the cell membranes of both cells, including receptors, signaling proteins and cytoskeletal elements. Kv1.3, the voltage-gated potassium channel of T cells has been shown previously to translocate into the synaptic area [2]. However, the exact mechanism and function of this redistribution was unknown, only suggesting its possible role in the regulation of the local membrane potential, allowing a sustained Ca^{2+} signal. We were able to show in this work that this redistribution is controlled by a scaffolding protein from the membrane-associated guanylate kinase (MAGUK) family, PSD-95. This protein, originally reported in neurons, is also expressed in human T cells, where it regulates the localization of

Kv1.3, and possibly allows the indirect interaction of several other proteins with the channel. We believe, that this finding may bring us closer to concluding what the exact role/roles Kv1.3 has at the IS and most importantly in immune response regulation.

2. SCIENTIFIC BACKGROUND

2.1 Dendritic cells, T lymphocytes

The first line of defense against pathogens is provided by the innate immune system, which is non-specific and only provides short-term immunity for the host. However, the innate immune system is crucial in the activation of the adaptive response, which features specialized cells against specific pathogens and creates immunological memory as well [3]. Dendritic cells (DC) have an important role in linking innate to adaptive immunity: they are capable of capturing and processing antigens, they can migrate to lymphoid organs in order to initiate immunity, and they are able to differentiate, mature rapidly responding to different stimuli [4]. Conventional DC differentiate from a common progenitor of macrophages via two independent pathways into $CD11c^+$ blood precursors with or without the expression of membrane cluster of differentiation 1 (CD1) molecules [5, 6]. CD1a is a type 1 membrane protein [7] that is stabilized by captured self- or pathogen-derived modified lipids [8] to activate CD1a-restricted T lymphocytes [9]. $CD11c^+CD1a^-$ DC replenish various tissues with interstitial DC, whereas the $CD11c^+CD1a^+$ subtype differentiate to Langerhans cells on epithelial surfaces [10]. DC also differentiate from blood monocytes driven by micro-environmental factors generated by inflammation, antigens, pathogens, or metabolites in peripheral tissues [11]. *In vitro* differentiation of monocytes to $CD1a^-$ and $CD1a^+$ DC requires granulocyte-macrophage colony-stimulating factor (GM-CSF) to support cell survival and IL-4 driving cell differentiation [12]. These DC subsets show immature tissue DC (IDC) features and can be further activated by stimulatory signals. It has been shown that $CD1a^-$ and $CD1a^+$ DC subsets exhibit different functional properties and are able to skew T cell polarization toward tolerogenic or immunogenic directions, respectively [13]. IDC may undergo drastic functional and phenotypic changes upon antigen encounter and concomitant danger signals, resulting in the transition toward mature DC (MDC). When activated, MDC migrate to draining lymph nodes and act as professional antigen presenting cells (APC) to prime and polarize naïve antigen (Ag)-specific T cells towards inflammatory or tolerogenic directions [14].

The most important functions of adaptive immunity are to differentiate between the host's own antigens and the foreign antigens through antigen presentation, to generate effective responses against pathogens and to create immunological memory. Different T lymphocyte subsets play a very important role in all of the above mentioned features. Following selection in the thymus, two major types of T cells can be distinguished according

to the T cell receptors (TCR) expressed on their surface. Approximately 90% of the cells express αβ chains, while a minority of T cells expresses γδ chains in the TCR. The latter are much less heterogenic than αβTCR T cells, and directly recognize their target antigen. αβTCR T cells can be further sorted either according to their lineage markers or their functional activities. The two best known markers are CD4 and CD8 that separate two distinct T cell subsets with different functions. $CD4^+$ cells produce various cytokines as effector T helper cells following the recognition of antigens presented on the surface of MHC class II molecules (which are expressed only on professional APC). Cytotoxic T lymphocytes on the other hand express CD8, and recognize antigenic peptides through MHC class I molecules, which are present on every nucleated cell type. However, depending on the functional status of T cells, we can distinguish between naïve, effector and memory T lymphocytes [3].

The fate (activation, maturation) of both dendritic cells and T cells depends in a great deal on different ion channels in their plasma membrane. The next sections will focus on ion channels in general, and on their functions in dendritic and T cells.

2.1.1 Ion channels in general

Ion channels are transmembrane, pore-forming proteins that can be found in every cell type. Two characteristics separate ion channels from other transporter molecules: the rate of ion transport through the pores is very high and the ion transport always follows the electrochemical gradient [15]. Ion channels can be classified according to their selectivity (highly-, mildly- or non-selective) or their gating (e.g. voltage-, ligand-gated, mechanosensitive). Because this study focuses on a voltage-gated sodium and a voltage-gated potassium channel, these will be described in detail in the upcoming sections.

Voltage-gated sodium channels (VGSC) are made up of a single approximately 260 kDa polypeptide chain (α-subunit) that is associated with one or more auxiliary β subunits [16]. The latter are not necessary for channel expression, however they modify the kinetics and voltage-dependence of channel gating [17]. The α-subunit contains four homologous domains and each is made up of six alpha helices (segments, S) that span the plasma membrane. The voltage sensor is the S4 helix, containing positively charged amino acid residues. The central pore of the channels is formed by the S5-S6 segments of the four domains and the pore loop amidst them (Figure 2.1) [18, 19].

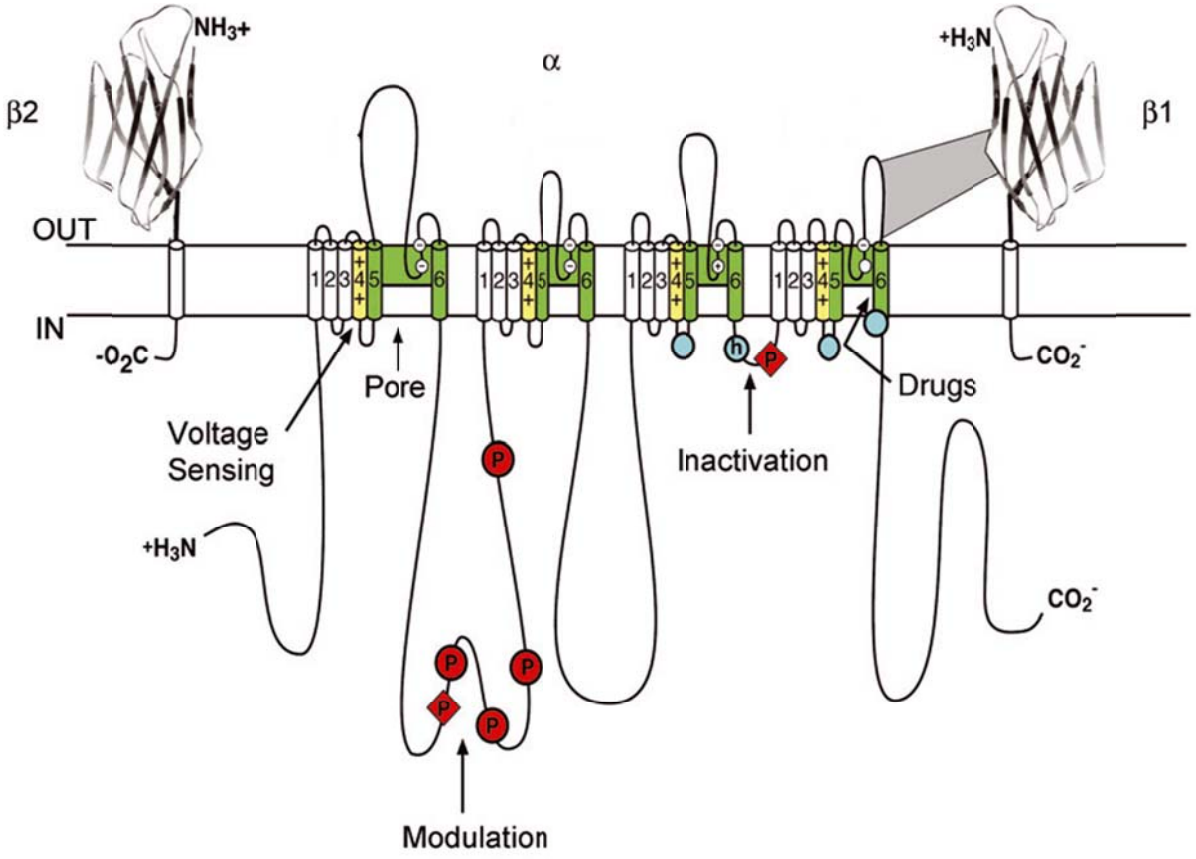

The α-subunits are also responsible for the binding of pharmacological agents that affect sodium channels [18]. One receptor site for local anesthetics and at least six receptor sites for different neurotoxins have been identified [20]. Tetrodotoxin (**T**TX) and saxitoxin (STX) are two non-peptide pore blockers that bind to neurotoxin receptor site 1 located at the extracellular pore opening of the channel.

Voltage-gated potassium channels (VGPC) have a similar structure to VGSCs, except that the four homologous domains are formed by separate polypeptide chains that are held together by non-covalent bonds (Figure 2.2) [21]. The voltage sensor is again the S4 helix, which contains positively charged amino acids. The pore is formed by the extracellular loops between the S5 and S6 segments and contains the typical four-amino-acid motif (GYGD) that is responsible for K^+ selectivity [22, 23].

VGPCs can be identified by means of various peptide and small-molecule inhibitors. For instance, tetraethylammonium (TEA) is a non-selective blocker of VGPCs, reducing the peak amplitude of K^+ current and blocking the slow, C-type inactivation of the channels [24]. One of the first peptide inhibitors Charybdotoxin (ChTX) is a 37 amino acid long polypeptide isolated from the *Leiurus quiquestratus* scorpion. It has been described as a high affinity blocker of potassium channels [25], blocking Kv1.3 channels at nanomolar levels [26]. More and more selective blockers are developed or discovered every year as they can be efficiently applied in clinical therapy to treat for example autoimmune diseases [27-29].

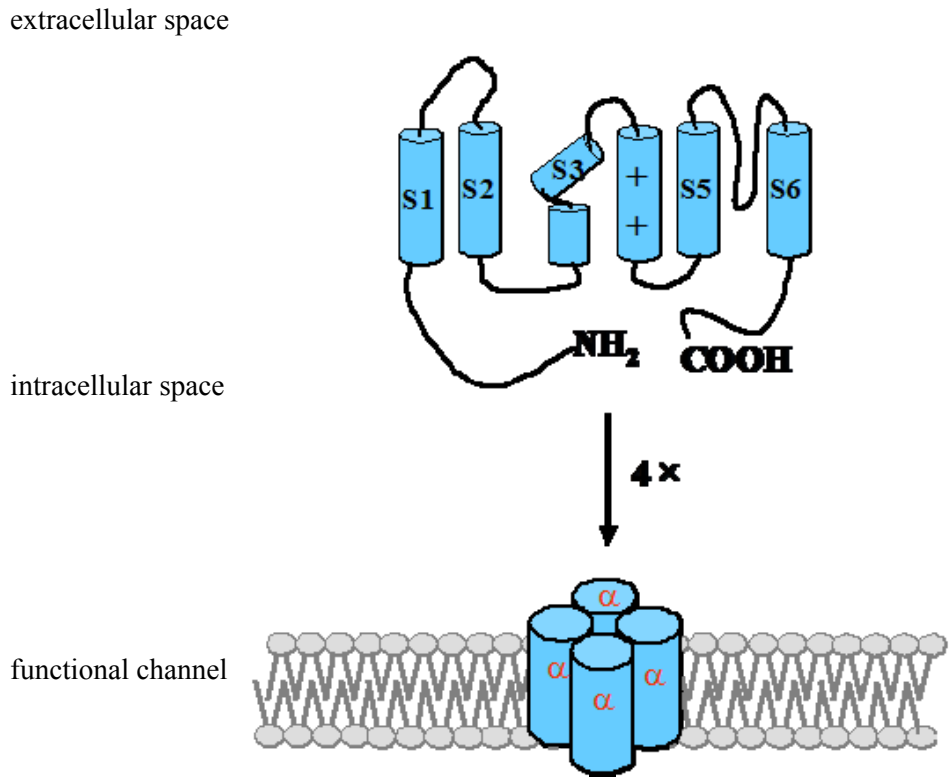

Figure 2.2 ***Structure of voltage-gated potassium channels***.
Four α subunits, each composed of 6 alpha-helices (S1-S6, see top panel), make up a functional channel.

2.1.1.1 Ion channels in dendritic cells, the Nav1.7 channel

The above mentioned voltage-gated ion channels were first described in excitable cells, where they are involved in the electrogenesis of action potential [30]. Since then several studies have shown the existence of ion channels in non-excitable cells as well, including immune cells [31-33]. Numerous signaling pathways depend on the intracellular Ca^{2+} concentration in DC, which is controlled by various ion channels: RyR1 receptors, P2Y receptors, L-type calcium channels, and the calcium release-activated calcium channel (CRAC) [34-37]. Voltage-gated potassium channels help to maintain a negative membrane potential required for efficient Ca^{2+} signaling in these cells [38]. During immune cell differentiation the expression of VGPC may change, suggesting their inevitable effect on various cellular functions. Microglia cells, which exclusively reside to the central nervous system, express multiple VGSC, playing a role in cell migration and phagocytosis [39]. It was also described that sodium channels act during the activation and phagocytosis of macrophages and microglia, suggesting the anti-inflammatory role of sodium channel blockers [40].

The Nav1.7 channel is a voltage-gated sodium channel that was originally described in neurons [41, 42], but since then has been shown in DC as well [1]. The biophysical properties of the channel have been investigated extensively: the voltage dependence of steady-state activation, which defines the distribution of the ion channels between the open and closed state at a given membrane potential, characterized with the $V_{1/2}$ is approximately -20 mV, meaning that about 50% of the Nav1.7 channels are open at this potential. Nav1.7 shows fast inactivation kinetics between 1-2 ms (typical for Na^+ channels), which is due to the fast inactivation gate. This gate is formed by the short intracellular loop connecting the S3 and S4 segments of the α-subunit and forms an intracellular block that folds into the channel structure in such a way that it occludes the pore [43]. According to pharmacological studies Nav1.7 currents are TTX (TTX, $K_d \approx 25$ nM) sensitive [44].

In neuronal cells the α-subunit of Nav1.7 was shown to amplify small depolarization events to generate threshold currents close to the resting membrane potential [45]. The Nav1.7 protein is encoded by the *SCN9A* gene, expressed mainly in sympathetic ganglia and nociceptive dorsal root ganglion neurons [42, 44]. According to various studies, Nav1.7 could play a role in pain induction via its altered transcription or mutation. Upregulation of Nav1.7 expression and activity results in increased pain sensation, and therapies based on silencing the *SCN9A* gene or blocking Nav1.7 activity could emerge as means for effective pain relief

[46]. Moreover, mutations of the *SCN9A* gene that cause excessive channel activities revealed the inherited pain syndrome erythermalgia and paroxysmal extreme pain disorder [47]. Mice showed reduced responses to mechanical, thermal, and inflammatory pain, when lacking the *SCN9A* gene due to a specific deletion in nociceptive sensory neurons [48]. Furthermore, the expression of Nav1.7 is enhanced in pathophysiological conditions, such as metastatic prostate cancer, where several cellular activities are potentiated due to Nav1.7 activity [49]. Even though Nav1.7 is a potential therapeutic target for pain modulation the major factors, which regulate the expression of *SCN9A* have not yet been identified. Moreover, Nav1.7 was characterized as a novel VGSC in monocyte-derived DC, which shows a developmental switch to VGPC Kv1.3 during *in vitro* DC maturation [1]. However, the exact role of VGSC and Nav1.7 in particular, in the regulation of Na^+ flux to immune cells and their contribution to cellular functions are still poorly understood.

2.1.1.2 T lymphocytes and ion channels, the Kv1.3 channel

Just like in dendritic cells, ion channels expressed in T lymphocytes regulate Ca^{2+} signaling, thus have a crucial impact on cell activation and differentiation [50]. CRAC channels are responsible for the generation of Ca^{2+} currents in these cells [51-53], and the negative membrane potential is ensured by two potassium channels. Intermediate-conductance Ca^{2+} -activated potassium channel (IKCa1, or also termed KCa3.1, *KCNN4* gene encoded) is sensitive to the rise of intracellular Ca^{2+} concentration, opening of the channel leads to the hyperpolarization of the plasma membrane [54]. On the other hand, a voltage-dependent K^+ current has been described in T cells as well [55] that can be attributed to the Kv1.3 channel (coded by the *KCNA3* gene) [56]. Interestingly, while the membrane potential of resting T cells is controlled primarily by Kv1.3 channels (~200-400 channels/cell), this function is taken over by KCa3.1 channels in activated cells [57]. Besides ensuring the necessary driving force for Ca^{2+} influx, Kv1.3 also works together with a Cl^- channel (Cl_{swell}) to regulate cellular volume [58].

The Kv1.3 channel belongs to the *Shaker* family of potassium channels [59]. *Shaker* type channels open quickly after a depolarizing impulse, after which they become inactivated. During activation the S4 transmembrane segment moves towards the extracellular space due to the positively charged amino acids in this region, thereby altering the conformation of the channel [60]. The activation threshold potential for Kv1.3 channels is between -40-(-50) mV. The voltage dependence of steady-state activation can be characterized by the Boltzmann-equation, which reaches its maximum between +20 - +30 mV, when the probability of

channel opening is approximately 1. The inactivation of *Shaker* channels can occur through N-type or so-called “fast inactivation” [61]. The N-type inactivation features the “ball and chain” model, widely accepted in the literature [62, 63]. According to this model a peptide region containing some positively charged amino acids (“ball”) is attached to every channel subunit through a peptide chain (“chain”) at the intracellular, N-terminal side of the channel. During inactivation, this “ball” plugs in the pore of the channel. Kv1.3 lacks this inactivating region, thus only slow inactivation can take place in this channel type. This is highly sensitive to the amino acids forming the extracellular pore of the channel and to the ion composition of the extra- and intracellular space [64]. The selectivity filter at the extracellular mouth of the pore constricts or collapses during slow inactivation [65, 66]. The slow inactivation consists of the closing of the gate at the end of the pore (P-type inactivation), followed by conformational changes in this region that stabilizes the conformation of the voltage sensors and the non-conducting state of the channel as well (C-type inactivation) [67].

2.2 *In vivo* T cell activation, the immunological synapse

Helper T cells are one of the key components in establishing adaptive immune response. The crucial step that triggers T cell activation and proliferation is the interaction between MHCII molecules of professional APC with the T cell receptor (TCR)/CD3 complex

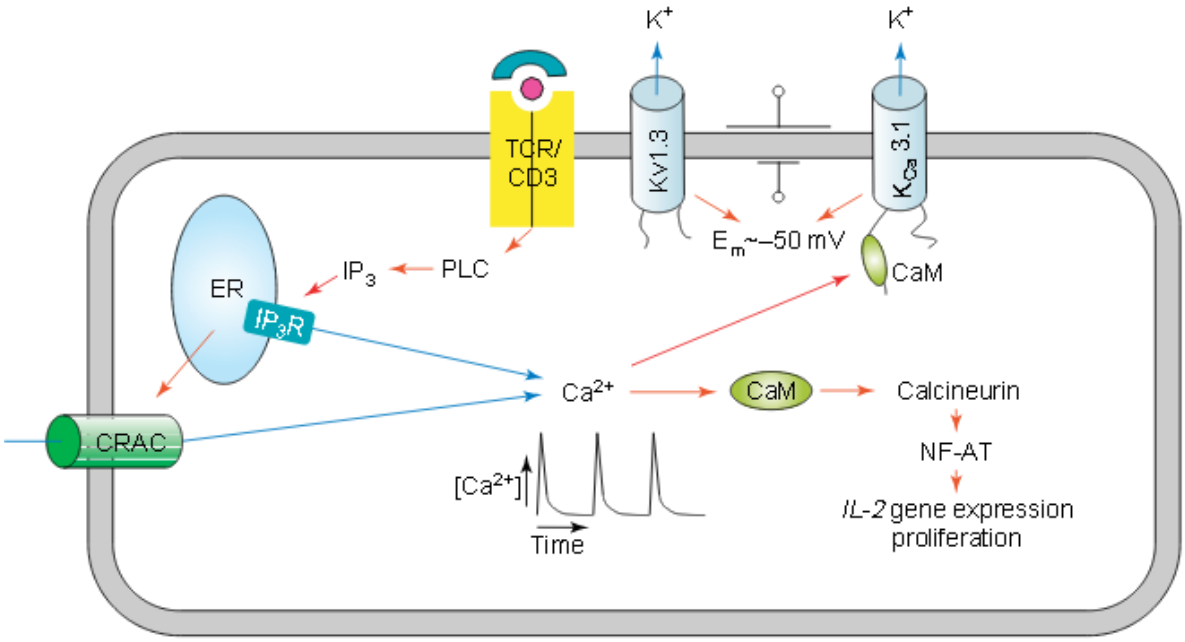

Figure 2.3 ***Role of ion channels in in vivo T cell activation.***
Upon TCR activation Ca^{2+} is released from intracellular stores, which activates the CRAC channels in the plasma membrane, resulting in Ca^{2+} influx from the extracellular space. KCa3.1/IKCa1 and Kv1.3 channels hyperpolarize the plasma membrane, providing appropriate driving force for prolonged Ca^{2+} influx. As a second messenger Ca^{2+} regulates signaling cascades within the T cell, eventually leading to proliferation (Panyi *et al.*, 2004).

[68]. This initial signaling step results in the activation of phospholipase C-γ (PLC-γ). This enzyme catalyses the cleavage of phosphatidylinositol 4,5-bisphosphate (PIP_2) into diacyl glycerol (DAG) and inositol 1,4,5-trisphosphate (IP_3). DAG is responsible for the activation of protein kinase C (PKC), which in turn phosphorylates several intracellular substrates. The other crucial component of this signaling cascade is the two-phase elevation of the intracellular Ca^{2+} concentration. IP_3 is the key element in the initial Ca^{2+} influx: binding of IP_3 to its receptors on the endoplasmic reticulum results in Ca^{2+} release from the endoplasmic stores. This in turn activates stromal interaction molecule 1 (STIM1), which translocates to a

region of the endoplasmic membrane where it can activate Orai1 molecules. Orai1 forms the pore of CRAC channels, through which Ca^{2+} ions can flow into the cell, creating the second, prolonged increase in the cytosolic Ca^{2+} concentration [53, 69]. This results in the opening of both potassium channels (KCa3.1/IKCa1 and Kv1.3) in the plasma membrane, which ensures the necessary driving force for Ca^{2+} influx (Figure 2.3 [70]). The persistent, oscillating Ca^{2+} concentration elevation activates the phosphatase calcineurin through calmodulin. Calcineurin in turn dephosphorylate the transcription factor, nuclear factor of activated T-cells (NF-AT) in the cytoplasm, which then translocates to the nucleus, and activates the IL-2 gene. This signaling cascade in concert with other pathways (MAP kinase, Ras, Fos) induces the proliferation of T cells [71, 72].

As mentioned above, the first step of T cell activation is the interaction of MHCII molecules with the TCR/CD3 complex, forming the immunological synapse (IS), during which the antigen presentation may occur. During IS formation plasma membrane proteins of both the APC and T cell rearrange and segregate into the contact area between the two cells [73] creating the so called supramolecular activation cluster (SMAC), consisting of two concentric rings of molecules [74]. These separate rings were termed central supramolecular activation cluster (c-SMAC) and peripheral supramolecular activation cluster (p-SMAC), as they include different molecules. The TCR and various intracellular signaling molecules like protein kinase CΘ (PKCΘ) and the lymphocyte-specific protein tyrosin kinase (LCK) are restricted to the c-SMAC, whereas the p-SMAC includes talin, a protein bound to the actin cytoskeleton, and the integrin lymphocyte function-associated antigen-1(LFA-1), surrounding the TCR (Figure 2.4) [74].

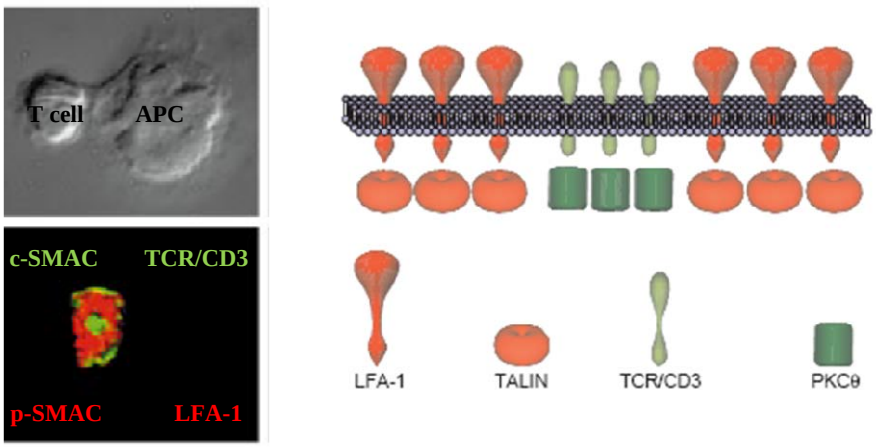

Figure 2.4 ***Structure of the immunological synapse I.***
Structure of the immunological synapse with regard to supramolecular activation clusters (c-SMAC and p-SMAC) and their most important proteins (Monks *et al*., 1998).

Later a third, distal supramolecular activation cluster (d-SMAC) has been recognized as well, rich in CD45 and actin. Interestingly, T cells that form immunological synapses with DC do not show this typical bull's eye pattern, rather establish 'multifocal IS', where the TCR clusters at multiple sites at the interface between T cells and DC [75]. However, these clusters only show a lateral organization of the immunological synapse, whereas Dustin et. al. suggests the organization of the IS into three functional layers, which represents its true, three dimensional structure, containing various molecules: a receptor interaction layer, including TCR/CD3, LFA-1, LAT (linker of activated T cells), and several CD molecules, a signaling layer containing ZAP70 (Zeta-chain-associated protein kinase 70), LCK, PKCΘ, talin, ITK (protein tyrosine kinase), PLCγ, paxillin, FAK1 (focal adhesion kinase 1), and PYK2 (protein tyrosine kinase). Finally, a cytoskeletal layer including molecules such as vinculin or F-actin (Figure 2.5 [76]).

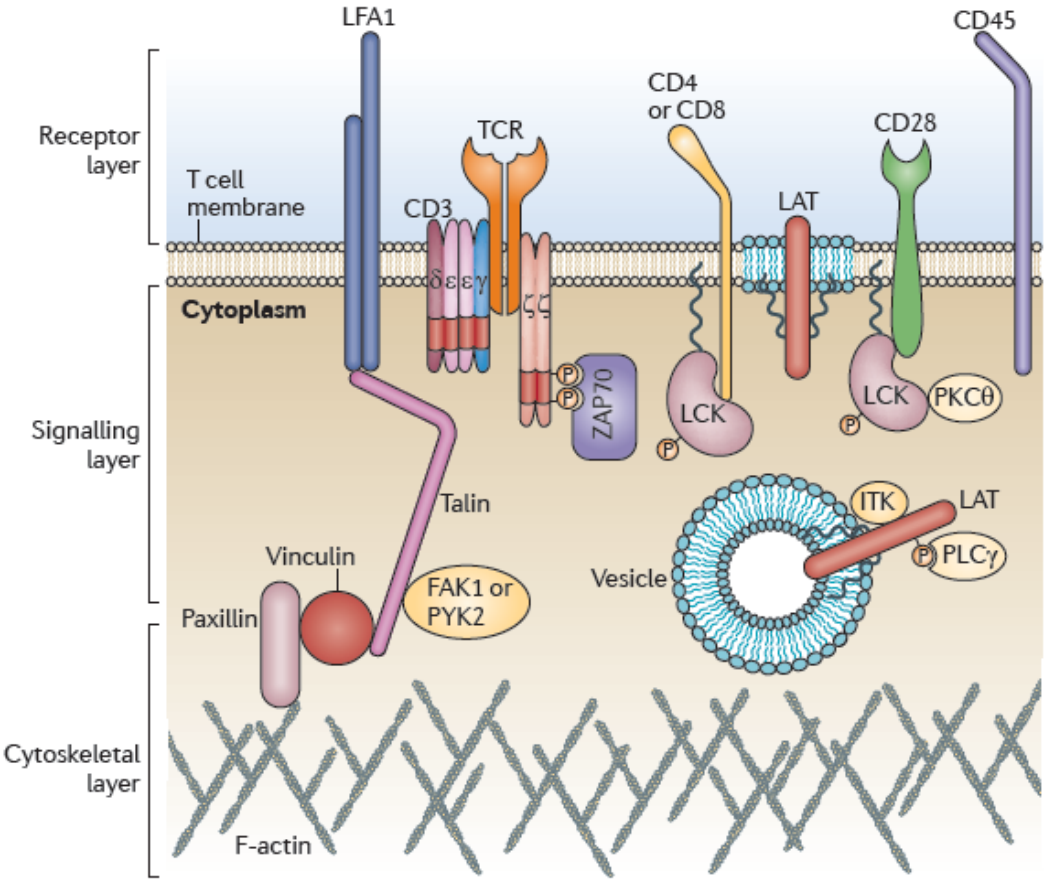

Figure 2.5 ***Structure of the immunological synapse II.***
Structure of the immunological synapse considering the three functional (receptor, signaling, cytoskeletal) layers (Dustin *et al*., 2011).

Previously our laboratory has shown that FLAG-tagged Kv1.3 channels expressed in Jurkat T cells co-localize with CD3 molecules [77]. In addition, when expressed in cytotoxic T cells, the Kv1.3 channels concentrated between the T cell - target cell interface, namely at the cytotoxic IS (Figure 2.6) [2]. The same polarized distribution was shown for Kv1.3 and KCa3.1/IKCa1 channels at the IS between a T cell and an APC [78]. Later it has been described, that Stim1 and Orai1 proteins also redistribute to the IS between DC and T cells [79]. Blocking Kv1.3 or CRAC channels has no effect on molecular clustering [78-80], however the longer term stability of the IS may be affected. There are some evidences suggesting the functional role of Kv1.3 channels at the synapse: 1) the regulation of Kv1.3 channels by Lck, 2) the interaction of Kv1.3 with Lck through adaptor proteins, 3) the association of Kv1.3 with Lck and PKC through its accessory subunits (Kvβ) [81-85]. Regardless of these, the exact purpose and the mechanism of this redistribution are still unknown.

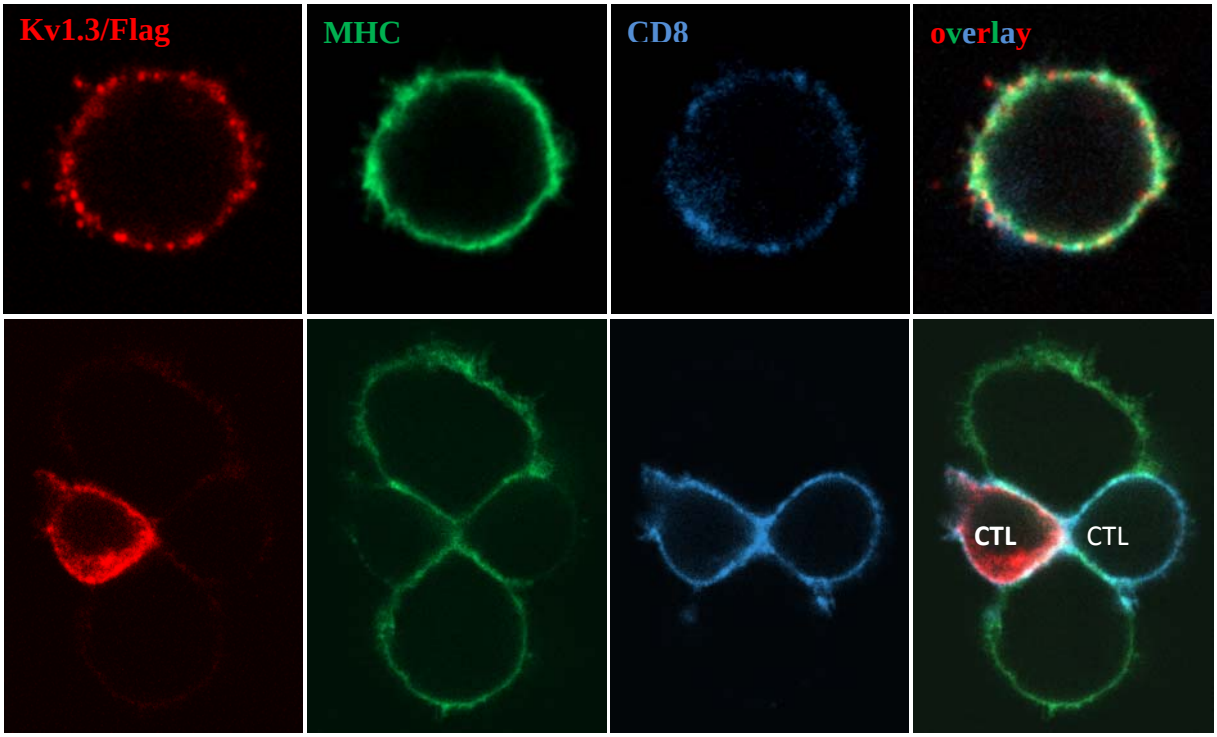

Figure 2.6 ***Redistribution of FLAG-tagged Kv1.3 channels to the immunological synapse formed between cytotoxic T cells (CTL) and a target cell.***
Resting T cells show a diffuse Kv1.3 distribution within their plasma membrane (upper panel), whereas the channels relocalize to the synaptic area upon interaction with the target cell (lower panel) (Panyi *et al*., 2004).

2.3 Ion channels and autoimmune diseases

The first disease that was described as an autoimmune disorder related to ion channels was myasthenia gravis [86, 87]. Since then, several other ion channel-attributed autoimmune syndromes have been shown, in which the channels become the targets of auto-antibodies [88, 89]. However, in some disorders the ion channels are expressed on the surface of auto-reactive effector cells, thus play a role in the autoimmune reaction itself, rather than being the target molecules themselves. Due to antigen stimulation, naïve T lymphocytes differentiate into central memory T cells (T_{CM}) and in case of further antigen stimulation into effector memory T cells (T_{EM}). Auto-reactive effector T cells (which display T_{EM} phenotype) have been shown to play a role in diseases such as rheumatoid arthritis, type 1 diabetes mellitus and multiple sclerosis. As mentioned in section 2.1.1.2, Kv1.3 and KCa3.1 are the two potassium channels expressed in T cells. It was demonstrated that activated/effector T_{EM} cells isolated from patients with the above mentioned diseases express many more Kv1.3 channels compared to activated naïve or T_{CM} cells (Kv1.3-dominated K^+ channel expression). On the contrary, KCa3.1 channels are much more abundant in the latter two cell types, than in T_{EM} [90, 91] (Figure 2.7). Because of this unique channel pattern, the activity of these autoreactive T_{EM} cells can be manipulated by the application of specific Kv1.3 channel blockers, which could lead to suppression of their effector function *in vitro* or *in vivo* in animal models [92].

It has also been suggested that the exact localization of Kv1.3 channels during immunological synapse formation may affect auto-reactivity of T cells. Nicolaou et al. showed that cross-linking these channels using external antibodies prevents their translocation to the IS, suggesting that the recruitment of Kv1.3 channels to the IS probably occurs through lateral movement in the plasma membrane. Blocking Kv1.3 channel movement to the IS has no effect on IS formation itself, however, it results in a magnified Ca^{2+} amplitude, implying the role of Kv1.3 channels in Ca^{2+} response [93]. The changes in Ca^{2+} signaling could alter the regulation of transcription factors that are important in T cell activation and proliferation. The same workgroup described, that systemic lupus erythematosus (SLE) T cells show exaggerated response to Ag stimulation due to more sustained increase in intracellular Ca^{2+} levels. Interestingly, resting T lymphocytes display a long-lasting recruitment of Kv1.3 channels in the IS, whereas pre-activated T cells show a different time course: Kv1.3 channels have a maximal recruitment at the first minute and progressively move out of the synapse by the 30^{th} minute following IS formation. The latter was observed in resting SLE T cells as well, implying that the premature loss of Kv1.3 from the IS in these cells could result in improper

Ca^{2+} regulation [94]. In line with this, they showed that the presence of Kv1.3 prevents the development of an exaggerated Ca^{2+} response, and that sustained Ca^{2+} signaling in SLE T cells highly correlates with short-lived Kv1.3 localization in the IS [95].

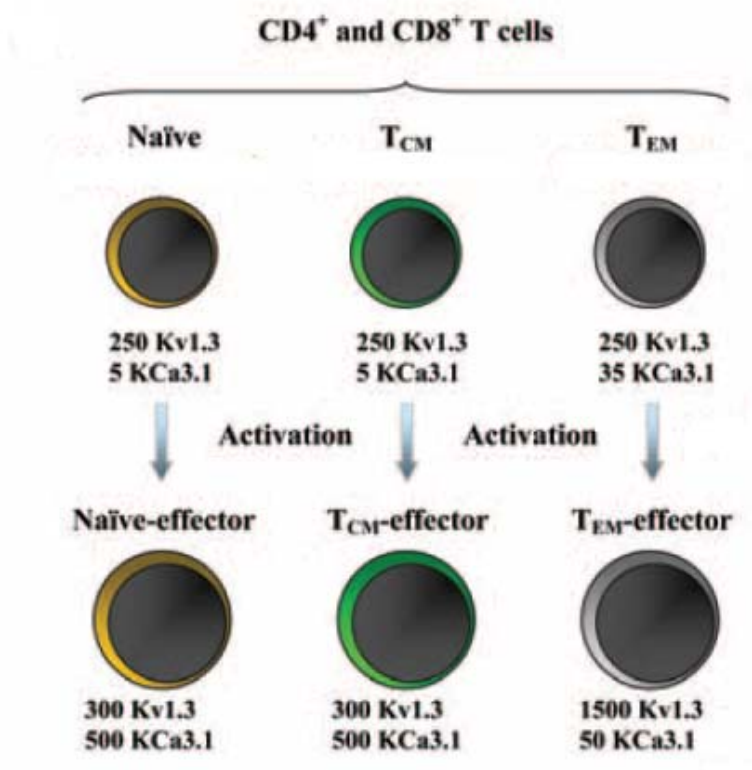

Figure 2.7 ***Expression of Kv1.3 and KCa3.1 channels in the different human T cell subsets.***
Activation of naïve and TCM cells dramatically increases the number of KCa3.1 channels, whereas effector memory T cells express more Kv1.3 channels following activation (Beeton *et al*., 2005).

2.4 MAGUK proteins

Membrane-associated guanylate kinases (MAGUK) form a widely expressed scaffolding protein family that is essential in neurological synapse formation. Ten subfamilies have been identified according to the genomic sequences of their typical domains. These subfamilies are: discs large 1-4 (DLG1-4), discs large 5 (DLG5), zona occludens (ZO), caspase recruitment domain containing MAGUK protein (CARMA), membrane protein palmytoilated 1 (MPP1), membrane protein palmytoilated 2-4 (MPP2-4), membrane protein palmytoilated 5 (MPP5), calcium/calmodulin-dependent serine protein kinase 3 (CASK), calcium channel β subunit (CACNB), and MAGUK with an inverted repeat (MAGI) [96] (Figure 2.7 and Table 2.1, [97]). DLG, MPP, CASK, CACNB, and MAGI proteins are primarily expressed in the central nervous system and control neuronal synapse formation and function [98-101]. The members of the ZO subfamily play an important role in the maintenance of the blood-brain barrier [102], while CARMA proteins are expressed in different tissues, where they regulate antibody recognition and inflammation in hematopoietic cells [103].

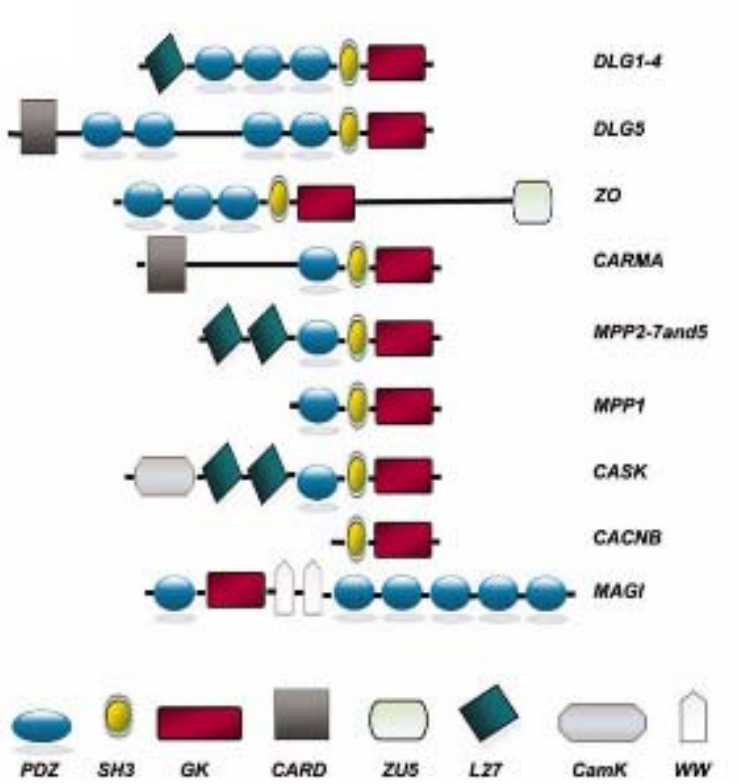

Figure 2.8 ***MAGUK protein subfamilies according to their domain structure.***
(Oliva *et al*., 2011)

MAGUK Subfamily	Vertebrate Proteins (alternative name)
MPP1	MPP1 (P55)
MPP2-7	MPP2 (DLG2), MPP3 (DLG3), MPP4 (DLG6), MPP7
MPP5	MMP5 (PALS1)
DLG	DLG1 (SAP-97), DLG2 (PSD-93), DLG3 (SAP-102, NE-Dlg), DLG4 (PSD-95)
DLG5	DLG5
ZO	TJP1-3 (ZO1-3)
CASK	CASK
CARMA	CARD11 (CARMA2), CARD10 (CARMA3), CARD14 (CARMA2)
MAGI	MAGI
CACNB	Voltage-dependent L-type calcium channel β subunit

Table 2.1 MAGUK family proteins

Post-synaptic density protein-95 (PSD-95) and synapse-associated protein 97 (SAP97) belong to the DLG1-4 subfamily (Figure 2.8 [97]), and have been extensively studied in neurons. According to its name, PSD-95 is mainly expressed in the post-synaptic density (PSD), while SAP97 can be found in the presynaptic and axonal regions [104]. Both proteins have two isoforms: the α-isoforms have a shorter N-terminal that can be reversibly palmytoilated on cystein residues, allowing the association with lipid bilayers. β-isoforms on the other hand contain an N-terminal L27 domain (named after *C. elegans* scaffolding proteins Lin-2 and Lin-7 [105]) that promotes homo- and/or hetero-oligomerization with multiple proteins [106-108]. PSD-95 is expressed mostly in the α-isoform, while SAP97 can be found mainly in β-isoform (Figure 2.9 [97]). They both contain three type I PDZ (PSD-95/DLG/ZO1) domains in their N-terminal half, an src homology 3 (SH3) domain, and a guanylate kinase (GK)-like sequence (enzymatically inactive) at their C-terminal regions [109], as shown in Figure 2.8 and 2.9. PSD-95 and SAP97 have a high degree of sequence identity (73.6% amino acid sequence identity), the main difference between them lies in the so called HOOK region. This sequence is between the SH3 and GK domains, and is shorter in length in case of PSD-95. The PDZ domains are composed of approximately 100 amino acids, which can interact with several proteins through a specific C-terminal peptide motif (X-T/S-X-V/I) of the target protein, including receptors and ion channels [110-112]. The purpose of this interaction appears to be the regulation of receptor/ion channel clustering at synaptic sites. On the other hand, it is possible that PSD-95 and SAP97 are also key elements in intracellular signaling. Various proteins, including the guanylate-kinase-associated protein (GKAP) have been shown to interact with the GK-domain of DLG proteins [113], implying that they could

play a role in creating a scaffolding complex by anchoring different signaling proteins, thus keeping them at close proximity at specific sites.

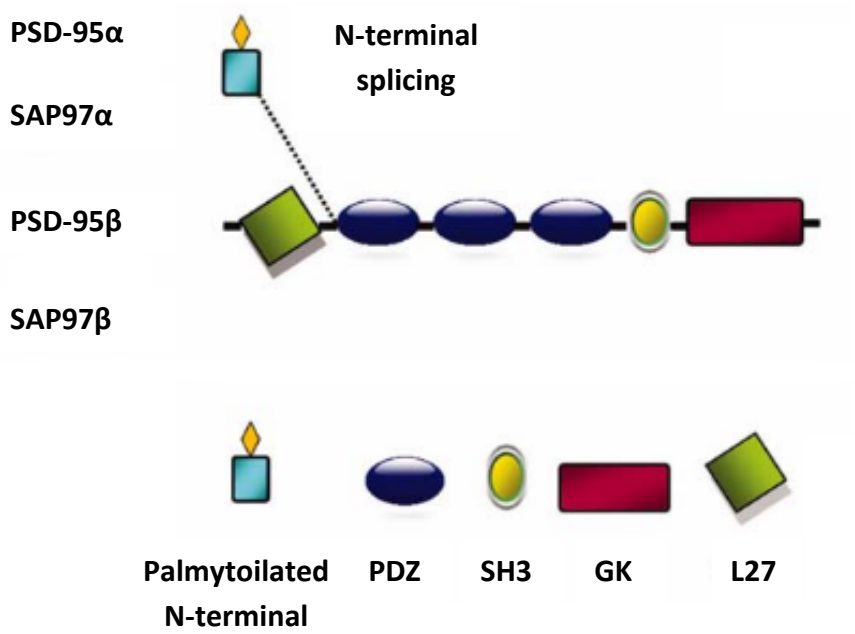

Figure 2.9 ***Splice variants of PSD-95 and SAP97 proteins.***
PSD-95 is mainly expressed in the α-isoform, which enables reversible palmytoilation as opposed to SAP97 of which the β-isoform is more abundant (Oliva *et al*., 2011).

2.4.1 Voltage-gated potassium channels and DLG proteins

As mentioned previously, DLG proteins, including PSD-95 and SAP97 interact with various ion channels, such as voltage-gated potassium channels in neurons [114]. By the means of yeast two-hybrid system, Kim and colleagues showed that a *Shaker*-type potassium channel, Kv1.4, interacts with PSD-95 and SAP97, and this interaction occurs through the first two PDZ motifs of the scaffolding proteins. They also revealed that the last 11 amino acids of the channel are sufficient, but the last 4 amino acids are essential for the interaction of the channel with PSD-95. The last three amino acids (TDV) of Shaker-type potassium channels appear to be highly conserved, and they found that both PSD-95 and SAP97 bound to Kv1.1, Kv1.2 and Kv1.3. This suggests the importance of the TDV sequence in the interaction, which was confirmed by mutational analysis. PSD-95 interaction with Kv1.4 was abolished upon the substitution of threonin to alanin (TDV→ADV), or of valine to alanine or glutamate (TDV→TDA/TDE) [114]. They also found that PSD-95 appears in the cytoplasm, while Kv1.4 is located diffusely on the cell surface of COS7 cells, when expressed separately. However, the co-expression of the two proteins resulted in their co-localization in irregular membrane-patches on the cell surface. Interestingly, co-expression of Kv1.4 with SAP97 (which when expressed by itself also shows cytoplasmic distribution) resulted in their co-localization not at the plasma membrane, but in intracellular aggregates [115]. Later it was shown, that when expressed in COS1 cells, PSD-95 is predominantly at the cell periphery, while SAP97 shows perinuclear localization [116]. This dissimilarity may be due to the difference in isoform expression: as mentioned before, PSD-95 can be found mainly in the α-isoform, containing two cystein residues as targets for palmytoilation that may result in the association with membranes. In contrast, the abundant β-isoform of SAP97 lacks these residues, which could explain the perinuclear localization. Because PSD-95 is originally present close to the plasma membrane, it is possible that it anchors various Kv channels to the plasma membrane, rather than mediates their intracellular trafficking. The same applies for SAP97, except that this scaffolding protein may be responsible for the retention of the voltage gated potassium channels to the endoplasmic reticulum. All these imply that PSD-95 and SAP97 could both have an important role in ion channel clustering and distribution in neurons.

Kv1.3 also interacts with both PSD-95 and SAP97, and interestingly both scaffolding proteins are expressed in murine T cells [84, 117]. However it must be mentioned, that it has not been shown so far if this interaction occurs through the C-terminal, PDZ binding domain

of the channel. Because Kv1.3 has SH3 binding domains on its N- and C-terminal as well, the possibility that PSD-95 and/or SAP97 bind to the channel through this domain cannot be completely ruled out either. Taken together, it is an intriguing question whether these scaffolding proteins are also expressed in human T cells, where they could potentially affect ion channel (e.g. Kv1.3) clustering and distribution especially during immunological synapse formation, somewhat analogous to neuronal synapses.

3. AIMS OF THE STUDY

As mentioned previously, voltage-gated ion channels play an important role in the regulation of different immune cells, and thus in immune response in general. Nav1.7 channels have been shown to influence several neuronal functions, but their existence has also been described in immune, specifically dendritic cells. However, the question that which DC functions could be regulated by this channel has not been addressed so far. According to this, in the first part of our study we had the following objectives:

Investigating the expression and function of Nav1.7 channels in immature dendritic cells:

- Is the Nav1.7 expression dendritic cell subtype specific?
- Is this channel functional in DC?
- What DC functions may be affected by the channel?

Kv1.3 channels regulate the membrane potential of T cells where they relocate to the immunological synapse during antigen presentation, but how and why this translocation occurs is unknown. Several scaffolding proteins have been shown to affect the cellular localization of various voltage-gated potassium channels in neurons, but the presence and possible effect of these proteins on ion channels in immune cells still needs to be elucidated. Based on this, the aims of the second part of our study were as follows:

Addressing the question of how Kv1.3 channels redistribute to the immunological synapse:

- Do human T cells express PSD-95 and SAP97?
- Do these proteins interact with Kv1.3, and if yes, through which region of the channel protein?
- Does the binding site removal of Kv1.3 or the knock-down of PSD-95 or SAP97 affect the redistribution of the ion channel during immunological synapse formation?

4. MATERIALS AND METHODS

4.1 Reagents

All reagents were purchased from Sigma-Aldrich (St. Louis, MO, USA), unless stated otherwise.

4.2 Buffers, solutions

4.2.1 Buffers, solutions for molecular biology

1xTAE: 4 mM Tris, 0.1 mM EDTA, 0.114% acetic acid, pH 8.5

2xYT: 16 g/l trypton, 10 g/l yeast extract, 5g/l NaCl, pH 7,0

5xSDS sample buffer: 50% glycerin, 10% SDS, 310 mM Tris, 100 mM DTT, 0.01% bromophenol blue

Blotting buffer: 25 mM Tris, 192 mM glycine, 0.285 mM SDS

LB (Luria-Bertani) agar: 10 g/l tryptone, 5 g/l yeast extract, 10 g/l NaCl, 1.5% agar, pH 7.0

LB medium: 10 g/l tryptone, 5 g/l yeast extract, 10 g/l NaCl, pH 7.0

PBS: 20 mM Na_2HPO_4, 115 mM NaCl, pH 7.4

SOB medium: 20 g/l bacto-tryptone, 5 g/l bacto-yeast extract, 10 mM NaCl, 2.5 mM KCl

SOC: 20 g/l tryptone, 2g/l yeast extract, 0.6 g/l NaCl, 10 mM $MgCl_2$, 10 mM $MgSO_4$, 20 mM glucose, pH 7.0

Transformation buffer: 10 mM HEPES, 55 mM $MnCl_2$, 15 mM $CaCl_2$, 250 mM KCl, pH 6.7

TBS: 25 mM Tris-HCl, 150 mM NaCl, pH 7.5

TBST: 25 mM Tris-HCl, 150 mM NaCl, 0.1% Tween-20, pH 7.5

Transfer buffer: 120 mM Tris-HCl, 40 mM glycine, 20 v/v% methanol

4.2.2 Buffers, solutions for patch clamping

Normal bath solution (in mM): 145 NaCl, 5 KCl, 1 $MgCl_2$, 2.5 $CaCl_2$, 5.5 glucose and 10 HEPES (pH 7.35, 305 mOsm)

Na^+-free bath solution (in mM): 145 choline-Cl, 5 KCl, 1 $MgCl_2$, 2.5 $CaCl_2$, 5.5 glucose, 10 HEPES (pH 7.35, 305 mOsm)

High K^+ bath solution (in mM): 150 KCl, 1 $MgCl_2$, 2.5 $CaCl_2$, 5.5 glucose, 10 HEPES (pH 7.35, 305 mOsm)

Pipette solution (in mM): 140 KF, 5 mM NaCl, 11 K_2EGTA, 1 $CaCl_2$, 2 $MgCl_2$, and 10 HEPES (pH 7.20, ~295 mOsm)

Pipette solution in perforated-patch mode (in mM): 150 KCl, 2 $MgCl_2$, 1 $CaCl_2$, 5 HEPES, 10 EGTA (pH 7.2) and 0.3 g/l Nystatin

Pipette solution for IKCa1 current measurements (in mM): 150 KCl, 5 HEPES, 10 EGTA, 8.7 $CaCl_2$, 2 $MgCl_2$, (pH 7.2, free Ca^{2+} was app. 1 μM)

4.3 Dendritic cells and cell culture

Human monocyte-derived DCs were generated from $CD14^+$ blood monocytes at the Department of Immunology, where the phenotypic characterization and sorting of the dendritic cells were performed as well.

The composition of the activating cytokine cocktail was the following: 10 ng/ml TNF-α, 5 ng/ml IL-1β, 20 ng/ml IL-6, 75 ng/ml GM-CSF, 1 μg/ml prostaglandin E2 (PGE2).

Jurkat and Raji cells (ATCC, Germany) were cultured in RPMI solution supplemented with 10% FBS, L-glutamine (2 mM), Penicillin (100 unit/liter) and Streptomycin (100 mg/liter). HEK-293T (human embryonic kidney-293.T), tsA-201 and CHO (chinese hamster ovary) cells (ATCC, Germany) were cultured in DMEM medium, which also contained 10% FBS, L-glutamine (2 mM), Penicillin (100 unit/liter) and Streptomycin (100 mg/liter). Cells were maintained at 37°C in a humidified atmosphere of 5% of CO_2 and 95% air. Cells were passaged every 2-3 days.

4.4 Reverse transcription (RT) and polymerase chain reaction (PCR)

Total RNA was isolated from approximately 5×10^6 Jurkat cells with an RNA isolation kit (GenElute Mammalian Total RNA Miniprep Kit). Reverse transcription was performed with Revert Aid H Minus enzyme using the First Strand cDNA Synthesis Kit (Fermentas, Biocenter Ltd., Hungary). Coding sequences were amplified using 0.002 units of Phusion High-Fidelity Polymerase (Thermo Fisher Scientific, Inc., Waltham). The following forward and reverse primers were applied, respectively: for PSD-95: 5'-

CTAGAAGCCCCAGGATATGAGTTGC and 5'-CTGTCACTCAGGTAGGCATTGCTGG, for SAP97: 5'-AGATTTCCAGCCTTCCAAGCTCTAC and 5'-GCTGATTTC CAACACCTCCAGCAAT (Bio-Science Ltd., Hungary), and sequence identities were verified at the Debrecen Clinical Genomics Center.

Q-PCR experiments for the quantification of Nav1.7 gene expression were carried out at the Department of Immunology.

4.5 Plasmids, cloning

PSD-95 and SAP97 containing plasmids were obtained from Prof. J.S. Trimmer, University of California. The various Kv1.3 channels containing a monomeric green fluorescent protein (mGFP) N-terminal tag (wild type (WT) and ΔC mutant (last 94 amino acids deleted)) were subcloned into the retroviral pBMN-LacZ vector (from Nolan's Lab).

4.5.1 Agarose gel electrophoresis

DNA fragments were separated in 1% agarose gels. Agarose was dissolved in 1xTAE by heating and ethidium bromide was added to visualize the DNA. Samples were mixed with 6x DNA loading buffer (Promega Corporation, USA), loaded into the gel and the DNA fragments were separated at 100V in 1xTAE buffer. Fragments were cut out on an UV illuminator table.

4.5.2 DNA extraction from agarose gel

DNA was purified from the agarose gel using phenol extraction method [118]. DNAse and RNAse free water was used for elution, the purity and concentration of the DNA was measured by NanoDrop 2000 Spectrophotometer (Thermo Fisher Scientific, Inc., Waltham).

4.5.3 Restriction digestion

HindIII and NotI restriction enzymes (Thermo Fisher Scientific, Inc., Waltham, USA) were employed. The amounts of restriction enzymes used were kept lower than 10% of the total reaction volume (between 2.5-5 units). Recognition sites of the enzymes are as follows:
HindIII: 5' A↓AGCTT 3'

NotI: 5' GC↓GGCCGC 3'

4.5.4 Ligation

During ligation the vector:insert molar ratio was 1:5. Five units of T4 DNA Ligase (Thermo Fisher Scientific, Inc., Waltham) were applied in each reaction. Ligation was performed at room temperature, for 1 hour.

4.5.5 Competent cell preparation

A single colony of *E. coli (JM109, DH5α)* was inoculated into 250 ml SOB medium containing $MgCl_2$. The culture was grown at 18°C with shaking at 200-250 rpm until OD_{600} reached 0.6, after which the culture was put on ice for 10 min. This was followed by centrifugation at 4°C with 2500*g* for 10 min. Cells were resuspended in 80 ml of ice cold TB buffer and centrifuged again (2500*g* for 10 min). Cells were then resuspended in 20 ml of ice cold TB buffer containing 7% DMSO. After this the bacteria were kept in an ice cold water bath for 10 minutes. Finally 200 µl aliquots were made and stored at -80°C [119].

4.5.6 Transformation

Plasmids were added to 200 µl competent cells thawed on ice. After 20 min incubation on ice, 50-60 seconds heat shock was applied (42°C), then cells were replaced on ice for at least 2 min. 800µl SOC medium was added to the samples which were then cultured at 180 rpm and 37°C for 50 min. After that bacteria were spread onto LB agar containing 100 µg/ml ampicillin. Controls were spread onto LB agar with and without the antibiotic. Plates were incubated overnight, at 37°C.

4.5.7 Plasmid preparation

A single colony of plasmid containing bacteria was inoculated into LB medium containing antibiotic and was grown at 37°C, 180 rpm overnight. PureYield Plasmid Miniprep System (Promega Corporation, USA) was used to purify plasmid DNA. For larger scale plasmid preparation, the overnight culture was diluted 1:100 and further grown overnight and PureYield Plasmid Maxiprep System (Promega Corporation, USA) was applied.

4.6 Transfection of plasmids and small interfering RNA

To express PSD-95 and SAP97 in tsA-201 cells 2 µg DNA/10 µl Lipofectamine 2000 reagent (Invitrogen Corporation, Carlsbad, CA, USA) was mixed and added to the 35 mm

petri dishes containing cells at ≈80% confluency according to the manufacturer's instruction. Cells were used for further experiments 24 hours later.

The mix of three different constructs of Nav1.7-specific and control small interfering RNA (Applied Biosystems) was transfected into differentiating IDC on day three at a final concentration of 1 pM using the GenePulser X Cell electroporator and 0.4-cm cuvettes (Bio-Rad Laboratories, Hercules, CA, USA). Two days after the transfection the level of Nav1.7 mRNA expression was tested by Q-PCR.

4.7 SDS-PAGE and Western blotting

Protein samples were separated by 10-12% SDS-PAGE and transferred to PVDF membranes (Millipore, Billerica, MA) after electrophoresis. The membranes were blocked with milk powder, and immunoblotted with mouse-anti-PSD-95, mouse-anti-SAP97 (Antibodies Incorporated, Davis, CA) or rabbit-anti-actin primary and anti-mouse IgG HRP-linked or anti-rabbit IgG HRP-linked secondary antibodies (Cell Signaling Technology, Inc., Beverly, MA), respectively. Blots were developed with ECL reagent (Thermo Scientific Inc., Vantaa, Finland).

4.8 GST pull-down assay

Escherichia coli BL21 transformed with pGEX-4T-2 containing glutathione S-transferase (GST) (obtained from the Department of Chemistry) or pGEX-4T-2 containing the N-terminal or C-terminal coding DNA sequence (N-terminal: first 184, C-terminal: last 94 amino acids) of Kv1.3 (from *KCNA3* gene, accession number: NM_002232) fused with GST were induced with 1 mM isopropyl β-D-thiogalactoside and grown at room temperature with shaking for 2 hours. Cells were harvested by centrifugation, sonicated in lysis buffer (50 mM Tris-HCl (pH 7.5), 0.1 % Tween 20, 0.2 % 2-mercaptoethanol, Protease Inhibitor Cocktail Set III (Calbiochem, Darmstadt, Germany)), and proteins were isolated by affinity chromatography on GST SpinTrap Purification Module (GE Healthcare, Piscataway, NJ) according to the manufacturer's protocol. Jurkat cells were washed twice with 1x ice-cold PBS and lysed with sonication in lysis buffer. The Jurkat cell lysates were incubated with the Sepharose-bead-immobilized fusion proteins (GST, GST-Kv1.3-N-terminus, or GST-Kv1.3-C-terminus) overnight at 4°C. The beads were washed two times with 1x PBS and afterwards the GST fusion proteins were eluted with 10 mM gluthatione. Elutes were tested for protein expression by SDS-PAGE and specific protein expression was confirmed by Western blotting (see above, section 4.2).

4.9 Viral infection

Transduction protocol for CHO and Jurkat cells was obtained from the Nolan lab web page (http://www.stanford.edu/group/nolan/). The main steps are shown in section 4.9.1.

4.9.1 Retroviral transduction

HEK 293.T cells plated the previous day were transfected with the following plasmids using calcium phosphate transfection method: 17 µg plasmid of interest (pBMN-Z plasmid (Figure 4.1), containing the appropriate insert), 12 µg VSVG and 4 µg PAX2 (latter two are helper plasmids). Also, 25µM chloroquine was added to the cells to aid transfection. Cells were then incubated for 4-6 hours at 37°C, after which the transfection medium was replaced with fresh DMEM. Cells were then kept at normal culturing conditions. 48 hours after the transfection the supernatant was collected from the cells and filtered with a 0.45 micron filter. Half of this supernatant was added to the target (Jurkat/CHO) cells along with 10µg/ml polybrene to increase the infection efficiency. Jurkats or CHO cells were then incubated for one day, then the original supernatant was removed and replaced with the second half of the viral supernatant, also adding polybrene (boosting). 4-6 hours later all supernatant was removed from the cells which were carefully and thoroughly washed and resuspended in appropriate cell culture medium.

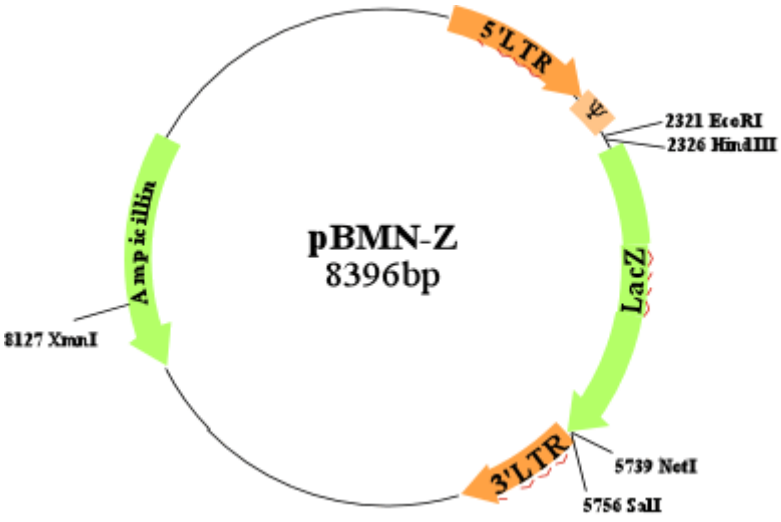

Figure 4.1 ***Map of pBMN-LacZ plasmid.***
(Obtained from the Addgene webpage.)

4.9.2. Lentiviral knockdown of PSD-95 and SAP97

PSD-95 or SAP97 knockdown cells were obtained using the same viral transduction protocol using Mission shRNA by Sigma-Aldrich, except that different plasmids were used: 10 µg plasmid of interest (pLKO.1-puro plasmid (Figure 4.2) containing the appropriate insert), 5 µg MDL, 2.5 µg MD2G and 2.5 µg RSV (latter three are helper plasmids). Two different shRNA sequences were tested for both targets, which were the following: for PSD-95: CCGGACGAGAGTGGTCAAGGTTAAACTCGAGTTTAACCTTGACCACTCTCGTTTTTTG and CCGGACGATCATCGCTCAGTATAAACTCGAGTTTATACTGAGCGATGATCGTTTTTTG, for SAP97: CCGGCGGGTCAATGACTGTATATTACTCGAGTAATATACAGTCATTGACCCGTTTTT and CCGGCCCACAAGTATGTATATGAATCTCGAGATTCATATACATACTTGTGGGTTTTT. Knockdown cells were selected with 3 µg/ml puromycin.

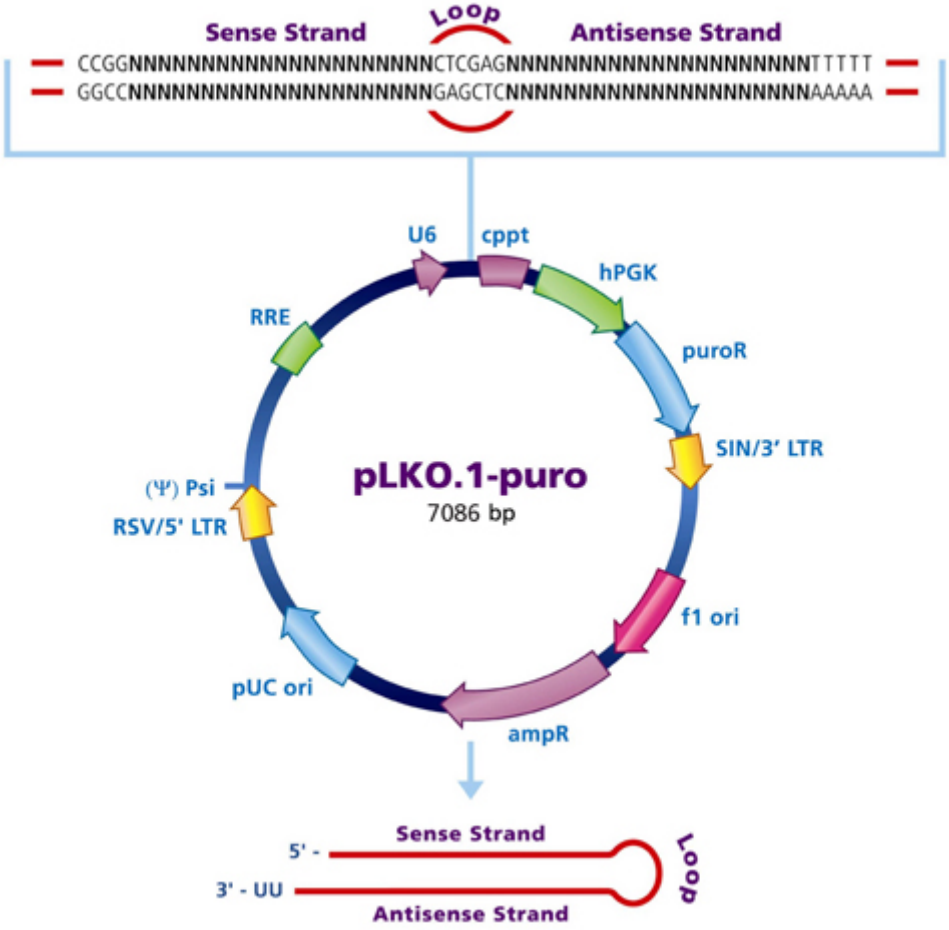

Figure 4.2 ***Map of pLKO.1-puro plasmid.***
(Obtained from the Sigma-Aldrich webpage.)

4.10 Immunological synapse formation and immunofluorescence

The Jurkat T cell line is specific for *Staphylococcus* enterotoxin E (SEE, Toxin Technologies, Sarasota, FL, USA). The B cell lymphoma Raji cells were used as APCs. Raji cells were pulsed with 10 μg/ml *Staphylococcus* enterotoxin E (SEE) for 30 min. Cell conjugates were formed by mixing Jurkat cells with Raji cells at a 1:1 ratio, and co-centrifugating them at 200 g for 1 min at 37°C. The mixtures were plated on poly-L-lysine coated coverslips and were incubated for 1, 5, 10, 20 or 30 min at 37°C in a humidified atmosphere of 5% of CO_2 and 95% air, and were then put on ice for labeling. The cells were washed once with 1×TBS, and fixed with 2% paraformaldehyde in 1 x TBS for 10 min. Between each step, the cells were rinsed three times with 1 x TBS. Cells were labeled with primary CD3 antibody (Invitrogen Corporation, Carlsbad, CA, USA) followed by the appropriate secondary antibody (Alexa Fluor 647, GAMIG, Invitrogen Corporation, Carlsbad, CA, USA). Both antibodies were diluted in 1×TBS containing 1% BSA and incubated with the cells for 30 min. Coverslips were rinsed and mounted in Mowiol Antifade.

4.11 Confocal microscopy and evaluation

Confocal images were taken using Olympus FV1000 confocal microscope (the thickness of the slices were app. 1 μm). For excitation of mGFP the line 488 nm of Ar-ion laser, for Alexa 647 the line 633 nm of He-Ne laser was used and emitted light was detected through 505-550 nm bandpass and 650 nm longpass filters, respectively. To quantify the accumulation of Kv1.3 channels in the IS (judged by the CD3 polarization in the contact area of the T cell and the B cell) we used the following expression (accumulation ratio, AR):

$$AR = \frac{\left(I_{IS} - I_{BG}\right) \cdot AREA_{IS}}{\frac{(I_{outside} - I_{BG}) \cdot AREA_{outside} - (I_{inside} - I_{BG}) \cdot AREA_{inside}}{AREA_{outside} - AREA_{inside}}}$$

,where I_{IS}, $I_{outside}$, I_{inside} and I_{BG} is the mean fluorescent intensity of mGFP (Kv1.3 channels) in the IS, outside the cell (including the membrane and intracellular region), inside the cell (only intracellular region) and background intensity detected at a cell-free area of the image, respectively. $AREA_i$ denotes the area of the described sections (Figure 4.3). The regions of interest were always selected according to the extracellular CD3 labeling to ensure the neglect

of possible intracellular mGFP-Kv1.3 signals. For analysis MacBiophotonics ImageJ software was used. A cell was regarded Kv1.3 polarized if the value of AR was higher than 1.5.

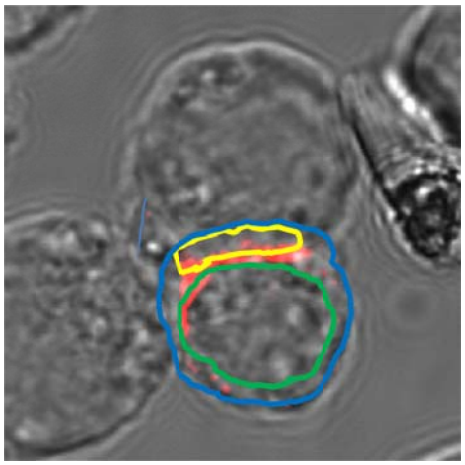

I_{IS} and $AREA_{IS}$: mean intensity and area of the IS

$I_{outside}$: mean intensity in the whole cell

I_{inside}: mean intensity in the cytosol of cell

$AREA_{membrane} = AREA_{outside} - AREA_{inside}$

I_{BG}: mean background intensity

4.12 Electrophysiology

4.12.1 Patch-clamping of dendritic cells

Standard whole-cell patch-clamp techniques were used in voltage-clamp (current detection) or current-clamp (membrane potential measurement) configuration, as described previously ([120]). All electrophysiological measurements were performed at room temperature (approximately 21-22 °C). Whole-cell measurements were carried out using Multiclamp 700B and Axopatch-200A amplifiers connected to personal computers using Axon Instruments Digidata 1440 or 1320 data acquisition boards (Molecular Devices, Sunnyvale, CA). For data acquisition and analysis the pClamp9 and 10 software packages (Molecular Devices, Sunnyvale, CA) were used. Pipettes were pulled from GC 150 F-15 borosilicate glass capillaries (Clark Biomedical Instruments, Pangboume, UK) in five stages and fire-polished to gain electrodes of 2-MΩ resistance in the bath. Series resistance compensation up to 85% was used to minimize voltage errors and achieve good voltage clamp conditions (V_{err}<5mV). $CD1a^+$ cells were visualized by anti-CD1a-FITC for patch-clamp recordings in a Nikon TE2000 fluorescence microscope.

Determination of IKCa1 channel numbers.

The whole-cell current was evoked by voltage-ramps and the magnitude of the current was measured at -85 mV (I_{-85}) and at -120 mV (I_{-120}). Since the reversal potential for K^+ is approximately -85 mV (E_K), calculated from the composition of the pipette and the normal bath solution using the Nernst equation, the current at this voltage is purely the leak current. In contrast, the current measured at -120 mV consists of the IKCa1 current and the leak. Because the leak current reverses at 0 mV and has linear current-voltage relationship, its value can be calculated at -120 mV using the formula: $I_{leak}(@\text{-}120mV)=\text{-}120/\text{-}85\times I_{-85}$, and can be subtracted from the whole-cell current measured at -120 mV to give the pure IKCa1 current at that voltage [$I_{IKCa1}(@\text{-}120mV)$]. Furthermore, the IKCa1 current does not show time- and voltage-dependent activation (current-voltage relationship is linear), hence the whole-cell conductance for IDC expressing only IKCal channels can be calculated: $G=I_{IKCa1}(@\text{-}120mV)/(\text{-}120\ mV\text{-}E_K)$ (where $I_{IKCa1}(@\text{-}120mV)$ is the current of IKCa1 channels at -120 mV and E_K is the reversal for K^+). The single channel conductivity of IKCa1 was determined earlier (γ=11 pS) ([121]), thus the number of channels in a cell is: $N=G/\gamma$.

Test substances.

Toxins (TTX, charybdotoxin: ChTx; Alomone Laboratories) were dissolved in bath solution supplemented with 0.1 mg/ml BSA to prevent nonspecific binding of the toxins to the plastic wall. TRAM-34 was dissolved in DMSO. Bath perfusion around the measured cell with different test solutions was achieved using a gravity-flow perfusion setup with 6 input lines and PE10 polyethylene tube output tip having flanged aperture to reduce the turbulence of the flow. Excess fluid was removed continuously.

4.12.2 Patch-clamping of Jurkat and CHO cells

Patch-clamp measurements were carried out using Axopatch-200B amplifiers connected to personal computers using Axon Instruments Digidata 1440 or 1322A data acquisition boards. For data acquisition and analysis the pClamp9 and the pClamp10 software package (Molecular Devices, Sunnyvale, CA) were used. Standard outside-out (CHO cells) or whole-cell (Jurkat cells) patch-clamp technique was used. Pipettes were pulled from GC 150 F-15 borosilicate glass capillaries (Clark Biomedical Instruments, UK) in four stages and fire-polished to give electrodes 4-5 MΩ resistance in the bath. Series resistance compensation up to 85% was used to minimize voltage errors and achieve good voltage clamp conditions in whole-cell configuration, and the P/5 protocol for online leaks subtraction was applied to minimize capacitance and leak errors during the determination of the activation kinetics.

The activation kinetics of the current was characterized by fitting the Hodgkin-Huxley (HH) model ($I(t) = I_a \times (1-\exp(-t/\tau_a))^4 + C$ where I_a is the amplitude of the activating current component; τ_a is the activation time constant of the current; C: constant) to the rising phase of the current traces evoked by 15-ms-long depolarizations to +50 mV. The activation time constant characteristic of a given cell was determined as the average of the time constants obtained upon three sequential depolarizations repeated every 15 s.

The inactivation kinetics of the current was characterized by fitting a single exponential function ($I(t) = I_0 \times \exp(-t/\tau_{in}) + C$, I_0: amplitude of current, τ_{in}: inactivation time constant, C: steady-state value of whole-cell current at the end of the pulse) to the decaying part of the current traces evoked by 2-s-long depolarizations to +40 mV from a holding potential of −120 mV. The inactivation time constant for a given cell was determined as for τ_a, except pulses were delivered every 60 s.

The voltage-dependence of steady-state activation relationships were obtained as follows. The cells were held at −120 mV holding potential and depolarized to various test

potentials ranging from −70 up to +50 mV in 10 mV steps at every 30 s. Peak whole-cell conductance (G(V)) at each test potential was calculated from the peak current (I_p) at test potential V and the K^+ reversal potential (E_r= -85 mV) using $G(V)=I_p/(V-E_r)$. The G(V) values were normalized for the maximum conductance and plotted as a function of test potential and the Boltzmann-function was fitted to the data points: $G_N = 1/(1+\exp[-(V-V_{½})/k]$, where G_N is the normalized conductance, V is the test potential, $V_{½}$ is the midpoint and k is the slope of the function.

4.13 Statistical analysis

In case of dendritic cells statistical analysis and sample comparisons were made by unpaired t-test and the level of significance was set to 0.05. The mean and standard error of the mean (SEM) of at least 4 or more independent experiments are shown. Chi square test with Yates correction was used for correlation analysis.

For Jurkat cells statistical comparison was carried out using unpaired t-test and ANOVA at a significance level of 0.05. The unadjusted p values of Holm-Sidak post-hoc test are given. The values are given as mean ± SEM. The mean frequency of Kv1.3 polarized cells was determined as the average of the frequencies for independent samples consisting of at least 10 cell conjugates at a time point.

5. RESULTS

5.1 Nav1.7 maintains the membrane potential and regulates the cytokine production of a monocyte-derived immature dendritic cell subset

5.1.1 Nav1.7 is expressed predominantly in the CD1a$^+$ subpopulation of monocyte-derived immature dendritic cells

Our workgroup has shown previously that Nav1.7 channels are expressed by monocyte-derived IDC and their expression is down-regulated upon differentiation into mature DCs [1]. CD1a$^-$ and CD1a$^+$ IDC subsets have been characterized previously by distinct functional activities hence we compared the Nav1.7 expression of these immature DC subsets. We detected a robust inward, rapidly activating and inactivating Na^+ current in CD1a$^+$ IDC evoked by a 15 ms-long depolarization to 0 mV from a holding of -120 mV upon perfusion with normal EC solution (Figure 5.1A). The incidence of Na^+ current detection in CD1a$^-$ IDC was significantly less frequent than in CD1a$^+$ cells (Chi square test with Yates correction: CD1a$^+$ (n=25) and CD1a$^-$ (n=19), p=0.021). We also found a considerable difference in the Na^+ current density (CD) of CD1a$^-$ and CD1a$^+$ IDC (CD, peak current at 0 mV divided by the capacitance of the cell, a quantity proportional to the number of channels/unit membrane area): it was significantly higher in the CD1a$^+$ subset (CD_{CD1a+}=-83 ± 7.6 pA/pF, CD_{CD1a-}=-43 ± 13.4 pA/pF (n=9, p=0.015) (Figure 5.1B). Still, there was no difference in the cell membrane capacitance of the two DC subtypes (11.9 ± 1.5 pF and 13.5 ± 1.5 pF for CD1a$^+$ and CD1a$^-$ cells, respectively, n=9, p=0.457). In addition, according to Q-PCR measurements carried out at the Department of Immunology, the relative expression of Nav1.7 mRNA was also higher in the immature CD1a$^+$ than in the CD1a$^-$ subset, but this expression level dramatically decreased upon DC maturation (data not shown,[1]). These results indicated that the role of the Nav1.7 channels is closely connected to the immature state of DC and acts primarily in the CD1a$^+$ subset.

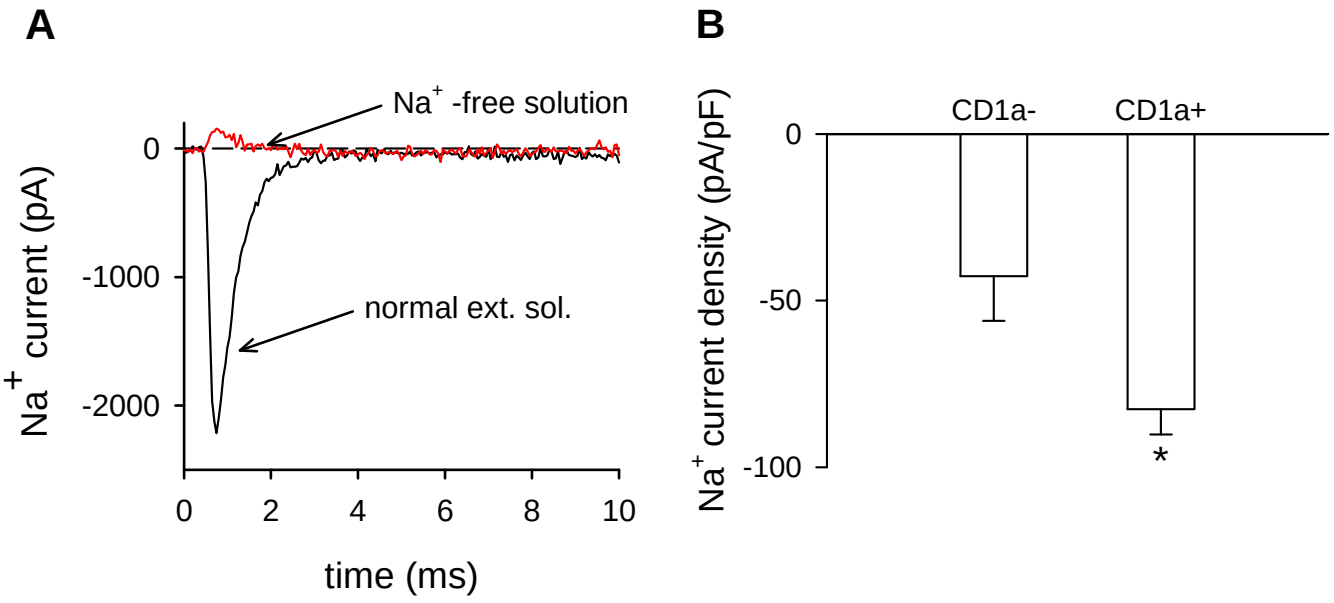

Figure 5.1 ***Expression levels of Nav1.7 in CD1a⁻ and CD1a⁺ IDC***.

A) Whole-cell Na^+ current in a $CD1a^+$ IDC recorded upon a 15 ms long depolarization to 0 mV from a holding potential of -120 mV. Arrows indicate the perfusion with normal and Na^+-free extracellular solutions. ***B)*** Current density of Nav1.7 channels in IDC. The peak Na^+-currents were determined at 0 mV and divided by the capacitance of the cell (measured in pF). This ratio was averaged for n=9 $CD1a^+$ and $CD1a^-$ cells, error bars indicate SEM, *: $p < 0.05$.

5.1.2 Intracellular Ca^{2+} elevation down-regulates the expression of Nav1.7

Several studies support the role of Ca^{2+} signaling in the activation of DC (reviewed in Ref. [122]) . Therefore, next we investigated whether sustained elevated Ca^{2+} concentration by itself could decrease Nav1.7 channel expression. Q-PCR measurements carried out at the Department of Immunology revealed that the elevation of intracellular Ca^{2+} concentration, induced either by the Ca^{2+} ionophore ionomycin or by the sarco(endo)plasmic reticulum Ca^{2+}-ATPase antagonist thapsigargin, was an effective inhibitor of Nav1.7 gene expression and had a comparable inhibitory capacity to that of an inflammatory cytokine cocktail (Figure 5.2A). Applying 5mM extracellular EGTA had no effect on the inhibition of Nav1.7 mRNA expression induced by the cytokine mix however it partially or completely reversed the ionomycin- and thapsigargin-induced Nav1.7 mRNA expression inhibition (Figure 5.2A).

To further verify the capability of intracellular Ca^{2+} elevation to down regulate Nav1.7 expression we examined the channel expression of $CD1a^+$ IDC after 24 h thapsigargin treatment using electrophysiology (Figure 5.2B). According to our expectations, the percentage of Nav1.7 expressing cells significantly decreased compared to the non-treated

cells, and this decrease was partially reversed by EGTA. These results suggest that the increase of intracellular Ca^{2+} level may trigger Nav1.7 channel down regulation.

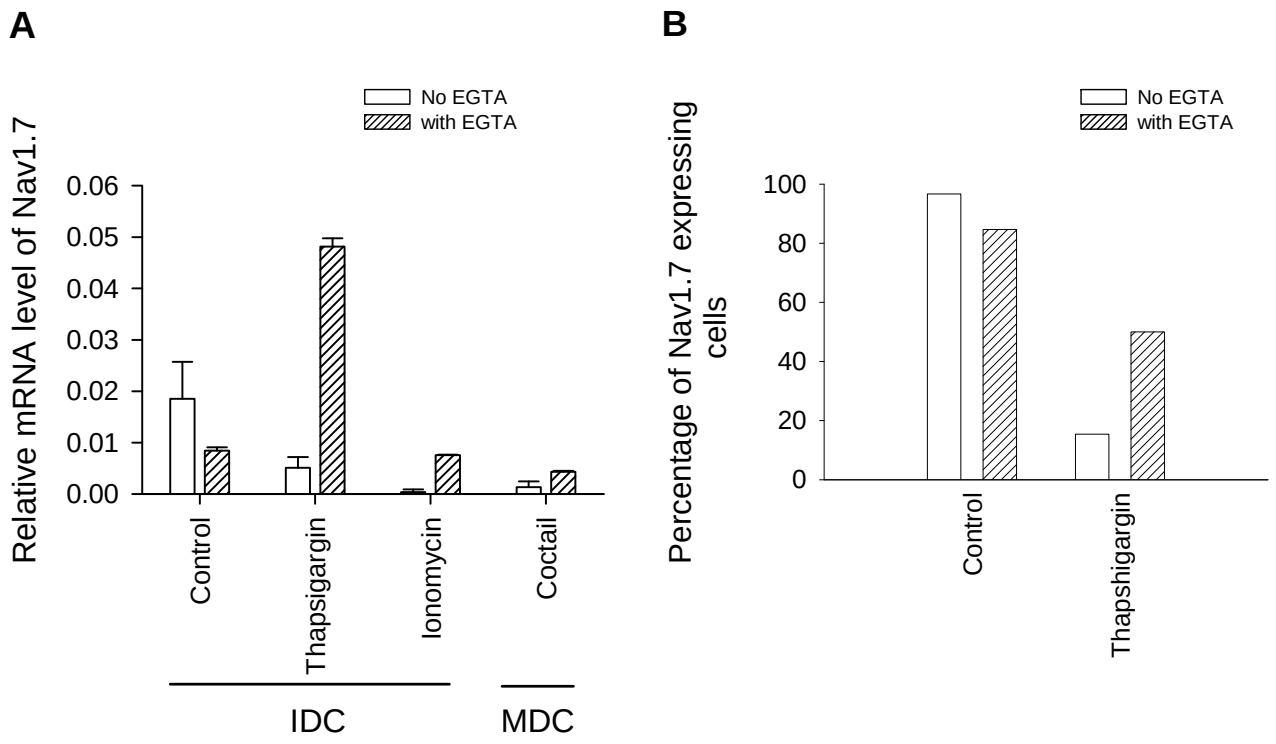

Figure 5.2 ***Effects of increased intracellular Ca^{2+} concentration on Nav1.7 gene expression in IDC.*** ***A)*** Nav1.7 gene expression in control IDC and in IDC treated with 250 nM thapsigargin, 180ng/ml ionomycin, or inflammatory mixture (cocktail) was measured with Q-PCR for 24 h in the absence (open bars) or the presence (hatched bars) of 5 mM EGTA and 10 mM $MgCl_2$. The expression level measured in MDC served as positive control (IDC samples treated with inflammatory cocktail). ***B)*** Percentage of Nav1.7 expressing $CD1a^+$ IDC in control and thapsigargin-treated cells in the absence (open bars) or presence (hatched bars) of EGTA. Cells were considered to express Nav1.7 if a characteristic inward current was recorded at 0 mV test potential and the peak current exceeded 100 pA. Statistical calculation was based on patch-clamp records from n > 13 in each group.

5.1.3 The membrane potential of $CD1a^+$ IDC is Nav1.7 channel dependant

Even though the exact role of VGSC in immune cells is still unknown, they are thought to contribute to the maintenance of the resting membrane potential. Therefore next we analyzed the membrane potential of both $CD1a^+$ and $CD1a^-$ IDC together with the corresponding MDC. Perforated whole-cell current-clamp measurements demonstrated that the resting membrane potential of $CD1a^+$ IDC is significantly depolarized (–8.7 ± 1.5 mV, n=14) as compared to $CD1a^-$ IDC or MDC (between -40 and -60 mV, with an average of -47

± 6.2 mV, n=7, Figure 5.3A). We surmised that the measured differences in membrane potential of the different cell types could be the result of the presence of functional Na^+ channels in $CD1a^+$ IDC. In order to test this hypothesis we determined the extracellular Na^+ sensitivity of the membrane potential in IDC. Transient exposure to a Na^+ free extracellular solution (which completely abolishes the inward Na^+ current in voltage-clamp experiments, see Figure 5.1A) hyperpolarized the membrane potential of $CD1a^+$ IDC to values close to those recorded in IDC and MDC of both $CD1a^-$ and $CD1a^+$ subtypes (Figure 5.3B). However, this Na^+ free extracellular solution had no effect on the membrane potential of $CD1a^-$ IDC (Figure 5.3C).

To further study the Nav1.7 dependence of the membrane potential, Nav1.7 gene silencing was carried out at the Department of Immunology using specific siRNA. Transfection of the Nav1.7-specific siRNA into IDC decreased the expression of Nav1.7 mRNA by ~60% (data not shown) and the number of Nav1.7 current-positive $CD1a^+$ IDC to 13% (87% inhibition) whereas 96% of $CD1a^+$ cells transfected with negative control siRNA remained positive for Na^+ current expression ($n \geq 20$ for control and *SCN9A* silenced cells). According to the current-clamp recordings the membrane potential of Nav1.7-specific siRNA-transfected $CD1a^+$ IDC were significantly more negative (-22.3 mV ± 1.5 mV (n=8) than in non-transfected $CD1a^+$ IDC ($p<0.001$, Figure 5.3A). In addition, there was no change in the membrane potential of *SCN9A* siRNA-transfected cells when exposed to a Na^+-free solution (Figure 5.3D), similarly to the behavior of $CD1a^-$ IDC lacking Nav1.7 channels (Figure 5.3C).

During the current-clamp measurements we also applied an extracellular high K^+ solution (150 mM K^+ concentration) in order to see whether it has an effect on the membrane potential of the different dendritic cell subtypes investigated (Figures 5.3B-D). Transient exposure of IDC to the solution depolarized the membrane potential to ~0 mV. This and the relatively negative membrane potential of $CD1a^-$ IDC (Figures 5.3A and C) suggested the presence of K^+ channels in the membrane. Since a previous study of our workgroup showed that IDC lack voltage-gated potassium channels [1], we assumed the presence of a non-voltage-gated K^+ channel in the membrane of IDC. Current traces recorded in $CD1a^-$ IDC upon a voltage-ramp protocol using a pipette solution containing 1 μM free Ca^{2+} are shown in Figure 5.4A. The biophysical and pharmacological properties of the current indicated the expression of IKCa1, a Ca^{2+}-activated K^+ channel: the current reversed at around -80 mV and could be blocked by 25 nM ChTx (K_d value for IKCa1 is ~5 nM) or with 125 nM TRAM-34, a selective antagonist of IKCa1 channels (K_d ~ 20-30 nM). The number of IKCa1

channels/cell was estimated for both the CD1a$^-$ and CD1a$^+$ IDC as detailed in the *Materials and methods*. We could not detect any significant difference between the two DC subsets (p=0.269) (Figure 5.4B). Therefore we concluded that the lack of IKCa1 channels cannot be responsible for the depolarized resting membrane potential of CD1a$^+$ IDC.

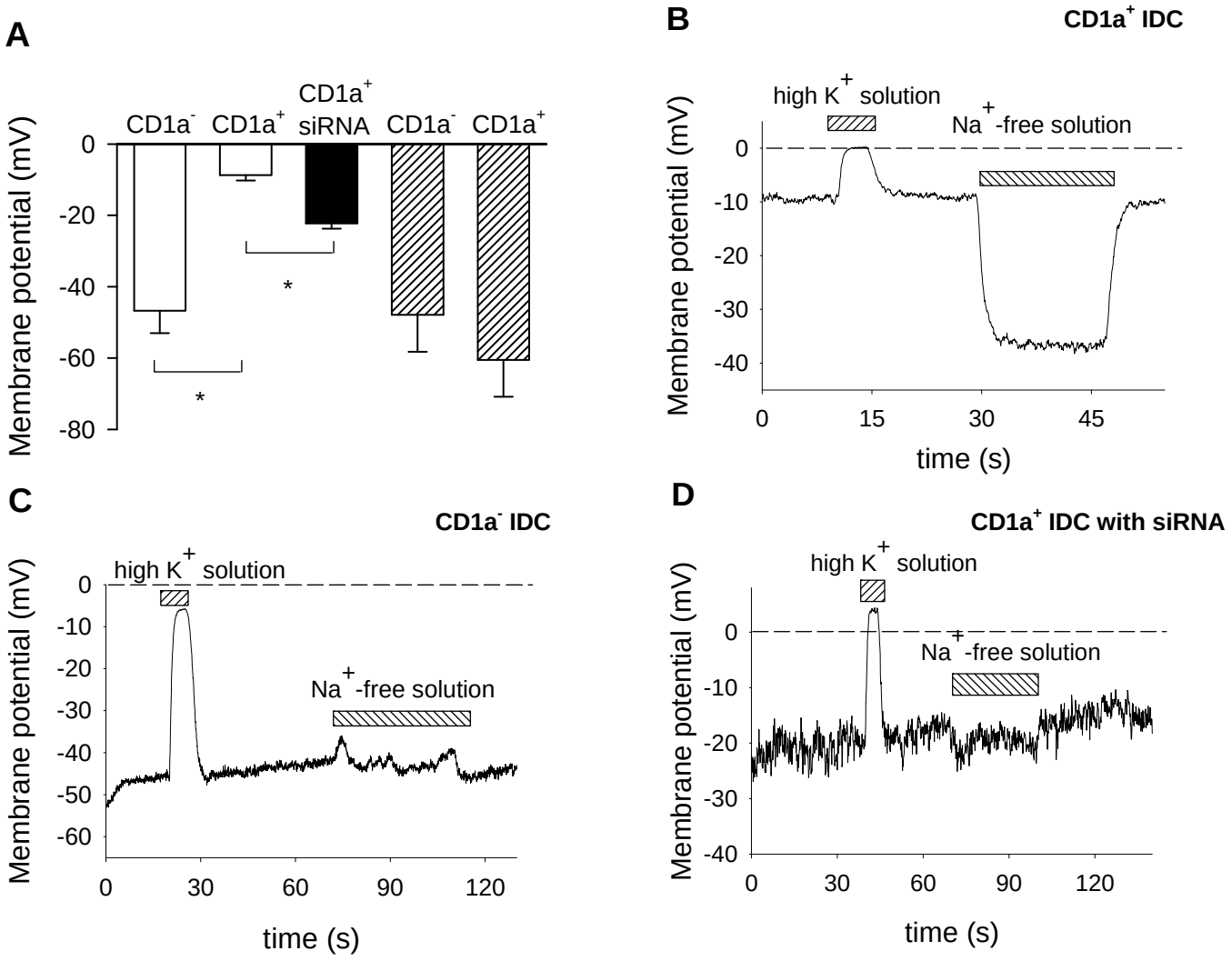

Figure 5.3 ***Membrane potential of CD1a$^+$ and CD1a$^-$ DC.***

Membrane potential of the cells was recorded in current-clamp configuration using perforated patch method. The holding current was 0 pA. CD1a$^+$ cells were identified in the patch-clamp microscope based on anti-CDa FITC fluorescent labeling. ***A)*** Membrane potential of CD1a$^-$ and CD1a$^+$ IDC (open bars), the corresponding MDC (hatched bars), and Nav1.7 siRNA transfected CD1a$^+$ IDC (filled bar) measured in normal extracellular solution. Errors indicate SEM for n > 7 cells measured in each group. *: $p < 0.05$. Membrane potential of a CD1a$^+$ ***(B)***, a CD1a$^-$ IDC ***(C)***, and a Nav1.7 siRNA transfected CD1a$^+$ IDC ***(D)***. Cells were perfused with normal extracellular solution, unless stated otherwise. The switch of the bath perfusion to a high K^+ bath solution (right-hatched bar, 150 mM K^+ concentration) or to a Na^+-free bath solution (left-hatched bar) is indicated by the horizontal bars. The dashed lines indicate the zero potential.

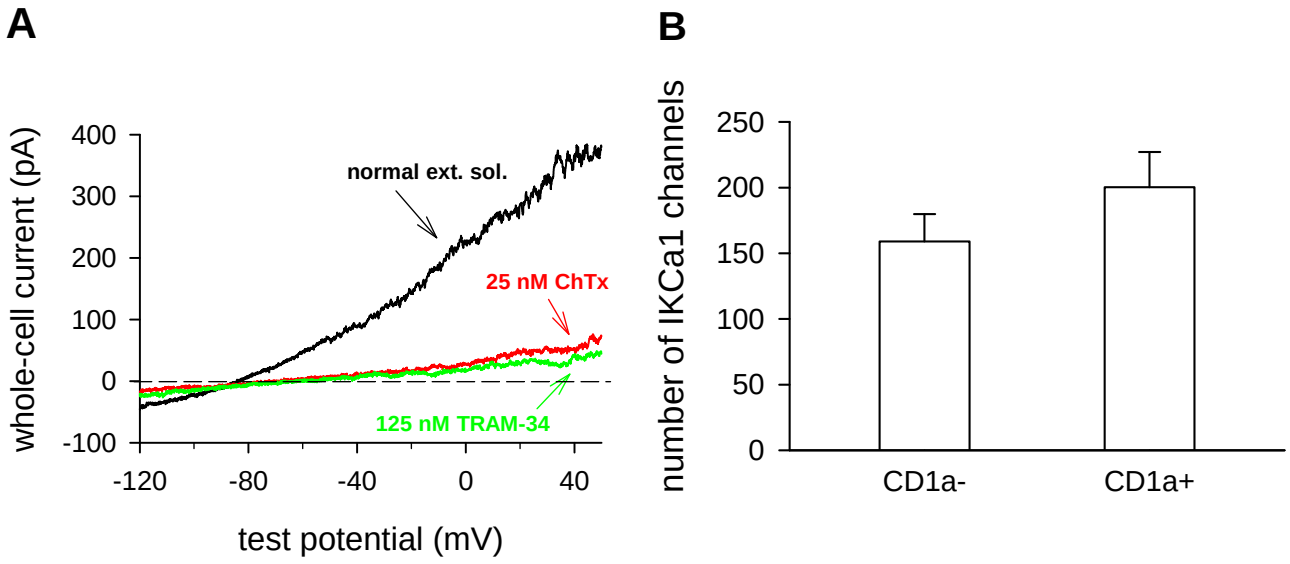

Figure 5.4 ***Expression and activity of the IKCa1/KCa3.1 channel in IDC.***

A) Whole-cell current recorded upon a voltage-ramp protocol in $CD1a^-$ IDC in normal extracellular solution during perfusion with ChTx or TRAM-34. The dashed line represents zero current level. ***B)*** The number of IKCa1 channels on $CD1a^+$ and $CD1a^-$ IDC was calculated as described in Materials and methods, n > 5, error bars indicate SEM.

5.1.4 Nav1.7 affects cytokine secretion of $CD1a^+$ IDC

Based on the literature that the inflammatory nature of monocyte-derived MDC can be attributed to the $CD1a^+$ subset [13], and our current finding that Nav1.7 channels are expressed primarily in this subpopulation of IDC, we hypothesized that the functional role of Nav1.7 in dendritic cells could be related to the maintenance of the immature state of the cells. Because of the elevated resting potential of $CD1a^+$ IDC (due to the Nav1.7 channels) they need a larger stimulus for activation than $CD1a^-$ IDC. 10-40 μM TTX was used to inhibit Nav1.7 channel function and to test its possible role in fine-tuning $CD1a^+$ IDC activation. According to our results the inhibition did not change the viability or the internalizing capacity of IDC (data not shown) nor did it affect the monocyte to IDC and the IDC to MDC differentiation pathway. On the other hand, CD83 expression was slightly elevated when cells were activated by optimal and suboptimal (10-fold dilution) concentrations of the inflammatory cocktail for a short (6h) period (24 ± 7% and 34 ± 23% at optimal and suboptimal concentrations, respectively, n=5), although statistically this effect was not significant (Figure 5.5A). A similar sensitizing effect of TTX treatment on IDC could be shown when the production of various IDC-derived cytokines was tested after activation by the cytokine cocktail. In these experiments IDC were treated with 40 μM TTX on day 2 and in combination with the cytokine cocktail on day 5. Following 6h of activation the excess of

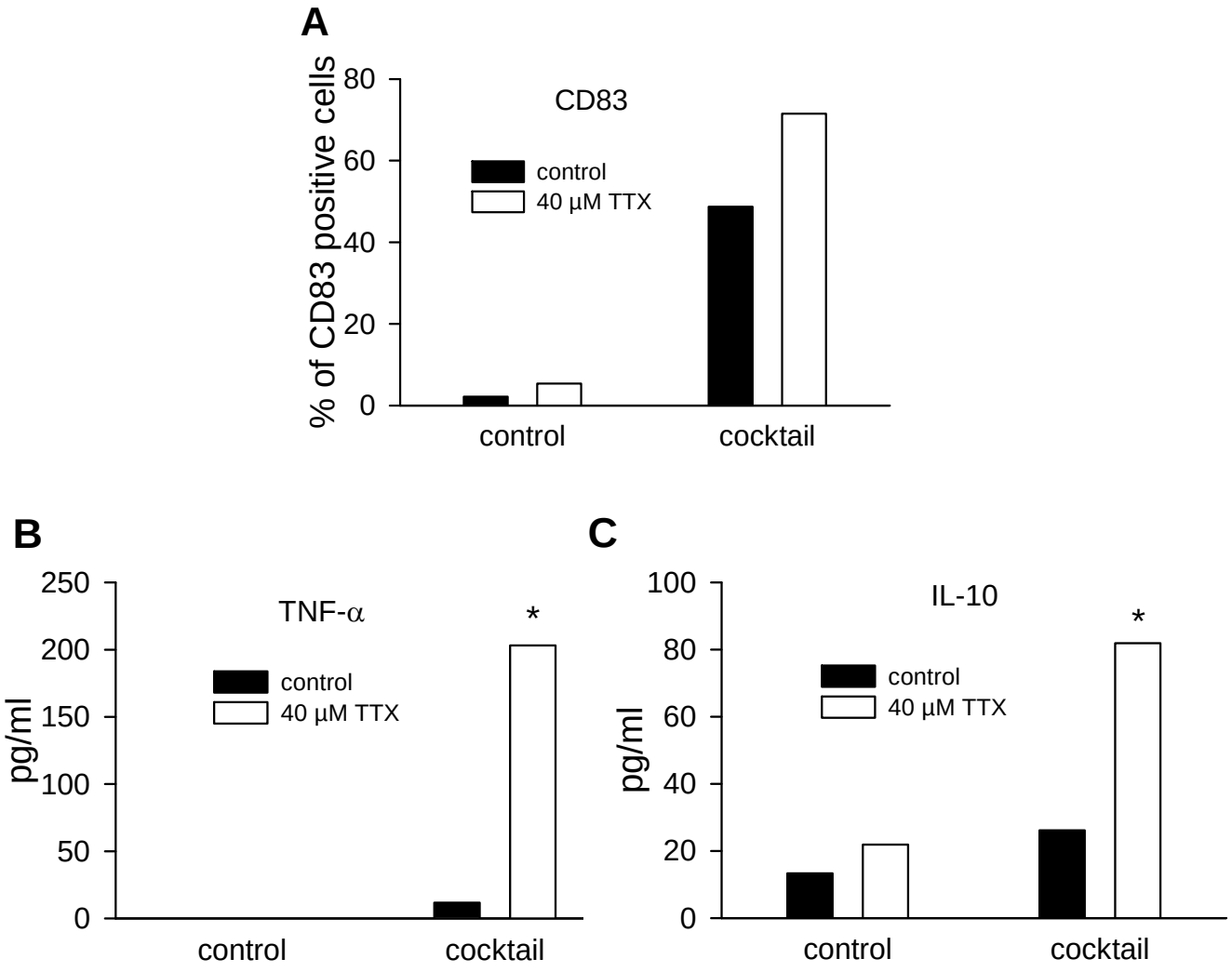

Figure 5.5 ***Effect of TTX-induced Nav1.7 block on the activation of DC***.

IDC were treated with 40 µM TTX on days 2 and 5 of differentiation. Activation of IDC was induced by addition of the inflammatory mixture used 10-fold diluted concentration on day 5, 1 h after TTX treatment. After 6 h, the excess of the mixture was removed by washing, and the activated MDC were cultured in fresh medium for another 16 h. ***A)*** The activation status of MDC was monitored by measuring the expression of CD83 and by determining the concentration of TNF-α ***(B)*** and IL-10 ***(C)*** cytokines by ELISA. Results obtained from DC of a selected donor (88% $CD1a^+$ cells) of four are documented.

added cytokines were removed by washing the cells and the activated DC were cultured for another 16h in fresh medium, and the supernatants were subjected to cytokine measurements. Although the absolute amounts of cytokines varied among individuals due to different $CD1a^+$ ratios in the donors [13], the increase of TNF-α (n=5; p=0.015; Figure 5.5B) and IL-10 (n=5; p=0.036; Figure 5.5C) secretion was 3–4 and 6–7 fold higher in TTX-treated samples as compared to untreated controls, respectively.

5.2 Protein interactions of Kv1.3 ion channel in the immunological synapse

5.2.1 Jurkat cells express PSD-95 and SAP97

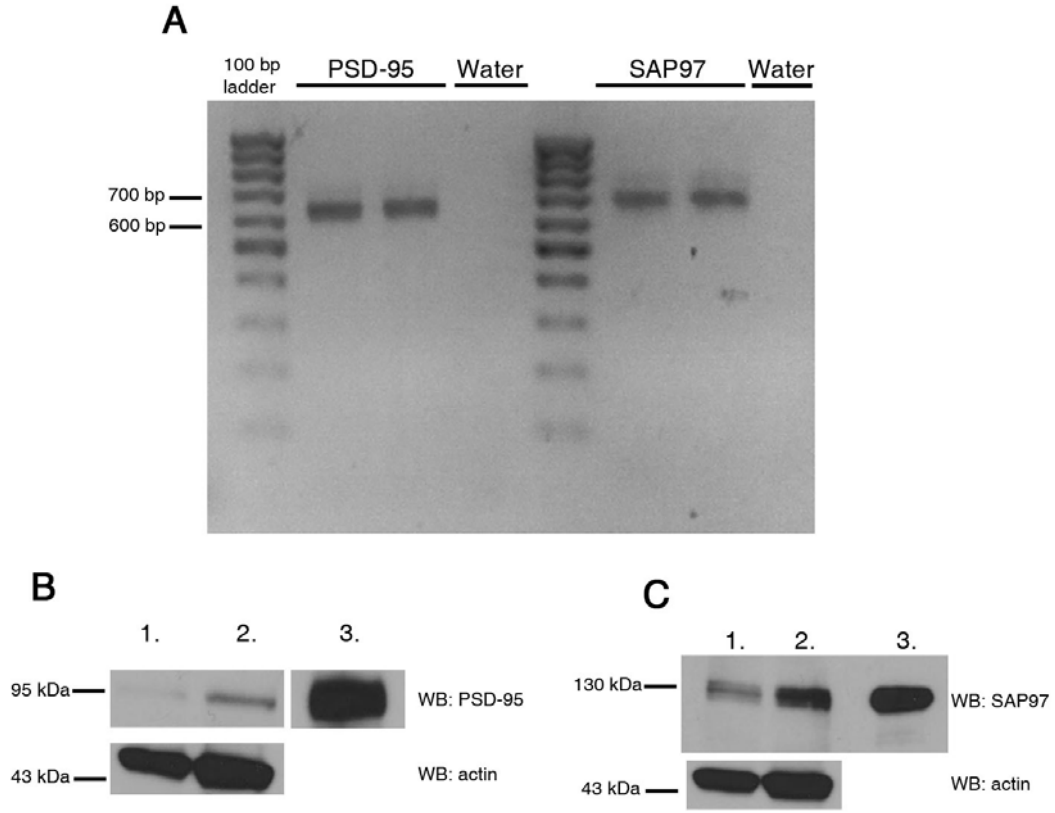

Figure 5.6 ***Jurkat cells express PSD-95 and SAP97.***
Panel ***A)*** shows PCR amplification of PSD-95 and SAP97 coding sequences from total Jurkat cDNA. Expected product sizes were 629 bp and 774 bp, respectively. ***B)*** Western blot of total cell lysates using a specific PSD-95 or ***C)*** SAP97 antibody. D38 cells transfected with PSD-95 or SAP97 served as positive controls. Actin blot was also performed to test the expression levels of PSD-95 and SAP97 in the different cell lines. *1)* Jurkat, *2)* Jurkat-mGFP-Kv1.3-WT, *3)* tsA-201 transfected with PSD-95 (***B***) or SAP97 (***C***).

As mentioned previously, PSD-95 and SAP97 are both scaffolding proteins expressed in neurons where they influence the localization of different Kv channels [116]. To understand whether these proteins could have an effect on Kv1.3 channel distribution in human T cells (Jurkat) we needed to test if they are expressed in these cells as well. Thus we isolated total RNA from Jurkat cells and used PSD-95 and SAP97 specific primers to perform reverse transcription PCR. The products were run on agarose gel, where we identified the specific products at the expected base pair sizes (Figure 5.6A). Also, sequence identity of the PCR products of both proteins was determined with nucleotide sequencing. To confirm the expression of PSD-95 and SAP97 at the protein level we performed Western blots from total

Jurkat cell lysates with a PSD-95 and a SAP97 specific antibody, respectively. tsA-201 cells transfected with either PSD-95 or SAP97 served as positive controls. We were able to detect specific lanes at 95 and 130 kDa, corresponding to the two proteins (Figure 5.6B-C), Therefore we could conclude that Jurkat cells do express both PSD-95 and SAP97.

5.2.2 PSD-95 and SAP97 interact with Kv1.3 through its C-terminal region

The next question that we addressed was whether the Kv1.3 channel interacts with PSD-95 and/or SAP97, and if it does, which part of the channel is involved in this interaction. As mentioned previously (section 2.4.1), the potential interaction sites (PDZ and SH3 binding domains) can be found on the N- and the C-terminal region of the channel, therefore we created GST-tagged bacterial expression constructs that contained either the first 184 (GST-Kv1.3-N-term.) or the last 94 amino acids (GST-Kv1.3-C-term) of Kv1.3 (see also *Materials and methods*, section 4.8). Total Jurkat cell lysates were incubated with immobilized recombinants of Kv1.3 channel termini or GST alone in our pull-down experiments. The eluted proteins were analyzed by Coomassie staining (Figure 5.7A) and also by Western blot (Figure 5.7B-C) using specific PSD-95 and SAP97 antibodies. The Coomassie staining clearly shows that both Kv1.3 constructs are expressed and purified efficiently from the bacterial extract. However, according to the Western blot it is apparent, that both PSD-95 and SAP97 bind only to the C-terminal region of Kv1.3, we could not identify any interaction through the N-terminal of the channel.

5.2.3 Over-expression of mGFP-tagged Kv1.3 constructs and knockdown of PSD-95 or SAP97 in Jurkat cells

Since in our future experiments we intended to investigate the localization of Kv1.3 under different circumstances with confocal microscopy, we needed Kv1.3 constructs that were tagged with a fluorescent protein that enabled the visualization of the channel. We chose the monomeric green fluorescent protein (mGFP) and added this tag not only to the wild type Kv1.3 (mGFP-Kv1.3-WT), but to a C-terminal truncated clone of the channel (mGFP-Kv1.3-ΔC) that lacks the potential binding site for PSD-95 and SAP97. Because of the C-terminal deletion we cloned the mGFP tags to the N-terminal region of the channel.

Over-expression of different exogenous proteins in suspension/immune cells can be a real challenge: the efficiency that one can reach is usually very low by using conventional transfection methods (cationic lipid reagent, electroporation). Therefore, we applied the retroviral transduction system, which we obtained from the Nolan Lab webpage (for details

see *Materials and methods*), to introduce our Kv1.3 constructs into Jurkat cells. This way we were able to reach approximately 30-50% transduction efficiency in our target cells (data not shown).

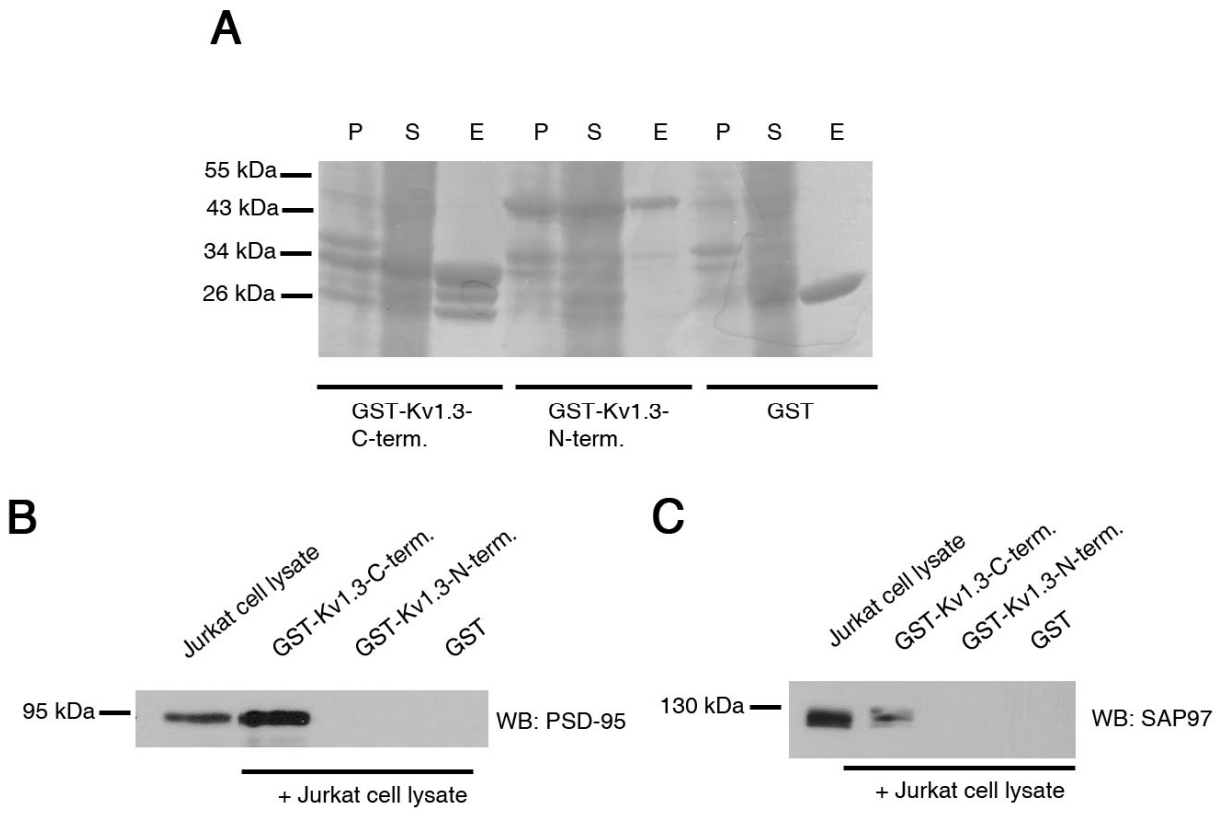

Figure 5.7 ***PSD-95 and SAP97 interact only with the C-terminal domain of Kv1.3***

A) Coomassie-staining of bacterially expressed glutathione S-tranferase (GST), GST-tagged C-terminal domain of Kv1.3 (GST-Kv1.3-C-term.), or GST-tagged N-terminal domain of Kv1.3 (GST-Kv1.3-N-term.) proteins shows the efficiency of the purification of bacterial extracts. Bacterial lysates were centrifuged after sonication, and the resulting pellets (P) and supernatants (S) were loaded on SDS-PAGE gels along with the elutes (E) of the GST pull-down assay. Western-blots probed with specific PSD-95 (***B***) or SAP97 (***C***) antibodies of Jurkat cell lysates (positive control) and the eluted fractions of the pull-down experiments that were obtained by incubating total Jurkat cell lysates with the Sepharose-bead-immobilized fusion proteins (GST, GST-Kv1.3-N-terminus, or GST-Kv1.3-C-terminus) are shown. PSD-95 and SAP97 was only detectable in the elute of GST-Kv1.3-C-terminal fusion protein and in the Jurkat cell lysate. Shown are representative data of at least three independent experiments. Also see Materials and methods for detailed explanation.

To further investigate the role of PSD-95 and SAP97 in T cells, we knocked down either of these proteins both in non-transduced and in mGFP-Kv1.3-WT over-expressing Jurkat cells. We used the lentiviral transduction method to introduce the specific shRNA

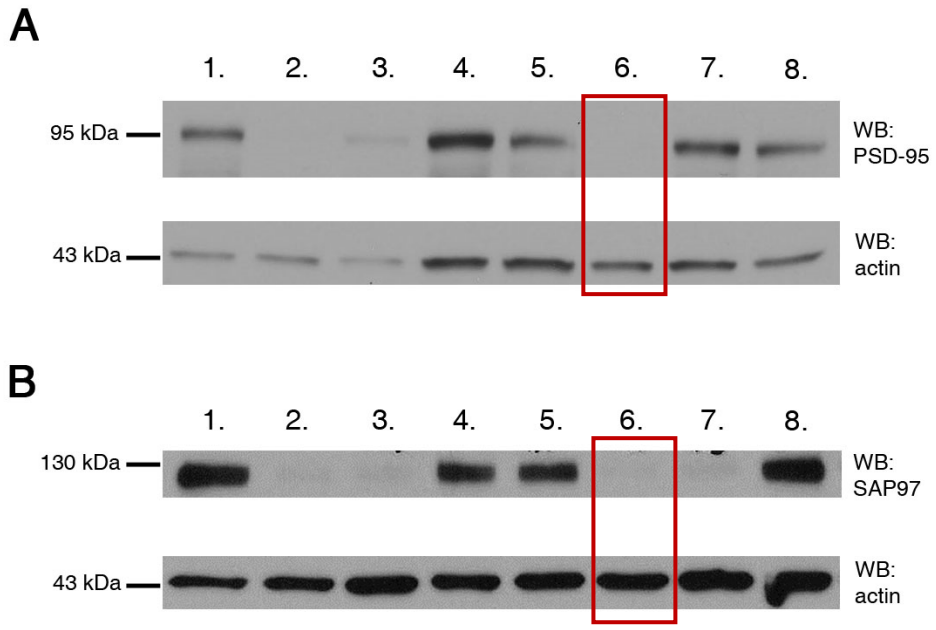

1) Jurkat

2) Jurkat-KD-PSD-95-27/Jurkat-KD-SAP97-01

3) Jurkat-KD-PSD-95-28/Jurkat-KD-SAP97-02

4) Jurkat-SCR-control

5) Jurkat-mGFP-Kv1.3-WT-pBMNZ

6) Jurkat-mGFP-Kv1.3-WT-KD-PSD-95-27/ Jurkat-mGFP-Kv1.3-WT-KD-SAP97-01

7) Jurkat-mGFP-Kv1.3-WT-KD-PSD-95-28/ Jurkat-mGFP-Kv1.3-WT-KD-SAP97-02

8) Jurkat-mGFP-Kv1.3-WT-SCR-control

Figure 5.8 ***shRNA knockdown of PSD-95 and SAP97***.

Jurkat and Jurkat-mGFP-Kv1.3-WT cells were transduced with two specific shRNA constructs each to down-regulate the expression level of PSD-95 (clone 27 and 28) or SAP97 (clone 01 and 02). Scrambled shRNA was used as transduction control. In case of PSD-95 construct 27 has been chosen for further experiments. Western blot of Jurkat cell lysates using ***A)*** anti-PSD-95 or ***B)*** anti-SAP97 antibodies. The cell lines chosen for further experiments are highlighted in red. The actin blot (bottom set: WB actin) shows the protein quantity loaded of each total cell lysate for both figure parts (***A-B***).

molecules into the cells, and applied two different clones in case of both proteins. The knock-down efficiency was checked with Western blot (Figure 5.8). We tested two shRNA sequences for both PSD-95 (Figure 5.8 panel A) and SAP97 (Figure 5.8 panel B) (numbers 27, 28 and 01, 02, respectively). According to the western blot experiments in the case of PSD-95 sequence number 27 was more effective in Jurkat-mGFP-Kv1.3-WT cells, thus we used these cells in our further experiments. In the case of SAP97 knock-down cells both shRNA clones were similarly effective, we chose sequence number 01 randomly.

5.2.4 Biophysical characterization of mGFP-tagged wild type and C-terminal deleted Kv1.3 channels

Before using the above mentioned mutated ion channels for microscopy it was crucial to investigate whether the mGFP tag and/or the C-terminal truncation had caused any change in the biophysical characteristics of Kv1.3. This was obtained by single-cell electrophysiology: we used the patch-clamp technique in outside-out patch configuration and compared the gating parameters of mGFP-Kv1.3-WT and mGFP-Kv1.3-ΔC channels that were expressed in CHO cells using retroviral transduction.

We found that the activation kinetics of mGFP-Kv1.3-WT and mGFP-Kv1.3-ΔC currents were identical: the rising phase of the current traces evoked by 15 ms depolarizing pulses to +50 mV overlap (Figure 5.9A). Quantitative description of the activation kinetics of the currents is given by the activation time constant (τ_a) obtained upon fitting the Hodgkin-Huxley equation to the rising phase of the current traces (see *Materials and methods* for details). The activation time constants for the mGFP-Kv1.3-WT and the mGFP-Kv1.3-ΔC constructs were not statistically different (τ_a was 0.54 ± 0.04 ms for mGFP-Kv1.3-WT (n=10) and 0.56 ± 0.02 ms for the mGFP-Kv1.3-ΔC (n=9), p= 0.698, Figure 5.9C).

The inactivation kinetics of the mGFP-Kv1.3-WT and mGFP-Kv1.3-ΔC currents is illustrated in Figure 5.9B. Again, the current traces are overlapping indicating that truncation of the C-terminal domain does not modify the inactivation kinetics. The inactivation time constants (τ_{in}), obtained by fitting a single exponential function to the decaying part of the current (see *Materials and methods* in details), were statistically not different for the mGFP-tagged WT and C-terminal deleted Kv1.3 channels (τ_{in} was 271 ± 31 ms for mGFP-Kv1.3-WT (n=7) and 240 ± 23 ms (n=6) for mGFP-Kv1.3-ΔC p=0.158, Figure 5.9D).

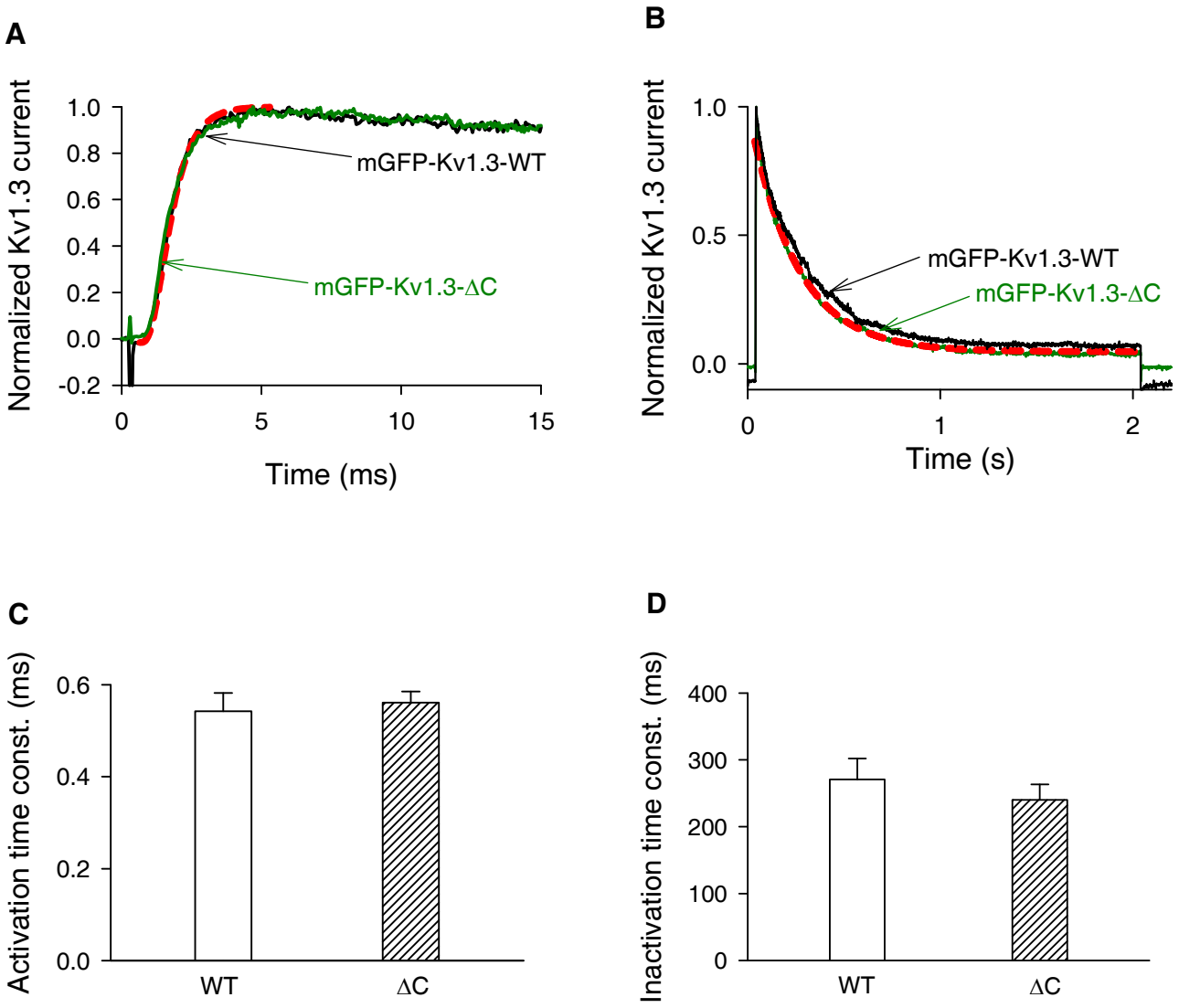

Figure 5.9 ***Biophysical properties of Kv1.3 channel constructs I.***

A) To study activation kinetics of mGFP-Kv1.3-WT and mGFP-Kv1.3-ΔC current CHO cell patches in outside-out configuration were depolarized to +50 mV from –120 mV for 15 ms (on-line leak subtraction was applied). Representative current traces are shown along with the best fitting curve obtained using Hodgkin-Huxley model (see Materials and methods) for the mGFP-Kv1.3-ΔC construct, (red dashed line, τ_a =0.59 ms). ***B)*** To study the inactivation kinetics of the currents outside-out patches were depolarized to +40 mV for 2 seconds from a holding potential of -120 mV. Typical current records for the mGFP-Kv1.3-WT and mGFP-Kv1.3-ΔC construct are shown along with the best-fit single exponential function to the decaying part of the trace obtained for the C-terminal truncated channel (red dashed line, τ_i=248 ms, see Materials and methods for details). ***C-D)*** The activation and inactivation time constants for mGFP-Kv1.3-WT (WT) and mGFP-Kv1.3-ΔC (ΔC) channels (mean ± SEM, n>6).

Finally, the equilibrium parameters of the voltage-dependence of steady-state activation, which defines the distribution of the channels between the open and closed state at a given membrane potential, were determined for both channel constructs: normalized conductance was plotted against test potential and data points were fitted with Boltzmann

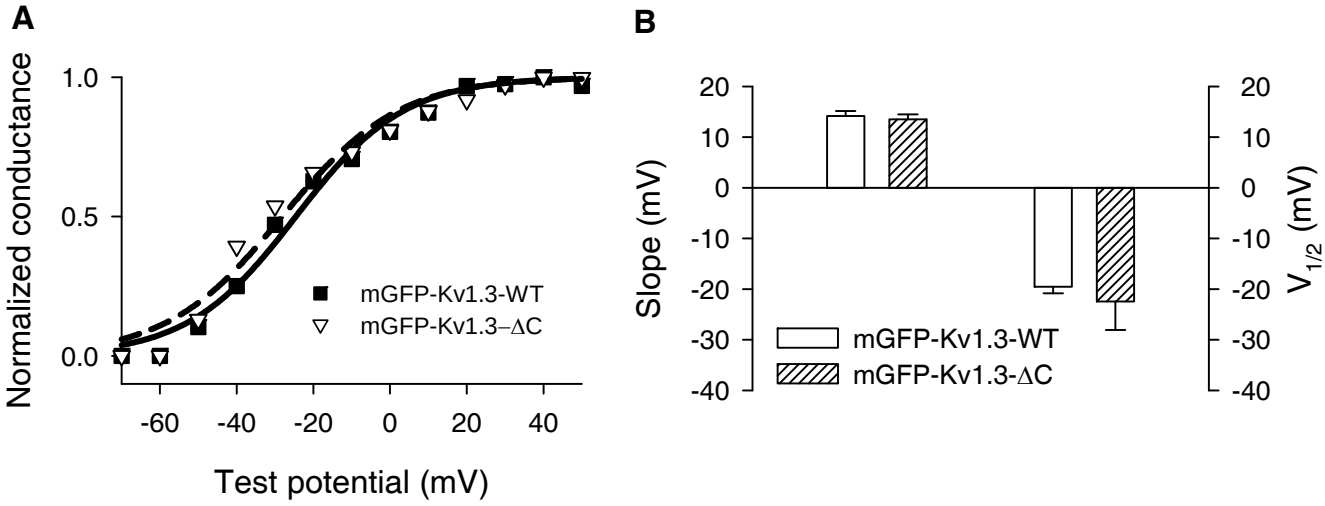

Figure 5.10 ***Biophysical properties of Kv1.3 channel constructs II.***

A) Voltage-dependence of steady-state activation of the Kv1.3 channels in CHO cells, outside-out configuration. The normalized conductance-test potential relationships were obtained and analyzed as described in the Materials and methods. Normalized conductance as a function of the test potential for mGFP-Kv1.3-WT(filled squares) and mGFP-Kv1.3-ΔC (empty triangles) along with the best fit Boltzmann-function (solid line: mGFP-Kv1.3-WT, dashed line: mGFP-Kv1.3-ΔC) are shown for two particular cells. The fitted parameters of the curve, the midpoint ($V_{½}$) and the slope (k, see Materials and methods) were $V_{½}$ = –24.6 mV, k=14.1 mV for mGFP-Kv1.3-WT and $V_{½}$= –28 mV and *k*=15.2 mV for the mGFP-Kv1.3-ΔC channels. ***B)*** Parameters of steady-state activation (slope (*k*) and midpoint ($V_{1/2}$)) are illustrated for the two channel constructs (mean ± SEM, n=7 and 5 for mGFP-Kv1.3-WT and mGFP-Kv1.3-ΔC).

function (Figure 5.10A). The small leftward shift in the normalized conductance-test potential curves for mGFP-Kv1.3-ΔC channels was not statistically significant (slope factor was 14.2 ± 1 mV and 13.5 ± 1 mV for mGFP-Kv1.3-WT (n=7) and mGFP-Kv1.3-ΔC (n=5), respectively, p=0.458; whereas $V_{1/2}$ was −19.5 ± 1.2 mV for mGFP-Kv1.3-WT (n=7) and −25.4 ± 5.4 mV for mGFP-Kv1.3-ΔC (n=5), p=0.282, Figure 5.10B). We believe that, since the biophysical

characteristics of the mGFP-Kv1.3-WT and C-terminal truncated mGFP-Kv1.3-ΔC channels are identical, any difference in the redistribution of the channels upon IS formation cannot be attributed to the altered ion channel function of the truncated channels.

5.2.5 Immunological synapse formation between Jurkat and Raji cells

To reveal if PSD-95 or SAP97 influences Kv1.3 redistribution at the immunological synapse, we initiated IS formation between Jurkat T cells (expressing the different Kv1.3 constructs) and Raji B cells (Figures 5.11 and 5.12). Raji cells were pretreated with *Staphylococcus Enterotoxin E* (SEE), then co-centrifuged and incubated with Jurkat cells. (For details on synapse formation, see *Materials and methods*.) The cells were fixed at five different time points (1, 5, 10, 20, and 30 min) after IS formation initiation in order to reveal the kinetics of Kv1.3 redistribution in the plasma membrane. Because it is well known that CD3 molecules rearrange into the immunological synapse [123], to verify synapse formation and to observe the physical boundaries of the IS, we used specific anti-CD3 immunofluorescent labeling as a positive control. All samples were analyzed by confocal microscopy.

5.2.6 C-terminal deletion of Kv1.3 or the knock-down of PSD-95 inhibits the accumulation of Kv.3 into the immunological synapse

In order to quantify the rearrangement of Kv1.3 channels upon IS formation we introduced the accumulation ratio (AR), which is proportional to the excess amount of Kv1.3 in the IS area compared to the even distribution of the channels in the membrane of standalone cells. (For details concerning the evaluation see *Materials and methods*.) As a negative control/justification for our evaluation method, we also analyzed standalone cells: we picked a random section of the plasma membrane, with similar area as the IS, to represent the contact area between the synapse forming cells and calculated the AR. In theory, the AR of standalone cells should be approximately 1. However, due to the patchy nature of Kv1.3 distribution in the membrane might be the consequence of its localization in lipid rafts [124], occasionally the calculated AR values were higher than 1 in these cells as well. In order to rule out these false positive data, we accepted Kv1.3 redistribution in the IS only at AR values being 1.5 or higher.

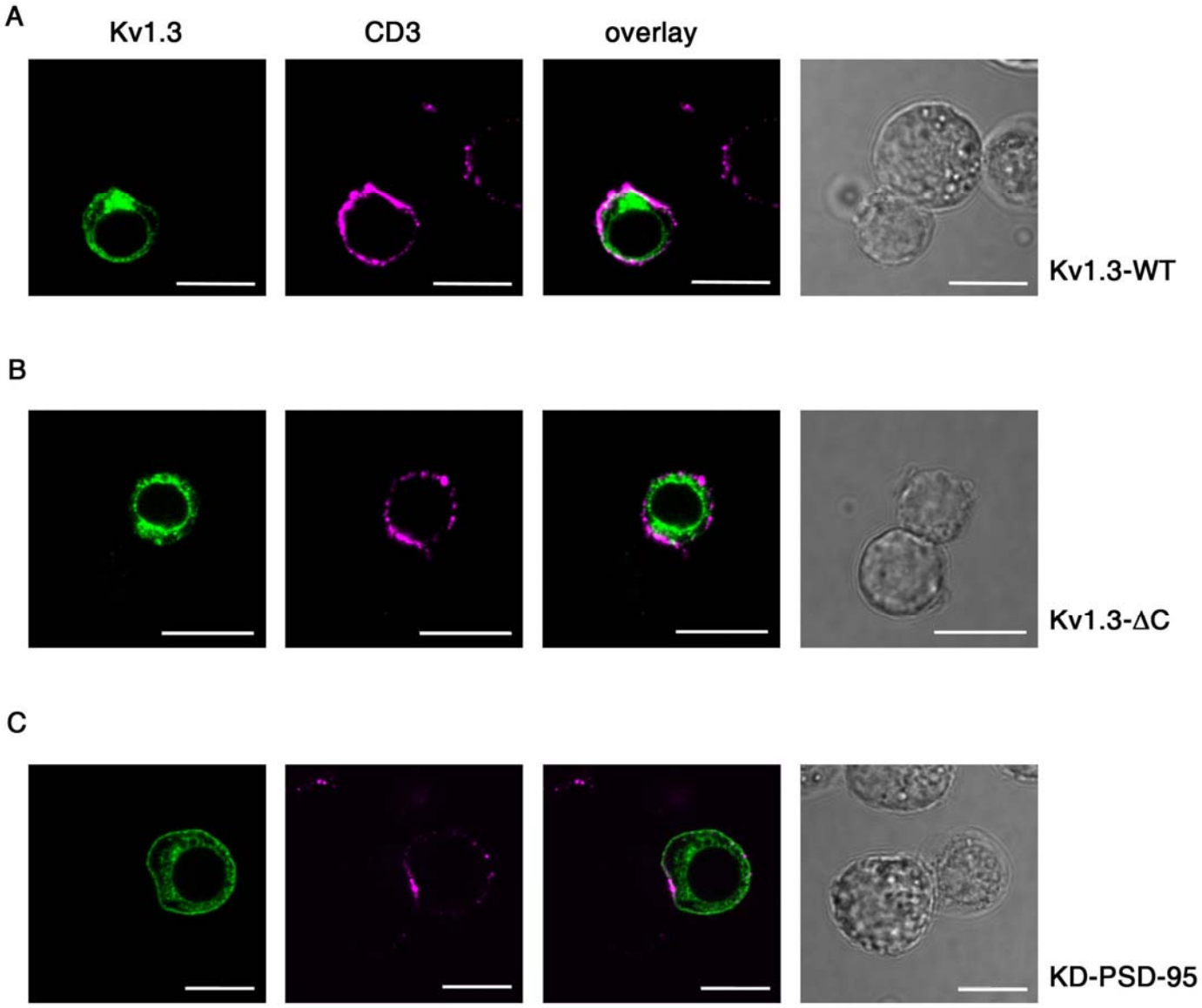

Figure 5.11 ***Recruitment of Kv1.3 and CD3 into the immunological synapse in control or PSD-95 knocked down Jurkat expressing wild-type or C-terminal truncated Kv1.3.***

Representative examples of immunological synapse formation between SEE-pulsed Raji B and ***A)*** Jurkat expressing the mGFP-tagged wild type Kv1.3 (Kv1.3-WT), ***B)*** Jurkat expressing the C-terminal truncated Kv1.3 (Kv1.3-ΔC), or ***C)*** PSD-95 knocked-down Jurkat expressing mGFP-tagged Kv1.3 (KD-PSD-95). The 1st column shows the Kv1.3 signal, mGFP-tagged channels are shown in green. Jurkat cells were also labeled with anti-CD3 primary and Alexa Fluor 647 GAMIG secondary antibodies to identify the synapses (2nd column, magenta). The 3rd column shows the overlay images of the Kv1.3 and anti-CD3 fluorescence signal whereas phase contrast images of the cells forming the IS are displayed in the 4th column. (For details concerning synapse formation and fluorescent labeling see Materials and methods, the images were taken at various time points.) Scale bar is 10 μm.

We analyzed at least 50 cells at each time point for all cell lines (except for Jurkat-mGFP-Kv1.3-WT cells-at 1 min n=38, and at 30 min n=32, for Jurkat-mGFP-Kv1.3-ΔC-at 10 min n=48). According to our results mGFP-tagged wild-type channels accumulate at a high rate in the immunological synapse: the AR was higher than 1.5 in approximately 30% of the cells 1 min after IS formation, and the fraction of Kv1.3 polarized cells monotonically decreased until the 30th minute (Figure 5.13A). On the other hand, the C-terminal truncated channels (mGFP-Kv1.3-ΔC) showed different accumulation kinetics: less than 10% percent of the cells showed Kv1.3 polarization at any given time point, nor did this parameter show any time dependence (Figure 5.13A). At approximately 30 minutes after IS formation the percentage of Kv1.3 polarized cells became similar in the case of the two cell lines. This correlates with the findings of Nicolaou et al. that the crucial time interval of molecular rearrangement during the immunological synapse is relatively short [78].

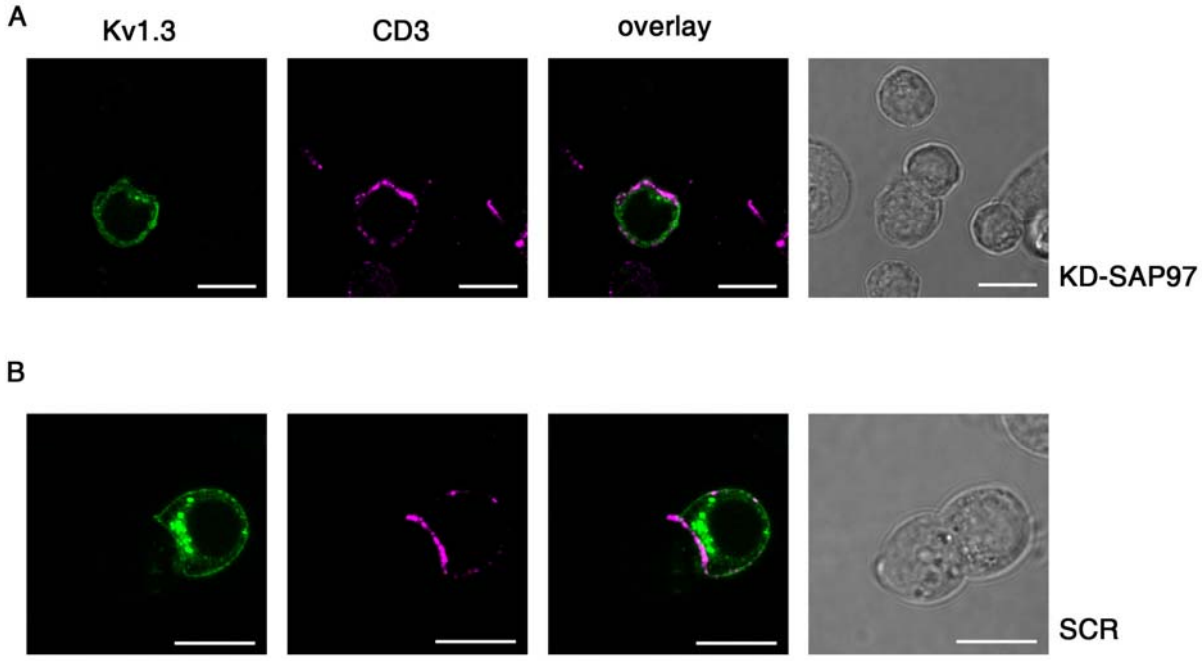

Figure 5.12 ***Recruitment of Kv1.3 and CD3 into the immunological synapse in SAP97 knocked down or scramble control Jurkat cells.***

Representative examples of immunological synapse formation between SEE-pulsed Raji B and **A)** SAP97 knocked-down Jurkat expressing mGFP-tagged Kv1.3 (KD-SAP97) or ***B)*** Jurkat transduced with scramble control shRNA (SCR). The 1st column shows the Kv1.3 signal, mGFP-tagged channels are shown in green. Jurkat cells were also labeled with anti-CD3 primary and Alexa Fluor 647 GAMIG secondary antibodies to identify the synapses (2nd column, magenta). The 3rd column shows the overlay images of the Kv1.3 and anti-CD3 fluorescence signal whereas phase contrast images of the cells forming the IS are displayed in the 4th column. (For details concerning synapse formation and fluorescent labeling see Materials and methods, the images were taken at various time points.) Scale bar is 10 μm.

Deleting the whole C-terminal tail of Kv1.3 may inhibit the binding of any intracellular scaffolding protein to the channel. Therefore, in order to see the specific effect of PSD-95 and SAP97 on channel redistribution we also compared the Kv1.3 polarization of

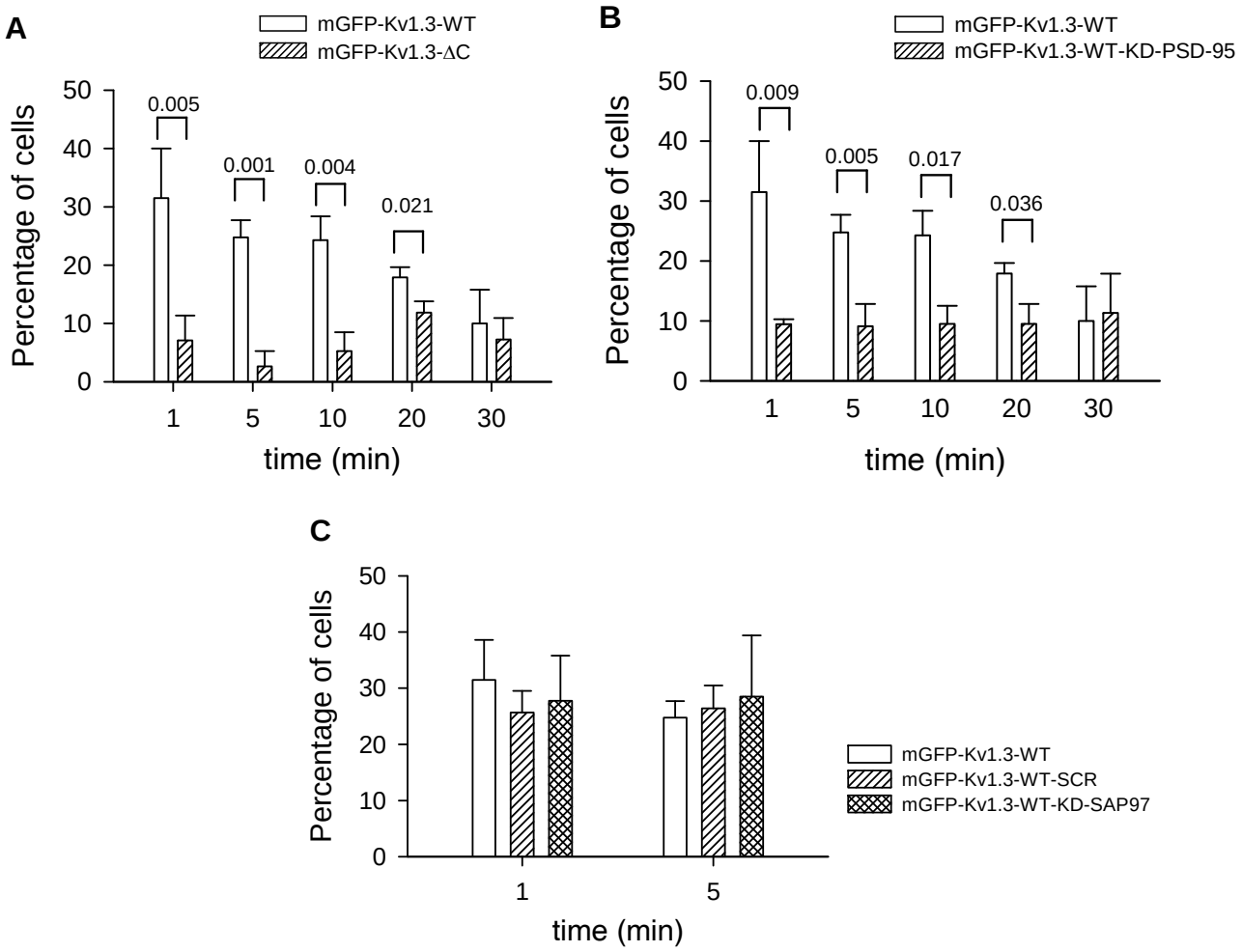

Figure 5.13 ***Accumulation of Kv1.3 channels in the IS depends on the C-terminus of Kv1.3 and the presence of PSD-95.***

The percentage of cells showing polarized Kv1.3 distribution during IS formation for ***A)*** Jurkat expressing the wild type (Jurkat-mGFP-Kv1.3-WT, empty bars) or C-terminal truncated (Jurkat-mGFP-Kv1.3-ΔC, hatched bars) Kv1.3 construct and ***B)*** control (Jurkat-mGFP-Kv1.3-WT) or PSD-95 knocked down (Jurkat-mGFP-Kv1.3-WT-KD-PSD-95) Jurkat cells expressing the same, mGPF-tagged Kv1.3 construct. The unadjusted p values are shown above the bars, only if there was statistical difference. ***C)*** Accumulation of Kv1.3 channels in the IS is not influenced by SAP97 or non-specific shRNA knockdown. The percentage of cells showing polarized Kv1.3 expression during IS formation for Jurkat expressing the wild type (Jurkat-mGFP-Kv1.3-WT, empty bars), SAP97 knocked-down (Jurkat-mGFP-Kv1.3-WT-KD-SAP-97, for 1 min: n=33, for 5 min: n=41) or scramble shRNA transfected Jurkat cells (Jurkat-mGFP-Kv1.3-SCR, for 1 min: n=29, for 5 min: n=85) transduced the same, mGPF-tagged Kv1.3 construct.

control and PSD-95 or SAP97 knockdown Jurkat cells upon IS formation. We found that PSD-95 depleted cells were similar to the C-terminal truncated channel expressing cells: the ratio of Kv1.3 polarized cells was significantly lower after 1 min compared to the normal cells, and the AR lacked any time-dependence up to the 30th minute (Figure 5.13B). In contrast, deletion of SAP97 or the introduction of non-specific scramble control shRNA into our model cell line had no effect on Kv1.3 distribution (Figure 5.13C) compared to the non-knockdown cells. These results support our hypothesis that PSD-95 may be one of the key scaffolding proteins that influence Kv1.3 distribution in the T cell membrane during immunological synapse formation.

5.2.7 The expression level of the different mGFP-tagged Kv1.3 channels is identical in Jurkat cells

As we showed previously (section 5.2.4.) the mGFP-Kv1.3-ΔC channel shares identical biophysical properties with the mGFP-Kv1.3-WT channel. However, the quantitative analysis of Kv1.3 channel's redistribution upon IS formation can also be fairly influenced by the expression level of Kv1.3 in the three different Jurkat cell lines: Jurkat-mGFP-Kv1.3-WT, Jurkat-mGFP-Kv1.3-ΔC and Jurkat-mGFP-Kv1.3-WT-KD-PSD95. Thus, using patch-clamping we measured the peak current and current density of Kv1.3 channels at 0 mV depolarization. Current density was defined as the ratio of peak current and the capacitance of the cell membrane. Figure 5.14A shows that the amplitude of Kv1.3 current is statistically the same for all three Jurkat cell lines (mean peak current was 4702 ± 540 pA for Jurkat-mGFP-Kv1.3-WT (n=10), 3618 ± 444 pA for Jurkat-mGFP-Kv1.3-ΔC (n=12) and 4297 ± 800 pA for Jurkat-mGFP-Kv1.3-WT-KD-PSD-95 (n=12), p=0.631). The whole cell capacitance was the following for the various cell lines: 3.85 ± 0.5 pF for Jurkat-mGFP-Kv1.3-WT, 3.5 ± 0.2 pF for Jurkat-mGFP-Kv1.3-ΔC and 5.1 ± 0.4 pF for Jurkat-mGFP-Kv1.3-WT-KD-PSD-95 cells. The current density, which is a good estimator of the channel number per unit area, was also found to be the same in these cell lines (the mean current density was 1284 ± 329 pA/pF for Jurkat-mGFP-Kv1.3-WT (n=10), 1109 ± 314 pA/pF for Jurkat-mGFP-Kv1.3-ΔC (n=12) and 960 ± 229 pA/pF for Jurkat-mGFP-Kv1.3-WT-KD-PSD-95 (n=12), p=0.541, Figure 5.14B). These data can exclude the possibility that the found difference in the accumulation of mGFP-tagged Kv1.3 channels in the IS could be due to the variation in the number of channels or in the channel density in the membrane of Jurkat cells lines.

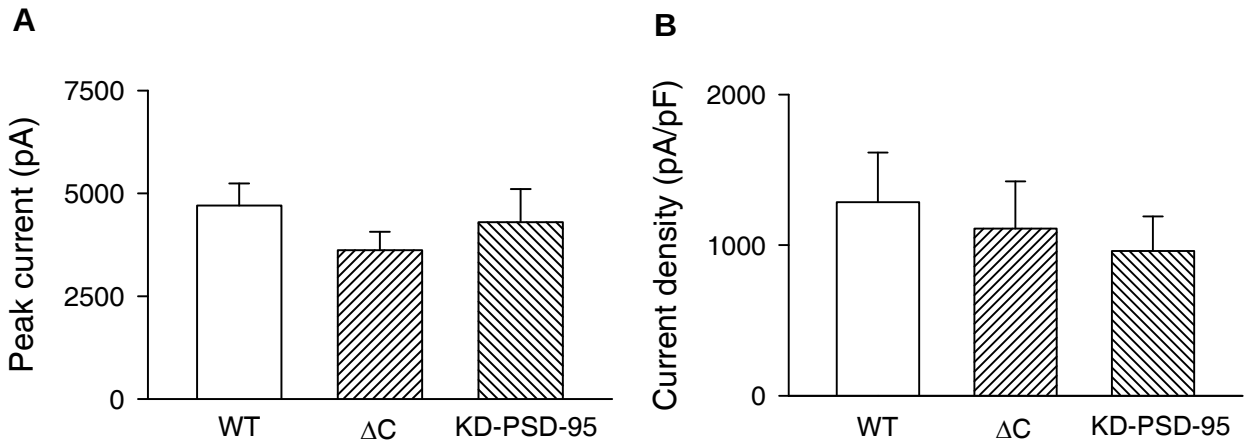

Figure 5.14 ***Expression of various Kv1.3 constructs in control and PSD-95 knocked-down Jurkat cells.***

A) Peak current was determined in whole-cell patch-clamped Jurkat cells upon depolarization to 0 mV from −120 mV for 30 milliseconds. The cells were transfected in a stable manner with the GFP-tagged wild type channel (mGFP-Kv1.3-WT, WT for short), the C-terminal deleted, GFP-tagged channel (mGFP-Kv1.3-ΔC, ΔC for short) or the mGFP-tagged wild-type channels were transfected into Jurkat cells having PSD-95 knocked-down using shRNA (mGFP-Kv1.3-WT-KD-PSD-95, KD-PSD95 for short). Online leak subtraction and series resistance compensation were applied. ***B)*** Kv1.3 current density of these three Jurkat cell lines calculated from the ratio of the peak current detected at 0 mV and the whole-cell capacitance. Error bars represent SEM on each panel.

6. DISCUSSION

6.1 Expression and function of Nav1.7 channels in CD1a$^+$ immature dendritic cells

The major function of IDC is to internalize exogenous soluble and particulate material and collect stimuli associated with environmental changes, and deliver this molecular information to the lymph-node resident T cells. Mobilization and maturation of DC to highly efficient APC with the unique capability to prime antigen-specific T lymphocytes requires inflammatory and danger signals. Activation-induced changes of DC include the down-regulation of some endocytic/phagocytic receptors; up-regulation of specific sets of cytokine and chemokine receptors, adhesion and co-stimulatory molecules; changes in morphology, cytoskeleton, mobility; and reorganization of the endo-lysosomal and MHC class II-rich intracellular compartments [4, 125]. Previous electrophysiological and pharmacological analysis performed in our laboratory showed a characteristic change in the expression of ion channels associated with the maturation of monocyte-derived DC. IDC were shown to express TTX-sensitive, rapidly inactivating voltage-gated Nav1.7 Na^+ channels whereas the dominant ion channel of MDC was the Kv1.3 K^+ channel [1].

This current study extends these findings by characterizing the expression pattern and functional activity of Nav1.7 channels in distinct DC subsets generated from a common precursor. According to our results the frequency of cells expressing Nav1.7 current and current density in Nav1.7-expressing cells is significantly higher in the CD1a$^+$ DC population than in CD1a$^-$ cells. This conclusion is based on ion current measurements performed on individual cells identified by their CD1a expression in the cell membrane.

Our data on the rapid activation-driven up- and down-regulation of the channel suggested direct transcriptional control of Nav1.7 expression. Transcriptional regulation of ion channel expression has been reported in naïve T cells, where the expression of the Ca^{2+}-activated K^+ channel IKCa1 is increased upon activation [126]. One of the most rapid signal transduction events in various cell types is the elevation of intracellular Ca^{2+} concentration. The importance, complexity and impact of Ca^{2+}-mediated signaling on the cell cycle of LPS-induced DC has recently been described in mice [127]. Various agents raising the intracellular concentration of Ca^{2+} have been investigated for their ability to alter the functions of sodium channels in the plasma membrane and at the level of mRNA expression [128-130]. Here we show the Ca^{2+}-dependent down-regulation of Nav1.7 both at the mRNA and protein levels in a subpopulation of human monocyte-derived DC, which may results in increased sensitivity to activation signals as documented by increased CD83 expression and TNF-α and IL-10

secretion in the presence of TTX. Therefore, the elevation of Ca^{2+} concentration, depending on the type and strength of the activating stimulus [131], is able to modulate the expression and function of Nav1.7 channels, which eventually leads to changes of the membrane potential. We propose that this process opens up a DC state ready to respond to activation signals.

To unveil the functional role of Nav1.7 channel expression in IDC we demonstrated that expression of the Nav1.7 channel in $CD1a^+$ IDC resulted in a depolarized resting membrane potential. This conclusion is supported by the results showing the following 1) removal of extracellular Na^+ hyperpolarizes the membrane of Nav1.7-expressing $CD1a^+$ IDC, but does not affect $CD1a^-$ IDC lacking Nav1.7 channels, 2) silencing of the Nav1.7 gene expression in $CD1a^+$ IDC results in a more negative and extracellular Na^+-independent resting membrane potential than in Nav1.7 expressing $CD1a^+$ IDC, and 3) the IKCa1/KCa3.1 channel is expressed in both $CD1a^-$ and $CD1a^+$ IDC at similar levels.

It has been demonstrated that VGSC contribute to the setting of the resting membrane potential in astrocytes [132, 133]. In addition, they are also implicated as key regulators of intracellular pH and cell migration [134, 135]. Our current-clamp experiments revealed that Nav1.7 channels are functional even at depolarized membrane potential; their presence is responsible for the maintenance of this depolarized state but act exclusively in $CD1a^+$ IDC. Even though the inactivation of Na^+ channels could be induced at depolarized membrane potentials, others have shown that even at ~ 0 mV an ample fraction of Nav1.7 channels are in available state [136, 137], and thus, the inward (depolarizing) Na^+ current may contribute to $CD1a^+$ IDC membrane potential regulation. This was supported by the fact, that the removal of extracellular Na^+, which abolishes the depolarizing Na^+ influx through Nav1.7, hyperpolarizes the membrane potential in $CD1a^+$ IDC. On the other hand, the hyperpolarized state of the cells could be an indirect consequence of the absence of extracellular Na^+, since this could alter the function of Na^+-dependent electrogenic transport mechanisms. In principle, the net inward current produced by the Na^+/Ca^{2+} exchanger run in forward mode could be responsible for extracellular Na^+-dependent membrane potential changes. However, we were able to eliminate this possibility by our siRNA experiment, which showed, that knocking down Nav1.7 results in a hyperpolarizing shift in $CD1a^+$ IDC, and insensitivity of the membrane potential to extracellular, similarly to $CD1a^-$ IDC with low Nav1.7 expression. These findings cannot be explained by the sensitivity of the membrane potential to Na^+/Ca^{2+} exchanger currents, rather can be interpreted as Nav1.7-dependence of the membrane potential. Taking all this into account, in combination with the similar number of IKCa1

channels on the different IDC subpopulations, our conclusion is that the Nav1.7 channel is an active regulator of the membrane potential in $CD1a^+$ IDC.

According to previous studies, the proper activation of Ca^{2+}-dependent signaling requires a negative membrane potential in various immune cells [128]. We propose that the presence and activity of IKCa1 channels in both IDC subtypes may be responsible for maintaining the negative membrane potential necessary for a sustained Ca^{2+} signaling during differentiation. The expression level of IKCa1 channels in $CD1a^+$ and $CD1a^-$ IDC is much higher than in other immune cells suggesting its exclusive role in the early phase of Ca^{2+}-dependent DC maturation.

The critical dependence of the membrane potential on Nav1.7 channels raised the question if different physiological responses of $CD1a^+$ IDC could be impaired upon Nav1.7 inhibition. Although in a previous study multiple functional studies were performed to demonstrate the effect of TTX on IDC functions, our workgroup failed to detect inhibition of DC differentiation, phagocytosis, pinocytosis or activation by the toxin [1]. However by using TTX we showed that Nav1.7 takes part in regulating the secretion of certain cytokines.

Taken together we showed that Nav1.7 channels in IDC are expressed in the cell membrane in contrast to microglia, where they are targeted to endosomes [39], and play a crucial role in the maintenance of the membrane potential, fine-tuning and setting the threshold of DC activation. We believe that the depolarized membrane potential (~ -10 mV) inhibits the activation of highly inflammatory $CD1a^+$ DC under a critical threshold and thus may protect these cells against unnecessary activation. When sensing danger signals strong enough to activate IDC maturation, the expression of Nav1.7 channel is rapidly down regulated allowing IDC to mature and transport their cargo to draining lymph nodes. Identification and functional characterization of the Nav1.7 channel in a human DC subset offers novel means of immune modulation and supports targeted drug design, whereas the novel, voltage-gated ion channel-dependent regulation of DC activation may have an impact on the targeted manipulation of DC functions in various clinical settings.

6.2 The role of PSD-95 in Kv1.3 channel rearrangement during immunological synapse formation

In the second part of this work we showed the influence of the intracellular adaptor protein, PSD-95, on the accumulation of Kv1.3 channels to the IS in human T cells. We demonstrated the following 1) PSD-95 and SAP97 are also present in human T cells (as for mouse lymphocytes [138]), 2) both PSD-95 and SAP97 interact directly with Kv1.3, but only

through the C terminus and not the N-terminal of the channel, 3) the biophysical characteristics of the Kv1.3 channel do not change significantly upon the deletion of the C terminal of the channel compared to WT Kv1.3, 4) a significantly lower percentage of cells transfected with the Kv1.3-ΔC construct showed polarized Kv1.3 expression upon IS formation as compared to cells expressing the WT channels, 5) knocking down PSD-95 gave similar results to the expression of Kv1.3-ΔC construct: the lack of this adaptor protein inhibited the polarization of Kv1.3 upon IS formation; 6) but SAP97-defficiency had no effect on Kv1.3 polarization. All these results underline the role of PSD-95 in the regulation of Kv1.3 redistribution into the IS.

It has been demonstrated by several groups, that different ion channels (Kv1.3, IKCa1, CRAC, P2X receptors), which are essential players in the Ca^{2+}-dependent activation of T cells, translocate into the IS in T cells [2, 78, 79, 94, 139]. The presence of potassium channels is a prerequisite for maintaining the negative membrane potential for adequate Ca^{2+} influx through CRAC channels which leads to the sustained elevated Ca^{2+} level necessary for downstream signaling pathways (NF-AT, IL-2 production). It has been shown that the entry of Ca^{2+} at the T cell APC contact site is facilitated by P2X1/4 and the Orai1-STIM1 complex [79, 139]. Mitochondria, which are also regulators of CRAC activity, were also demonstrated to move beneath the membrane region in contact with APCs [140]. The relocation of these organelles, which is coupled to the cytoskeleton meshwork, recruits the Ca^{2+} stores that buffer the intracellular Ca^{2+} concentration under the plasma membrane at the IS and prevent the inactivation of CRAC channels [141, 142]. All these emphasize the significance and functional importance of Kv1.3 recruitment to the IS, which we believe is guided by the PSD-95 adapter protein.

Anchoring proteins have been first described in neurons, where they participate in the membrane and vesicular trafficking of K^+ channels [114]. Their most important role is the transportation and anchoring of ion channels to different regions of a neuron, where the channels can locally and effectively control the membrane potential. Multiple studies in various expression systems explained how these proteins affect the membrane organization and intracellular targeting of Kv channels. PSD-95 was described to cluster with multiple channels in the Kv1 family. For example, it was demonstrated that PSD-95 immobilizes and clusters with Kv1.4 in HEK cells but the structural elements for these two mechanisms are different [143]. Furthermore, due to the clustering of PSD-95 with Kv1.4, the internalization of the channel can slow down [144]. Several studies indicated the interaction between Kv1.3 and PSD-95 in different expression systems, showing changes in channel distribution and/or

functional consequences. Marks and Fadool showed that clustering of Kv1.3 in HEK-293 cells is closely related to the PDZ binding domain on the C terminal of the channel [115, 117]. The physical interaction between Kv1.3 and PSD-95 showed by Marks and Fadool and the redistribution of PSD-95 into the IS formed between a thymocyte and a dendritic cell in mice [138] were combined in our study, where we showed with GST pull-down experiments, that PSD-95 and the C terminal of Kv1.3 are intimately coupled to each other in Jurkat T cells, and that this anchoring protein plays an essential role in regulation of Kv1.3 accumulation at the IS.

Some concerns had to be addressed because of the use of C-terminal truncated and N-terminal GFP-tagged channels. It has been shown that the interaction of Kv1.3 with PSD-95 induced use-dependent inhibition of, and modulation of the inactivation kinetics of the current, since the proline-rich sequences, which are necessary for functional modulations of the current by PSD-95, reside both N- and C-terminally of Kv1.3 [117]. It was also demonstrated recently that deletion of the PDZ domain from Kv1.3 (ΔTDV mutant) did not modify the cell surface expression of Kv1.3 in HEK cells; however, the incidence of cells with higher retention in the Golgi was more frequent for wild-type Kv1.3 than for the Kv1.3 ΔTDV mutant [145]. In contrast to the studies above we have not observed any change in the kinetic or steady-state parameters in the gating of the mGFP-Kv1.3-ΔC construct. Furthermore, the current densities were essentially the same regardless of the construct transfected (wild-type vs. Kv1.3-ΔC) or the cell type used (Jurkat vs. PSD-95 knockdown Jurkat). However, there are numerous non-canonical PDZ-binding domains other than the classical TDV sequence (S/T/Y-X-V/I/L) at the Kv1.3 C terminus (truncation of the complete intracellular carboxyl-tail can prevent binding of PSD-95/SAP-97 to these as well) [146]. Nonetheless, these might be exposed only under physiological circumstances and not during *in situ* binding-assays. Moreover, our results might indicate that PSD-95 and Kv1.3 interact in a different manner depending on the cell type used, or more likely, that interaction of the endogenous PSD-95 and transfected Kv1.3 in Jurkat cells (this study) can be different from that of a transfected channel and transfected PSD-95 as in other studies [117]. Regardless of the above, our results indicating identical biophysical parameters of Kv1.3 gating and current densities may exclude these factors as explanations for the differences observed in the redistribution of Kv1.3 in the cell membrane upon IS formation.

As it can be seen in Figure 5.13A-B neither the C-terminal deleted construct nor the knockdown of PSD-95 expression can fully prevent Kv1.3 polarization at the IS. In case of

the mGFP-Kv1.3-ΔC construct the reason behind this may be that the endogenous wild-type Kv1.3 subunit co-assemble with the transfected mGFP-Kv1.3-ΔC monomers, producing heterotetramers, as it was shown in Jurkat cells for endogenous wild-type and transfected kinetically tagged (A413V mutant) subunits of Kv1.3 [147]. Due to this co-expression there is always a subtle fraction of Kv1.3 tetramers which consist of one, two or three wild-type endogenous subunits having an intact C-terminal PDZ domain. For instance, given 2 percent of the total Kv1.3 subunits in a Jurkat cell are endogenous wild-type ones, approximately 8% of the total channel population contains at least one, full-length wild-type subunit, which can account for the non-zero fraction of Kv1.3 polarization in mGFP-Kv1.3-ΔC expressing cells (for calculation see [147]). As for the PSD-95 knockdown cells, the lack of PSD-95 at the cell population level (Figure 5.8) does not necessarily mean that a single cell cannot express this adaptor protein, regardless of the constant antibiotics selection. Since the percentage of T cells with Kv1.3 recruited at the IS do not change over time (it is around 10%, Figure 5.13B), we propose that cells with reduced but non-zero PSD-95 level were detected as Kv1.3 polarized. We should not, however, exclude the scenario that another, yet unidentified accessory protein of Kv1.3 may steer the channels to the IS.

According to Nicolaou et al., antibody cross-linking of Kv1.3 channels may result in the blocking of their compartmentalization and thus modification of Ca^{2+} signaling, which could have pathological consequences [93]. In addition, healthy and autoimmune T cells (from systemic lupus erythematosus, SLE patients) exhibit different Kv1.3 accumulation kinetics at the IS. This alters the development of Ca^{2+} responses in IS-engaged T cells and may explain the hyperactivity of SLE lymphocytes [94, 148]. Our results extend these earlier findings with the identification of one interaction partner of Kv1.3, PSD-95, which regulates the recruitment of the channels into the IS. Since PSD-95 has multiple PDZ domains, it may act as a linker between a putative cytoskeletal element, which is recruited into the IS, and Kv1.3. In this model Kv1.3 would passively follow the structural re-arrangements accompanying IS formation. On the other hand, in addition to the regulation of the Ca^{2+} entry via CRAC/P2X pathways the presence of Kv1.3 in the IS may also function as a "fishing rod" to collect adaptor proteins, including PSD-95, along with a great deal of signaling molecules.

We also showed, that SAP97 has no effect on Kv1.3 redistribution upon IS formation. SAP97 is only present at the IS for a short period of time, and it probably cannot aid the redistribution and accumulation of Kv1.3 channels in the IS appropriately [149]. Also, a recent study showed, that SAP97 has a T cell subset (regulatory T cells) specific feature: more SAP97 is recruited into the IS in these cells than in other $CD4^+$ T cells [150]. It has also been

described, that SAP97 serves as a linker in the PKAI induced phosphorylation and inhibition of the Kv1.3 channel, which in turn leads to T cell suppression via the SAP97–Lck–PKAI pathway [151]. Therefore, we suppose that SAP97 may participate in the regulation of other channel functions rather than in its lateral trafficking to the IS.

Based on our novel findings, it has now become possible to strategically inhibit the recruitment of Kv1.3 to the IS using a C-terminally truncated channel construct and directly address the consequences on membrane potential regulation, Ca^{2+} signaling and transmission of the mitogen signal. Taken together, we believe that the fundamental question, that what is the exact function of Kv1.3 channels at the IS, may soon be resolved.

7. SUMMARY

In this study we showed that $CD1a^+$ monocyte-derived immature dendritic cells (DC) express the voltage-gated Nav1.7 channel. We found that this voltage-gated sodium channel sets the membrane potential of these cells, thereby may modulate the threshold of dendritic cell activation, maturation. Inhibition of Nav1.7 channel by tetrodotoxin results in increased cytokine secretion of $CD1a^+$ immature dendritic cells (IDC) upon suboptimal cytokine cocktail stimulation, which suggests, that the channel has an important functional role during DC activation and differentiation. These facts confirmed our hypothesis that the presence of Nav1.7 channels in the plasma membrane of $CD1a^+$ IDC keeps the membrane potential at a "depolarized state" (app. -10 mV), thus protecting the cell from unnecessary or harmful activation below an actively set threshold. Since the transition of IDC to mature dendritic cells (MDC) is a crucial step in triggering both innate and adaptive immunity, these findings shed light to a new regulatory mechanism, by which DC functions may be controlled.

We also investigated the association of a voltage-gated potassium channel, Kv1.3, with two different scaffolding proteins in human T cells. We found that Kv1.3 interacts with both PSD-95 and SAP97, and this interaction occurs only through the C-terminal of the channel. Deleting this region of Kv1.3, or knocking down PSD-95 in a human T cell line significantly decreased the fraction of T cells displaying Kv1.3 accumulation at the immunological synapse upon T cell conjugation to an antigen presenting cell. On the other hand, SAP97 had no effect on Kv1.3 redistribution, implying that PSD-95 could be responsible for the rearrangement of the channel during the formation of this supramolecular cluster. The exact function of Kv1.3 channels at the immunological synapse is still not fully understood, however, we believe that elucidation of the mechanisms by which these channels can be recruited to the IS may help us in resolving this issue.

In summary this work focused on two different immune cell types and their dominant voltage-gated ion channels, which are both crucial in triggering an adequate immune response to different stimuli. Understanding the appropriate function and regulation of these channels may bring us closer to discovering possible causes of, and even therapies for various immune diseases.

8. ÖSSZEFOGLALÁS

Munkánk során sikerült kimutatnunk, hogy a monocita eredetű $CD1a^+$ éretlen dendritikus sejtek feszültség-kapuzott Nav1.7 ioncsatornákat fejeznek ki. Eredményeink alapján elmondható, hogy ez a feszültség-kapuzott nátrium csatorna szabályozza e sejtek membránpotenciálját, mely így befolyással lehet a dendritikus sejt aktivációs-küszöbérték beállítására. Az Nav1.7 csatorna gátlása tetrodotoxinnal a $CD1a^+$ éretlen dendritikus sejtek nagyobb mértékű citokintermelését eredményezi szuboptimális citokin-koktél stimuláció hatására, amely a csatorna funkcionális szerepére utal a dendritikus sejt differenciációja során. Mindezek a tények alátámasztják hipotézisünket, miszerint az Nav1.7 csatornák a $CD1a^+$ éretlen dendritikus sejtek membránját depolarizált állapotban tartják (kb. -10 mV), így biztosítva, hogy a sejtek csak az adott küszöbérték feletti stimulus hatására aktiválódnak. A dendritikus sejtek érése a veleszületett és az adaptív immunválaszra is hatással van, így ezen eredmények egy új szabályozó mechanizmust fednek fel, amely által a dendritikus sejtek működése szabályozódik.

Ezen kívül megvizsgáltuk a feszültség-kapuzott kálium csatorna, a Kv1.3 asszociációját két adapter fehérjével humán T sejtekben. Kimutattuk, hogy a Kv1.3 kölcsönhat mind a PSD-95, mind pedig a SAP97 fehérjével, és ez az interakció a csatorna C-terminális régióján keresztül valósul meg. Abban az esetben, ha eltávolítjuk a csatorna ezen szakaszát, vagy ha csendesítjük a sejtekben a PSD-95 fehérjét, jelentősen lecsökken a Kv1.3 polarizációt mutató azon T sejtek száma, melyek immunológiai szinapszisban vannak egy antigén prezentáló sejttel. Ezzel szemben a SAP97 csendesítése ugyanezen sejtekben nincs hatással a Kv1.3 ioncsatorna immunszinapszisbeli lokalizációjára. Mindezekből arra következtethetünk, hogy a PSD-95 fehérjének jelentős szerepe van a Kv1.3 csatorna ezen szupramolekuláris klaszterben való feldúsulásában. Mindazonáltal a Kv1.3 funkciója a szinapszisban továbbra sem tisztázott, de úgy gondoljuk hogy ezen eredmények segíthetnek a továbbiakban ezen kérdés megválaszolásában.

Összefoglalva elmondhatjuk, hogy munkánk során két különböző feszültség-kapuzott ioncsatornát vizsgáltunk két különböző típusú immunsejtben, amelyek azonban elengedhetetlenek a megfelelő immunválasz kialakításához. Ezen csatornák pontos funkciójának és szabályozásának ismerete segíthet különböző immunbetegségek okának és lehetséges gyógymódjának megismerésében.

9. REFERENCES

1. Zsiros, E., et al., *Developmental switch of the expression of ion channels in human dendritic cells.* J Immunol, 2009. **183**(7): p. 4483-92.
2. Panyi, G., et al., *Kv1.3 potassium channels are localized in the immunological synapse formed between cytotoxic and target cells.* Proc Natl Acad Sci U S A, 2004. **101**(5): p. 1285-90.
3. Janeway, C.A., et al., *Immunobiology: the immune system in health and disease*. 6th edition ed. 2005, New York: Garland Science Publishing.
4. Steinman, R.M. and H. Hemmi, *Dendritic cells: translating innate to adaptive immunity.* Curr Top Microbiol Immunol, 2006. **311**: p. 17-58.
5. Shortman, K. and Y.J. Liu, *Mouse and human dendritic cell subtypes.* Nat Rev Immunol, 2002. **2**(3): p. 151-61.
6. Caux, C., et al., *CD34+ hematopoietic progenitors from human cord blood differentiate along two independent dendritic cell pathways in response to GM-CSF+TNF alpha.* J Exp Med, 1996. **184**(2): p. 695-706.
7. Brigl, M. and M.B. Brenner, *CD1: antigen presentation and T cell function.* Annu Rev Immunol, 2004. **22**: p. 817-90.
8. Manolova, V., et al., *Functional CD1a is stabilized by exogenous lipids.* Eur J Immunol, 2006. **36**(5): p. 1083-92.
9. Moody, D.B. and S.A. Porcelli, *Intracellular pathways of CD1 antigen presentation.* Nat Rev Immunol, 2003. **3**(1): p. 11-22.
10. Caux, C., et al., *CD34+ hematopoietic progenitors from human cord blood differentiate along two independent dendritic cell pathways in response to granulocyte-macrophage colony-stimulating factor plus tumor necrosis factor alpha: II. Functional analysis.* Blood, 1997. **90**(4): p. 1458-70.
11. Randolph, G.J., et al., *Differentiation of phagocytic monocytes into lymph node dendritic cells in vivo.* Immunity, 1999. **11**(6): p. 753-61.
12. Sallusto, F. and A. Lanzavecchia, *Efficient presentation of soluble antigen by cultured human dendritic cells is maintained by granulocyte/macrophage colony-stimulating factor plus interleukin 4 and downregulated by tumor necrosis factor alpha.* J Exp Med, 1994. **179**(4): p. 1109-18.
13. Gogolak, P., et al., *Differentiation of CD1a- and CD1a+ monocyte-derived dendritic cells is biased by lipid environment and PPARgamma.* Blood, 2007. **109**(2): p. 643-52.
14. Dubsky, P., et al., *Human dendritic cell subsets for vaccination.* J Clin Immunol, 2005. **25**(6): p. 551-72.
15. B., H., *Ionic Channels of Excitable Membranes*. 2001.
16. Catterall, W.A., *Molecular properties of voltage-sensitive sodium channels.* Annu Rev Biochem, 1986. **55**: p. 953-85.
17. Isom, L.L., et al., *Primary structure and functional expression of the beta 1 subunit of the rat brain sodium channel.* Science, 1992. **256**(5058): p. 839-42.
18. Catterall, W.A., A.L. Goldin, and S.G. Waxman, *International Union of Pharmacology. XLVII. Nomenclature and structure-function relationships of voltage-gated sodium channels.* Pharmacol Rev, 2005. **57**(4): p. 397-409.
19. Catterall, W.A., *Voltage-gated sodium channels at 60: structure, function and pathophysiology.* J Physiol, 2012. **590**(Pt 11): p. 2577-89.
20. Cestele, S. and W.A. Catterall, *Molecular mechanisms of neurotoxin action on voltage-gated sodium channels.* Biochimie, 2000. **82**(9-10): p. 883-92.
21. MacKinnon, R., *Determination of the subunit stoichiometry of a voltage-activated potassium channel.* Nature, 1991. **350**(6315): p. 232-5.

22. Chapman, M.L., H.S. Krovetz, and A.M. VanDongen, *GYGD pore motifs in neighbouring potassium channel subunits interact to determine ion selectivity.* J Physiol, 2001. **530**(Pt 1): p. 21-33.
23. Ranganathan, R., J.H. Lewis, and R. MacKinnon, *Spatial localization of the K+ channel selectivity filter by mutant cycle-based structure analysis.* Neuron, 1996. **16**(1): p. 131-9.
24. Grissmer, S. and M. Cahalan, *TEA prevents inactivation while blocking open K+ channels in human T lymphocytes.* Biophys J, 1989. **55**(1): p. 203-6.
25. Sands, S.B., R.S. Lewis, and M.D. Cahalan, *Charybdotoxin blocks voltage-gated K+ channels in human and murine T lymphocytes.* J Gen Physiol, 1989. **93**(6): p. 1061-74.
26. Price, M., S.C. Lee, and C. Deutsch, *Charybdotoxin inhibits proliferation and interleukin 2 production in human peripheral blood lymphocytes.* Proc Natl Acad Sci U S A, 1989. **86**(24): p. 10171-5.
27. Chi, V., et al., *Development of a sea anemone toxin as an immunomodulator for therapy of autoimmune diseases.* Toxicon, 2012. **59**(4): p. 529-46.
28. Tytgat, J., et al., *A unified nomenclature for short-chain peptides isolated from scorpion venoms: alpha-KTx molecular subfamilies.* Trends Pharmacol Sci, 1999. **20**(11): p. 444-7.
29. Varga, Z., et al., *Vm24, a natural immunosuppressive peptide, potently and selectively blocks Kv1.3 potassium channels of human T cells.* Mol Pharmacol, 2012. **82**(3): p. 372-82.
30. Hodgkin, A.L. and A.F. Huxley, *A quantitative description of membrane current and its application to conduction and excitation in nerve.* J Physiol, 1952. **117**(4): p. 500-44.
31. Chandy, K.G., et al., *Voltage-gated potassium channels are required for human T lymphocyte activation.* J Exp Med, 1984. **160**(2): p. 369-85.
32. Ince, C., et al., *Ionic channels and membrane hyperpolarization in human macrophages.* J Membr Biol, 1987. **97**(3): p. 251-8.
33. Kim, S.Y., M.R. Silver, and T.E. DeCoursey, *Ion channels in human THP-1 monocytes.* J Membr Biol, 1996. **152**(2): p. 117-30.
34. Hsu, S., et al., *Fundamental Ca2+ signaling mechanisms in mouse dendritic cells: CRAC is the major Ca2+ entry pathway.* J Immunol, 2001. **166**(10): p. 6126-33.
35. Liu, Q.H., et al., *Expression and a role of functionally coupled P2Y receptors in human dendritic cells.* FEBS Lett, 1999. **445**(2-3): p. 402-8.
36. O'Connell, P.J., V.A. Klyachko, and G.P. Ahern, *Identification of functional type 1 ryanodine receptors in mouse dendritic cells.* FEBS Lett, 2002. **512**(1-3): p. 67-70.
37. Poggi, A., A. Rubartelli, and M.R. Zocchi, *Involvement of dihydropyridine-sensitive calcium channels in human dendritic cell function. Competition by HIV-1 Tat.* J Biol Chem, 1998. **273**(13): p. 7205-9.
38. Matzner, N., et al., *Ion channels modulating mouse dendritic cell functions.* J Immunol, 2008. **181**(10): p. 6803-9.
39. Black, J.A., S. Liu, and S.G. Waxman, *Sodium channel activity modulates multiple functions in microglia.* Glia, 2009. **57**(10): p. 1072-81.
40. Craner, M.J., et al., *Sodium channels contribute to microglia/macrophage activation and function in EAE and MS.* Glia, 2005. **49**(2): p. 220-9.
41. Rush, A.M., et al., *Electrophysiological properties of sodium current subtypes in small cells from adult rat dorsal root ganglia.* J Physiol, 1998. **511 (Pt 3)**: p. 771-89.
42. Sangameswaran, L., et al., *A novel tetrodotoxin-sensitive, voltage-gated sodium channel expressed in rat and human dorsal root ganglia.* J Biol Chem, 1997. **272**(23): p. 14805-9.
43. Vassilev, P.M., T. Scheuer, and W.A. Catterall, *Identification of an intracellular peptide segment involved in sodium channel inactivation.* Science, 1988. **241**(4873): p. 1658-61.
44. Klugbauer, N., et al., *Structure and functional expression of a new member of the tetrodotoxin-sensitive voltage-activated sodium channel family from human neuroendocrine cells.* Embo J, 1995. **14**(6): p. 1084-90.

45. Cummins, T.R., J.R. Howe, and S.G. Waxman, *Slow closed-state inactivation: a novel mechanism underlying ramp currents in cells expressing the hNE/PN1 sodium channel.* J Neurosci, 1998. **18**(23): p. 9607-19.
46. Waxman, S.G., *Neurobiology: a channel sets the gain on pain.* Nature, 2006. **444**(7121): p. 831-2.
47. Drenth, J.P. and S.G. Waxman, *Mutations in sodium-channel gene SCN9A cause a spectrum of human genetic pain disorders.* J Clin Invest, 2007. **117**(12): p. 3603-9.
48. Nassar, M.A., et al., *Nociceptor-specific gene deletion reveals a major role for Nav1.7 (PN1) in acute and inflammatory pain.* Proc Natl Acad Sci U S A, 2004. **101**(34): p. 12706-11.
49. Laniado, M.E., et al., *Expression and functional analysis of voltage-activated Na+ channels in human prostate cancer cell lines and their contribution to invasion in vitro.* Am J Pathol, 1997. **150**(4): p. 1213-21.
50. Varga, Z., et al., *Potassium channel expression in human CD4+ regulatory and naive T cells from healthy subjects and multiple sclerosis patients.* Immunol Lett, 2009. **124**(2): p. 95-101.
51. Hoth, M. and R. Penner, *Depletion of intracellular calcium stores activates a calcium current in mast cells.* Nature, 1992. **355**(6358): p. 353-6.
52. Hoth, M. and R. Penner, *Calcium release-activated calcium current in rat mast cells.* J Physiol, 1993. **465**: p. 359-86.
53. Zweifach, A. and R.S. Lewis, *Mitogen-regulated Ca2+ current of T lymphocytes is activated by depletion of intracellular Ca2+ stores.* Proc Natl Acad Sci U S A, 1993. **90**(13): p. 6295-9.
54. Fanger, C.M., et al., *Calcium-activated potassium channels sustain calcium signaling in T lymphocytes. Selective blockers and manipulated channel expression levels.* J Biol Chem, 2001. **276**(15): p. 12249-56.
55. Matteson, D.R. and C. Deutsch, *K channels in T lymphocytes: a patch clamp study using monoclonal antibody adhesion.* Nature, 1984. **307**(5950): p. 468-71.
56. Grissmer, S., et al., *Expression and chromosomal localization of a lymphocyte K+ channel gene.* Proc Natl Acad Sci U S A, 1990. **87**(23): p. 9411-5.
57. Cahalan, M.D., H. Wulff, and K.G. Chandy, *Molecular properties and physiological roles of ion channels in the immune system.* J Clin Immunol, 2001. **21**(4): p. 235-52.
58. Cahalan, M.D. and R.S. Lewis, *Role of potassium and chloride channels in volume regulation by T lymphocytes.* Soc Gen Physiol Ser, 1988. **43**: p. 281-301.
59. Chandy, K.G., *Simplified gene nomenclature.* Nature, 1991. **352**(6330): p. 26.
60. Ledwell, J.L. and R.W. Aldrich, *Mutations in the S4 region isolate the final voltage-dependent cooperative step in potassium channel activation.* J Gen Physiol, 1999. **113**(3): p. 389-414.
61. Panyi, G., *Biophysical and pharmacological aspects of K+ channels in T lymphocytes.* Eur Biophys J, 2005. **34**(6): p. 515-29.
62. Demo, S.D. and G. Yellen, *The inactivation gate of the Shaker K+ channel behaves like an open-channel blocker.* Neuron, 1991. **7**(5): p. 743-53.
63. Zagotta, W.N., T. Hoshi, and R.W. Aldrich, *Restoration of inactivation in mutants of Shaker potassium channels by a peptide derived from ShB.* Science, 1990. **250**(4980): p. 568-71.
64. Lopez-Barneo, J., et al., *Effects of external cations and mutations in the pore region on C-type inactivation of Shaker potassium channels.* Receptors Channels, 1993. **1**(1): p. 61-71.
65. Liu, Y., M.E. Jurman, and G. Yellen, *Dynamic rearrangement of the outer mouth of a K+ channel during gating.* Neuron, 1996. **16**(4): p. 859-67.
66. Loots, E. and E.Y. Isacoff, *Protein rearrangements underlying slow inactivation of the Shaker K+ channel.* J Gen Physiol, 1998. **112**(4): p. 377-89.
67. Olcese, R., et al., *Correlation between charge movement and ionic current during slow inactivation in Shaker K+ channels.* J Gen Physiol, 1997. **110**(5): p. 579-89.
68. Janeway, C.J., et al., *Immunobiology: The Immune System in Health and Disease.* 6th ed. 2004, New York: Garland Science.

69. Prakriya, M. and R.S. Lewis, *CRAC channels: activation, permeation, and the search for a molecular identity.* Cell Calcium, 2003. **33**(5-6): p. 311-21.
70. Panyi, G., et al., *Looking through ion channels: recharged concepts in T-cell signaling.* Trends Immunol, 2004. **25**(11): p. 565-9.
71. Crabtree, G.R., *Generic signals and specific outcomes: signaling through Ca2+, calcineurin, and NF-AT.* Cell, 1999. **96**(5): p. 611-4.
72. Rao, A., C. Luo, and P.G. Hogan, *Transcription factors of the NFAT family: regulation and function.* Annu Rev Immunol, 1997. **15**: p. 707-47.
73. Bromley, S.K., et al., *The immunological synapse.* Annu Rev Immunol, 2001. **19**: p. 375-96.
74. Monks, C.R., et al., *Three-dimensional segregation of supramolecular activation clusters in T cells.* Nature, 1998. **395**(6697): p. 82-6.
75. Brossard, C., et al., *Multifocal structure of the T cell - dendritic cell synapse.* Eur J Immunol, 2005. **35**(6): p. 1741-53.
76. Dustin, M.L. and D. Depoil, *New insights into the T cell synapse from single molecule techniques.* Nat Rev Immunol, 2011. **11**(10): p. 672-84.
77. Panyi, G., et al., *Colocalization and nonrandom distribution of Kv1.3 potassium channels and CD3 molecules in the plasma membrane of human T lymphocytes.* Proc Natl Acad Sci U S A, 2003. **100**(5): p. 2592-7.
78. Nicolaou, S.A., et al., *The Ca(2+)-activated K(+) channel KCa3.1 compartmentalizes in the immunological synapse of human T lymphocytes.* Am J Physiol Cell Physiol, 2007. **292**(4): p. C1431-9.
79. Lioudyno, M.I., et al., *Orai1 and STIM1 move to the immunological synapse and are up-regulated during T cell activation.* Proc Natl Acad Sci U S A, 2008. **105**(6): p. 2011-6.
80. Beeton, C., et al., *Kv1.3 channels are a therapeutic target for T cell-mediated autoimmune diseases.* Proc Natl Acad Sci U S A, 2006. **103**(46): p. 17414-9.
81. Chandy, K.G., et al., *K+ channels as targets for specific immunomodulation.* Trends Pharmacol Sci, 2004. **25**(5): p. 280-9.
82. Gong, J., et al., *Differential stimulation of PKC phosphorylation of potassium channels by ZIP1 and ZIP2.* Science, 1999. **285**(5433): p. 1565-9.
83. Gulbins, E., et al., *Ceramide-induced inhibition of T lymphocyte voltage-gated potassium channel is mediated by tyrosine kinases.* Proc Natl Acad Sci U S A, 1997. **94**(14): p. 7661-6.
84. Hanada, T., et al., *Human homologue of the Drosophila discs large tumor suppressor binds to p56lck tyrosine kinase and Shaker type Kv1.3 potassium channel in T lymphocytes.* J Biol Chem, 1997. **272**(43): p. 26899-904.
85. McCormack, T., et al., *The effects of Shaker beta-subunits on the human lymphocyte K+ channel Kv1.3.* J Biol Chem, 1999. **274**(29): p. 20123-6.
86. Drachman, D.B., et al., *Myasthenic antibodies cross-link acetylcholine receptors to accelerate degradation.* N Engl J Med, 1978. **298**(20): p. 1116-22.
87. Lennon, V.A., *Immunology of the acetylcholine receptor.* Immunol Commun, 1976. **5**(4): p. 323-44.
88. Gultekin, S.H., et al., *Paraneoplastic limbic encephalitis: neurological symptoms, immunological findings and tumour association in 50 patients.* Brain, 2000. **123 (Pt 7)**: p. 1481-94.
89. Shillito, P., et al., *Acquired neuromyotonia: evidence for autoantibodies directed against K+ channels of peripheral nerves.* Ann Neurol, 1995. **38**(5): p. 714-22.
90. Wulff, H., et al., *The voltage-gated Kv1.3 K(+) channel in effector memory T cells as new target for MS.* J Clin Invest, 2003. **111**(11): p. 1703-13.
91. Beeton, C. and K.G. Chandy, *Potassium channels, memory T cells, and multiple sclerosis.* Neuroscientist, 2005. **11**(6): p. 550-62.
92. Wulff, H., C. Beeton, and K.G. Chandy, *Potassium channels as therapeutic targets for autoimmune disorders.* Curr Opin Drug Discov Devel, 2003. **6**(5): p. 640-7.

93. Nicolaou, S.A., et al., *Localization of Kv1.3 channels in the immunological synapse modulates the calcium response to antigen stimulation in T lymphocytes.* J Immunol, 2009. **183**(10): p. 6296-302.
94. Nicolaou, S.A., et al., *Altered dynamics of Kv1.3 channel compartmentalization in the immunological synapse in systemic lupus erythematosus.* J Immunol, 2007. **179**(1): p. 346-56.
95. Nicolaou, S.A., et al., *Differential calcium signaling and Kv1.3 trafficking to the immunological synapse in systemic lupus erythematosus.* Cell Calcium, 2010. **47**(1): p. 19-28.
96. de Mendoza, A., H. Suga, and I. Ruiz-Trillo, *Evolution of the MAGUK protein gene family in premetazoan lineages.* BMC Evol Biol, 2010. **10**: p. 93.
97. Oliva, C., et al., *Role of the MAGUK protein family in synapse formation and function.* Dev Neurobiol, 2012. **72**(1): p. 57-72.
98. Deng, F., et al., *Stargazin and other transmembrane AMPA receptor regulating proteins interact with synaptic scaffolding protein MAGI-2 in brain.* J Neurosci, 2006. **26**(30): p. 7875-84.
99. Gosens, I., et al., *MPP1 links the Usher protein network and the Crumbs protein complex in the retina.* Hum Mol Genet, 2007. **16**(16): p. 1993-2003.
100. Jing-Ping, Z., et al., *p55 protein is a member of PSD scaffold proteins in the rat brain and interacts with various PSD proteins.* Brain Res Mol Brain Res, 2005. **135**(1-2): p. 204-16.
101. Laura, R.P., et al., *MAGI-1: a widely expressed, alternatively spliced tight junction protein.* Exp Cell Res, 2002. **275**(2): p. 155-70.
102. Wolburg, H. and A. Lippoldt, *Tight junctions of the blood-brain barrier: development, composition and regulation.* Vascul Pharmacol, 2002. **38**(6): p. 323-37.
103. McAllister-Lucas, L.M., et al., *The CARMA3-Bcl10-MALT1 signalosome promotes angiotensin II-dependent vascular inflammation and atherogenesis.* J Biol Chem, 2010. **285**(34): p. 25880-4.
104. Muller, B.M., et al., *Molecular characterization and spatial distribution of SAP97, a novel presynaptic protein homologous to SAP90 and the Drosophila discs-large tumor suppressor protein.* J Neurosci, 1995. **15**(3 Pt 2): p. 2354-66.
105. Kaech, S.M., C.W. Whitfield, and S.K. Kim, *The LIN-2/LIN-7/LIN-10 complex mediates basolateral membrane localization of the C. elegans EGF receptor LET-23 in vulval epithelial cells.* Cell, 1998. **94**(6): p. 761-71.
106. Feng, W., et al., *The tetrameric L27 domain complex as an organization platform for supramolecular assemblies.* Nat Struct Mol Biol, 2004. **11**(5): p. 475-80.
107. Li, Y., et al., *Structural basis for L27 domain-mediated assembly of signaling and cell polarity complexes.* Embo J, 2004. **23**(14): p. 2723-33.
108. Petrosky, K.Y., et al., *A general model for preferential hetero-oligomerization of LIN-2/7 domains: mechanism underlying directed assembly of supramolecular signaling complexes.* J Biol Chem, 2005. **280**(46): p. 38528-36.
109. Hata, Y., H. Nakanishi, and Y. Takai, *Synaptic PDZ domain-containing proteins.* Neurosci Res, 1998. **32**(1): p. 1-7.
110. Doyle, D.A., et al., *Crystal structures of a complexed and peptide-free membrane protein-binding domain: molecular basis of peptide recognition by PDZ.* Cell, 1996. **85**(7): p. 1067-76.
111. Gomperts, S.N., *Clustering membrane proteins: It's all coming together with the PSD-95/SAP90 protein family.* Cell, 1996. **84**(5): p. 659-62.
112. Sheng, M., *Excitatory synapses. Glutamate receptors put in their place.* Nature, 1997. **386**(6622): p. 221, 223.
113. Kim, E., et al., *GKAP, a novel synaptic protein that interacts with the guanylate kinase-like domain of the PSD-95/SAP90 family of channel clustering molecules.* J Cell Biol, 1997. **136**(3): p. 669-78.
114. Kim, E., et al., *Clustering of Shaker-type K+ channels by interaction with a family of membrane-associated guanylate kinases.* Nature, 1995. **378**(6552): p. 85-8.

115. Kim, E. and M. Sheng, *Differential K+ channel clustering activity of PSD-95 and SAP97, two related membrane-associated putative guanylate kinases.* Neuropharmacology, 1996. **35**(7): p. 993-1000.
116. Tiffany, A.M., et al., *PSD-95 and SAP97 exhibit distinct mechanisms for regulating K(+) channel surface expression and clustering.* J Cell Biol, 2000. **148**(1): p. 147-58.
117. Marks, D.R. and D.A. Fadool, *Post-synaptic density perturbs insulin-induced Kv1.3 channel modulation via a clustering mechanism involving the SH3 domain.* J Neurochem, 2007. **103**(4): p. 1608-27.
118. Maniatis, T., *Molecular Cloning: A Laboratory Manual*. 2012: Cold Spring Harbor Laboratory Press.
119. Inoue, H., H. Nojima, and H. Okayama, *High efficiency transformation of Escherichia coli with plasmids.* Gene, 1990. **96**(1): p. 23-8.
120. Hamill, O.P., et al., *Improved patch-clamp techniques for high-resolution current recording from cells and cell-free membrane patches.* Pflugers Arch, 1981. **391**(2): p. 85-100.
121. Grissmer, S., A.N. Nguyen, and M.D. Cahalan, *Calcium-activated potassium channels in resting and activated human T lymphocytes. Expression levels, calcium dependence, ion selectivity, and pharmacology.* J Gen Physiol, 1993. **102**(4): p. 601-30.
122. Connolly, S.F. and D.J. Kusner, *The regulation of dendritic cell function by calcium-signaling and its inhibition by microbial pathogens.* Immunol Res, 2007. **39**(1-3): p. 115-27.
123. Grakoui, A., et al., *The immunological synapse: a molecular machine controlling T cell activation.* Science, 1999. **285**(5425): p. 221-7.
124. Bock, J., et al., *Ceramide inhibits the potassium channel Kv1.3 by the formation of membrane platforms.* Biochem Biophys Res Commun, 2003. **305**(4): p. 890-7.
125. Koski, G.K., et al., *CD14+ monocytes as dendritic cell precursors: diverse maturation-inducing pathways lead to common activation of NF-kappab/RelB.* Crit Rev Immunol, 2001. **21**(1-3): p. 179-89.
126. Gogolak, P., et al., *Targeting dendritic cells for priming cellular immune responses.* J Mol Recognit, 2003. **16**(5): p. 299-317.
127. Flores-Romo, L., *In vivo maturation and migration of dendritic cells.* Immunology, 2001. **102**(3): p. 255-62.
128. Ghanshani, S., et al., *Up-regulation of the IKCa1 potassium channel during T-cell activation. Molecular mechanism and functional consequences.* J Biol Chem, 2000. **275**(47): p. 37137-49.
129. Offord, J. and W.A. Catterall, *Electrical activity, cAMP, and cytosolic calcium regulate mRNA encoding sodium channel alpha subunits in rat muscle cells.* Neuron, 1989. **2**(5): p. 1447-52.
130. Zanoni, I., et al., *CD14 regulates the dendritic cell life cycle after LPS exposure through NFAT activation.* Nature, 2009. **460**(7252): p. 264-8.
131. Hirsh, J.K. and F.N. Quandt, *Down-regulation of Na channel expression by A23187 in N1E-115 neuroblastoma cells.* Brain Res, 1996. **706**(2): p. 343-6.
132. Sontheimer, H., et al., *Astrocyte Na+ channels are required for maintenance of Na+/K(+)-ATPase activity.* J Neurosci, 1994. **14**(5 Pt 1): p. 2464-75.
133. Sontheimer, H. and S.G. Waxman, *Expression of voltage-activated ion channels by astrocytes and oligodendrocytes in the hippocampal slice.* J Neurophysiol, 1993. **70**(5): p. 1863-73.
134. Arcangeli, A., et al., *Targeting ion channels in cancer: a novel frontier in antineoplastic therapy.* Curr Med Chem, 2009. **16**(1): p. 66-93.
135. Grimes, J.A., et al., *Differential expression of voltage-activated Na+ currents in two prostatic tumour cell lines: contribution to invasiveness in vitro.* FEBS Lett, 1995. **369**(2-3): p. 290-4.
136. Jo, T., et al., *Voltage-gated sodium channel expressed in cultured human smooth muscle cells: involvement of SCN9A.* FEBS Lett, 2004. **567**(2-3): p. 339-43.
137. Meguro, K., et al., *Function and role of voltage-gated sodium channel NaV1.7 expressed in aortic smooth muscle cells.* Am J Physiol Heart Circ Physiol, 2009. **296**(1): p. H211-9.

138. Affaticati, P., et al., *Sustained calcium signalling and caspase-3 activation involve NMDA receptors in thymocytes in contact with dendritic cells.* Cell Death Differ, 2011. **18**(1): p. 99-108.
139. Woehrle, T., et al., *Pannexin-1 hemichannel-mediated ATP release together with P2X1 and P2X4 receptors regulate T-cell activation at the immune synapse.* Blood, 2010. **116**(18): p. 3475-84.
140. Quintana, A., et al., *T cell activation requires mitochondrial translocation to the immunological synapse.* Proc Natl Acad Sci U S A, 2007. **104**(36): p. 14418-23.
141. Quintana, A., et al., *Calcium microdomains at the immunological synapse: how ORAI channels, mitochondria and calcium pumps generate local calcium signals for efficient T-cell activation.* Embo J, 2011. **30**(19): p. 3895-912.
142. Schwindling, C., et al., *Mitochondria positioning controls local calcium influx in T cells.* J Immunol, 2010. **184**(1): p. 184-90.
143. Burke, N.A., et al., *Distinct structural requirements for clustering and immobilization of K+ channels by PSD-95.* J Gen Physiol, 1999. **113**(1): p. 71-80.
144. Jugloff, D.G., et al., *Internalization of the Kv1.4 potassium channel is suppressed by clustering interactions with PSD-95.* J Biol Chem, 2000. **275**(2): p. 1357-64.
145. Doczi, M.A., D.H. Damon, and A.D. Morielli, *A C-terminal PDZ binding domain modulates the function and localization of Kv1.3 channels.* Exp Cell Res, 2011. **317**(16): p. 2333-41.
146. Songyang, Z., et al., *Recognition of unique carboxyl-terminal motifs by distinct PDZ domains.* Science, 1997. **275**(5296): p. 73-7.
147. Panyi, G. and C. Deutsch, *Assembly and suppression of endogenous Kv1.3 channels in human T cells.* J Gen Physiol, 1996. **107**(3): p. 409-20.
148. Nicolaou, S.A., et al., *Differential calcium signaling and Kv1.3 trafficking to the immunological synapse in systemic lupus erythematosus.* Cell Calcium, 2007. **47**(1): p. 19-28.
149. Xavier, R. and B. Seed, *PDZ domains and the politics of polarity in lymphocytes.* Immunity, 2005. **22**(6): p. 655-6.
150. Zanin-Zhorov, A., et al., *Scaffold protein Disc large homolog 1 is required for T-cell receptor-induced activation of regulatory T-cell function.* Proc Natl Acad Sci U S A, 2012. **109**(5): p. 1625-30.
151. Kuras, Z., et al., *Modulation of Kv1.3 channels by protein kinase A I in T lymphocytes is mediated by the disc large 1-tyrosine kinase Lck complex.* Am J Physiol Cell Physiol, 2012. **302**(10): p. C1504-12.

10. LIST OF PUBLICATIONS

Register Number: DEENKÉTK/383/2013.
Item Number:
Subject: Ph.D. List of Publications

Candidate: Orsolya Szilágyi

Neptun ID: YDIWEL

Doctoral School: Doctoral School of Molecular Medicine

Mtmt ID: 10034484

List of publications related to the dissertation

1. **Szilágyi, O.**, Boratkó, A., Panyi, G., Hajdú, P.: The role of PSD-95 in the rearrangement of Kv1.3 channels to the immunological synapse.
Pflugers Arch. 465 (9), 1341-1353, 2013.
DOI: http://dx.doi.org/10.1007/s00424-013-1256-6
IF:4.866 (2012)

2. Kis-Tóth, K., Hajdú, P., Bácskai, I., **Szilágyi, O.**, Papp, F., Szántó, A., Posta, E., Gogolák, P., Panyi, G., Rajnavölgyi, É.: Voltage-Gated Sodium Channel Nav1.7 Maintains the Membrane Potential and Regulates the Activation and Chemokine-Induced Migration of a Monocyte-Derived Dendritic Cell Subset.
J. Immunol. 187 (3), 1273-1280, 2011.
DOI: http://dx.doi.org/10.4049/jimmunol.1003345
IF:5.788

List of other publications

3. Chimote, A.A., Hajdú, P., Kucher, V., Boiko, N., Kuras, Z., **Szilágyi, O.**, Yun, Y., Conforti, L.: Selective Inhibition of KCa3.1 Channels Mediates Adenosine Regulation of the Motility of Human T Cells.
J. Immunol. Epub ahead of print (2013)
DOI: http://dx.doi.org/10.4049/jimmunol.1300702
IF:5.52 (2012)

4. Izsépi, E., Himer, L., **Szilágyi, O.**, Hajdú, P., Panyi, G., László, G., Matkó, J.: Membrane microdomain organization, calcium signal, and NFAT activation as an important axis in polarized Th cell function.
Cytometry A. 83 (2), 185-196, 2013.
DOI: http://dx.doi.org/10.1002/cyto.a.22234
IF:3.711 (2012)

5. Somodi, S., Balajthy, A., **Szilágyi, O.**, Pethő, Z., Harangi, M., Paragh, G., Panyi, G., Hajdú, P.: Analysis of the K+ current in human CD4+ T lymphocytes in hypercholesterolemic state.
Cell. Immunol. 281 (1), 20-26, 2013.
DOI: http://dx.doi.org/10.1016/j.cellimm.2013.01.004
IF:1.743 (2012)

6. Hajdú, P., **Szilágyi, O.**, Tóth, Á., Krasznai, Z., Pocsai, K., Panyi, G.: Answer to the "comment on functional consequences of Kv1.3 ion channel rearrangement into the immunological synapse" by Stefan Bittner et al. [Immunol. Lett. 125 (Aug 15 (2)) (2009) 156-157].
Immunol. Lett. 129 (1), 47-49, 2010.
DOI: http://dx.doi.org/10.1016/j.imlet.2009.12.026
IF:2.511

7. Tóth, Á., **Szilágyi, O.**, Krasznai, Z., Panyi, G., Hajdú, P.: Functional consequences of Kv1.3 ion channel rearrangement into the immunological synapse.
Immunol. Lett. 125 (1), 15-21, 2009.
DOI: http://dx.doi.org/10.1016/j.imlet.2009.05.004
IF:2.906

Total IF of journals (all publications): 27.045

Total IF of journals (publications related to the dissertation): 10.654

The Candidate's publication data submitted to the Publication Database of the University of Debrecen have been validated by Kenezy Life Sciences Library on the basis of Web of Science, Scopus and Journal Citation Report (Impact Factor) databases.

28 November, 2013

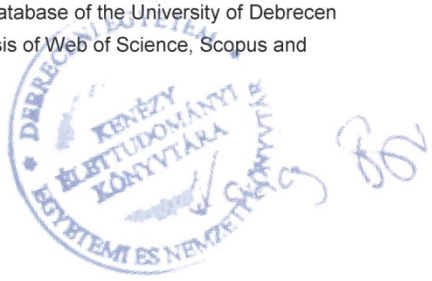

11. ORAL AND POSTER PRESENTATIONS

Oral presentations:

Szilágyi Orsolya, Boratkó Anita, Panyi György, Hajdu Péter. A PSD-95 a Kv1.3 ioncsatorna immunológiai szinapszisban való feldúsulásában (Ernst Jenő award), Veszprém, 2013, XXIV. Congress of the Hungarian Biophysical Society

Orsolya Szilágyi, Anita Boratkó, György Panyi, Péter Hajdu. The role of PSD-95 in the rearrangement of Kv1.3 channels to the immunological synapse, Mátraháza, 2013, Immune-related Pathologies: Understanding Leukocyte Signaling and Emerging therapies (IMPULSE)

Poster presentations:

Szilágyi Orsolya, Tóth Ágnes, Bartók Ádám, Krasznai Zoltán, Panyi György, Hajdú Péter: Fluoreszcens fehérjével konjugált Kv1.3 csatornák komparatív vizsgálata, Sümeg, 2008, Membrane Transport Conference

Szilágyi Orsolya, Papp Ferenc, Herceg Mónika, Gáspár Rezső, Batista C. V. F., Zamudio F. Z., Varga Zoltán, Possani L. D. Pharmacological and biophysical studies of a toxin from the scorpion Tytius stigmurus, Leuven, Belgium, 2008, IST Conference

Ágnes Tóth, **Orsolya Szilágyi**, Ákos Fábián, Zoltán Krasznai, György Panyi, Péter Hajdú. Functional Consequences of Kv1.3 Ion Channel Rearrangement Into The Immunological Synapse, Strbske Pleso, Slovakia, 2008, 8th EFIS-EJI Tatra Immunology Conference

Ádám Bartók, Ferenc Papp, Mónika Herceg, **Orsolya Szilágyi**, Rezső Gáspár. Pharmacological and biophysical studies of a toxin from the scorpion Tytius stigmurus, Sümeg, 2008, Membrane Transport Conference

Orsolya Szilágyi, Mónika Herceg, Gerrardo Corzo, Ferenc Papp, Zoltán Varga, Omar Barraza, Pavel G. Espino, Ricardo C. Rodríguez de la Vega, Rezső Gáspár, György Panyi, Lourival D. Possani. A selective blocker of Kv1.2 and Kv1.3 potassium channels from the soluble venom of the scorpion Centruroides suffusus suffusus, Boston, USA, 2009, Biophysical Society 53rd Annual Meeting

Szilágyi Orsolya, Tóth Ágnes, Krasznai Zoltán, Panyi György, Hajdú Péter. Kv1.3 csatornák immunológiai szinapszisba történő átrendeződésének funkcionális következményei, Pécs, 2009, XXIII. Congress of the Hungarian Biophysical Society

Papp Ferenc, **Szilágyi Orsolya**, Herceg Mónika, Corzo Gerrardo, Varga Zoltán, Barraza Omar, Pavel G. Espino, Ricardo C. Rodríguez de la Vega, Gáspár Rezső, Lourival D. Possani, Panyi György. A Centruroides suffusus skorpió venomjából izolált toxin kálium-csatornát gátol, Pécs, 2009, XXIII. Congress of the Hungarian Biophysical Society

Peter Hajdu, Katalin Kis-Toth, Ferenc Papp, Attila Szanto, Edit Posta, Ildiko Bacskai, Peter Gogolak, **Orsolya Szilagyi**, Eva Rajnavolgyi, Gyorgy Panyi. Voltage-gated Sodium Channel Nav1.7 Maintains The Membrane Potential And Regulates Chemokine-induced Migration Of A Subpopulation Of Monocyte-derived Dendritic Cells (poszter) Baltimore, USA, 2011, Biophysical Society 55th Annual Meeting

Orsolya Szilágyi, György Panyi, Anita Boratkó, Péter Hajdú. The possible role of PSD-95/SAP90 in the rearrangement of Kv1.3 channels to the immunological synapse , Visegrád, 2011, Immune-related Pathologies: Understanding Leukocyte Signaling and Emerging therapies (IMPULSE)

Orsolya Szilágyi, György Panyi, Anita Boratkó, Péter Hajdú. The possible role of PSD-95/SAP90 in the rearrangement of Kv1.3 channels to the immunological synapse, San Diego, USA, 2012, Biophysical Society 56th Annual Meeting

Orsolya Szilágyi, György Panyi, Anita Boratkó, Péter Hajdú. The possible role of PSD-95/SAP90 in the rearrangement of Kv1.3 channels to the immunological synapse, Sümeg, 2012, Membrane Transport Conference

Domján Brigitta, Papp Ferenc, Szántó G. Tibor, Bartók Ádám, **Szilágyi Orsolya**, Bacsó Zsolt, Panyi György, Krasznai Zoltán. RF expozíció akut hatásai Nav1.5 ioncsatornák működésére, Sümeg, 2012, Membrane Transport Conference

Orsolya Szilágyi, Anita Boratkó, György Panyi, Péter Hajdu. The role of PSD-95 in the rearrangement of Kv1.3 channels to the immunological synapse, Saint Petersburg, Russia, 2013, FEBS Congress

12. KEYWORDS

ion channel

patch-clamp

dendritic cell

T cell

Nav1.7

Kv1.3

immunological synapse

MAGUK proteins

KULCSSZAVAK

ioncsatorna

patch-clamp

dendritikus sejt

T sejt

Nav1.7

Kv1.3

immunológiai szinapszis

MAGUK fehérjék

13. ACKNOWLEDGEMENTS

First and foremost I would like to express my deepest gratitude to my supervisor Dr. Péter Hajdu, who has been my mentor throughout my PhD education.

I would also like to thank the head of the Department of Biophysics and Cell biology, Prof. Dr. János Szöllősi for supporting my work.

I am grateful to Prof. Dr. György Panyi the leader of the Electrophysiology Laboratory for providing me with the opportunity to work in his group.

The constant and helpful assistance provided by Cecília Nagy is especially appreciated.

I must thank the past and present members of our laboratory: Dr. Zoltán Krasznai, Dr. Zoltán Varga, Dr. Sándor Somodi, Dr. Tibor G. Szántó, Dr. Ferenc Papp, Ádám Bartók, Dr. Ágnes Tóth, Brigitta Domján, Dr. András Balajthy and Zoltán Pethő, who have not only helped me during my work professionally, but have also ensured a great atmosphere to work in.

Finally I would like to thank my Family, who have always supported me.

The experimental work was performed by the support of the TÁMOP-4.2.2.A-11/1-KONV/2012-0025 project. The doctoral training program was supported by the TÁMOP-4.2.2/B-10/1-2010-0024 project. This research was supported by the European Union and the State of Hungary, co-financed by the European Social Fund in the framework of TÁMOP 4.2.4. A/2-11-1-2012-0001 ‘National Excellence Program’.